

ELECTRICAL PROPERTIES OF ALUMINOSILICATE GLAZES CONTAINING  
NIOBIUM DOPED TITANIUM DIOXIDE.

A Thesis Presented  
for the Degree  
of  
Doctor of Philosophy  
by  
Jasbinder Singh Sanghera

Department of Metallurgy and Materials Science,  
Imperial College of Science and Technology,  
The University of London.

July, 1985

ABSTRACT

The thesis describes a novel approach in providing a uniform distribution of electrically conducting particles of  $\text{TiO}_2$  doped with  $\text{Nb}_2\text{O}_5$  in an aluminosilicate glass. This is achieved by heat treatment of a homogeneous glass at  $800^\circ\text{C}$  to produce glass in glass phase separation by a spinodal decomposition mechanism. A dispersion of sub-micron titania-rich droplets in a silica rich matrix is produced. Subsequent treatment at  $1000^\circ\text{C}$  enables the titania-rich phase to crystallise, producing a fine and uniform dispersion of rutile ( $\text{TiO}_2$ ) needles. The presence of a few weight per cent  $\text{Nb}_2\text{O}_5$  in the glass gives rise to  $\text{TiO}_2$  crystals doped with  $\text{Nb}^{5+}$  ions and the partially crystalline materials exhibit semiconducting properties.

The properties of the glasses and crystallised glasses have been investigated using optical and electron microscopy, x-ray diffraction analysis and bulk D C conductivity measurements over the range from room temperature to  $500^\circ\text{C}$ .

The microstructure of the materials has been related to the D C conductivities. The effects of varying the  $\text{TiO}_2$  and  $\text{Nb}_2\text{O}_5$  contents and the ratio of  $\text{Nb}_2\text{O}_5$  to  $\text{TiO}_2$  have been studied; while the range of heat treatments to optimise the electrical conductivities have been investigated.

The suitability of the materials as semiconducting glaze coatings for application to high voltage insulators, which requires a knowledge of the physical properties of the glaze and substrate, has been determined.

CONTENTS

ABSTRACT

<u>CHAPTER 1</u>		<u>Page</u>
1.1	Introduction	13
1.2	History of Semiconducting Glazes	14
	1.2.1 Iron oxide based glazes	15
	1.2.2 Reduced titania glazes	18
	1.2.3 Tin oxide based glazes	21
	1.2.4 Criteria for selection of a semiconducting crystalline phase for a semiconducting glaze	24
1.3	Glass Formation and Crystallisation	26
	1.3.1 Glass formation	26
	1.3.2 Theories of glass formation	28
	1.3.2.1 Structural theories	28
	1.3.2.2 Thermodynamic theories	35
	1.3.2.3 Kinetic theories	37
1.4	Crystallisation of Glasses	41
	1.4.1 Homogeneous nucleation	41
	1.4.2 Heterogeneous nucleation	46
	1.4.3 Liquid-liquid phase separation	47
	1.4.4 Crystal growth	50
1.5	Glass-Ceramics	57
1.6	Electrical Conduction in Crystalline Solids	61
	(i) Non-stoichiometry	65
	(ii) Conduction in inverse spinels (B[AB]O <sub>4</sub> )	66
	(iii) Valency controlled semiconductors	67
1.7	Electrical Conduction in Oxide Glasses	68
	1.7.1 Ionic conduction in glasses	68
	1.7.2 Electronic conduction in glasses	70
1.8	Temperature Dependence of D.C. Conductivity	75
	1.8.1 Band conduction	75
	1.8.2 Thermally assisted tunnelling	75
	1.8.3 Tunnelling conduction near E <sub>F</sub>	75
	1.8.4 Polaron Hopping	76
1.9	TiO <sub>2</sub> /Nb <sub>2</sub> O <sub>5</sub> System	81

<u>CHAPTER 2 EXPERIMENTAL DETAILS</u>		<u>Page</u>
2.1	Glass Preparation	87
2.2	Optical Microscopy	88
2.3	X-ray Powder Diffraction Analysis	88
2.4	Transmission Electron Microscopy	89
2.5	Scanning Electron Microscopy	90
2.6	Electron Probe Microanalysis	90
2.7	D.C. Conductivity Measurements	90
2.8	TiO <sub>2</sub> /Nb <sub>2</sub> O <sub>5</sub> Solid Solution Formation	92
2.9	Determination of the wt% Crystalline TiO <sub>2</sub> Present in Partially Crystalline Glass Samples	93
2.10	Determination of the Coefficient of Linear Expansion, $\alpha$	97
<u>CHAPTER 3 EXPERIMENTAL RESULTS</u>		
3.1	Composition of the Glasses	98
3.2	Initial Heat Treatment Study	100
3.3	Electron Probe Microanalysis (EPMA) Results	110
3.4	D.C. Resistivity Results	112
3.5	TiO <sub>2</sub> /Nb <sub>2</sub> O <sub>5</sub> Solid Solution Results	155
3.6	Determination of the Wt% Crystalline TiO <sub>2</sub>	168
3.7	Results for the Coefficient of Linear Expansion, $\alpha$	171
<u>CHAPTER 4 DISCUSSION</u>		
4.1	Crystallisation Behaviour of the Glasses	173
	4.1.1 Glass preparation	173
	4.1.2 Phase separation	174
	4.1.3 Crystal growth	176
4.2	Solid Solution Formation in the TiO <sub>2</sub> /Nb <sub>2</sub> O <sub>5</sub> System	178

<u>CHAPTER 4 continued</u>		<u>Page</u>
4.3	Wt% Crystalline TiO <sub>2</sub> in Partially Crystalline Samples	181
4.4	D C Resistivity Measurements of the Glasses	186
	4.4.1 Glasses containing 10 wt% TiO <sub>2</sub>	186
	4.4.2 Glasses containing 15 wt% TiO <sub>2</sub>	192
4.5	Suitability of TiO <sub>2</sub> Aluminosilicates as Insulator Glaze Material	199
	4.5.1 Coefficients of linear expansion, $\alpha$	201
<u>CHAPTER 5 CONCLUSIONS AND SUGGESTIONS FOR FUTURE WORK</u>		
5.1	Conclusions	205
5.2	Suggestions for Further Studies	208
ACKNOWLEDGEMENTS		210
REFERENCES		211

TABLES

		<u>Page</u>
1.1	Preparation of non-crystalline materials from solid, liquid and gaseous phases	27
3.1	Compositon of the glasses (wt%)	99
3.2	Preliminary heat treatments performed on J0 and J3 glasses	103
3.3	EPMA analysis of partially crystalline J3 glass heat treated at 3 hours 800°C + 0.5 hours 1000°C	111
3.4	Heat treatment of J0 glass	115
3.5	Heat treatment of J1 glass	116
3.6	Electrical properties of partially crystalline samples of J1 glass	117
3.7	Electrical properties of partially crystalline samples of J1 glass	119
3.8	Heat treatment of J2 glass	121
3.9	Electrical properties of partially crystalline samples of J2 glass	122
3.10	Heat treatment of J3 glass	124
3.11	Electrical properties of partially crystalline samples of J3 glass	125
3.12	Heat treatment of J4 glass	127
3.13	Electrical properties of partially crystalline samples of J4 glass	128
3.14	Heat treatment of J5 glass	130
3.15	Heat treatment of J6 glass	131
3.16	Heat treatment of J7 glass	132
3.17	Heat treatment of J8 glass	133
3.18	Electrical properties of partially crystalline samples of J8 glass	134
3.19	Heat treatment of J9 glass	136

<u>TABLES CONTINUED</u>		<u>Page</u>
3.20	Electrical properties of partially crystalline samples of J9 glass	137
3.21	Heat treatment of J10 glass	139
3.22	Electrical properties of partially crystalline samples of J10 glass	140
3.23	Heat treatment of J11 glass	142
3.24	Electrical properties of partially crystalline samples of J11 glass	143
3.25	Heat treatment of J12 glass	145
3.26	Electrical properties of partially crystalline samples of J12 glass	146
3.27	Heat treatment of J13 glass	148
3.28	Electrical properties of partially crystalline samples of J13 glass	149
3.29	Heat treatment of JS11 glass	151
3.30	Electrical properties of partially crystalline samples of JS11 glass	152
3.31	Composition of the solid solution samples	158
3.32	X-ray diffractometer data for determination of absolute lattice parameter " $a_0$ " for pure rutile, $TiO_2$	159
3.33	X-ray diffractometer data for determination of absolute lattice parameter " $c_0$ " for pure rutile, $TiO_2$	160
3.34	X-ray diffractometer data for determination of absolute lattice parameter " $a_0$ " for rutile doped with 1.9 mole% $Nb_2O_5$	162
3.35	X-ray diffraction data for determination of absolute lattice parameter " $c_0$ " for rutile doped with 1.9 mole% $Nb_2O_5$	163
3.36	Variation of the lattice parameters of rutile with the addition of $Nb_2O_5$ dopant	165
3.37	Determination of the wt% of crystalline $TiO_2$ in partially crystalline samples	170

TABLES CONTINUED

		<u>Page</u>
3.38	The coefficient of linear expansion, $\alpha$ , of various samples	172
4.1	Volume% of crystalline $\text{TiO}_2$ in partially crystalline samples	185



<u>FIGURES</u>		<u>Page</u>
1.1	Structure of the compound $X_2O_3$ in (a) the crystalline and (b) the glassy form	31
1.2	Structure of a $Na_2O - SiO_2$ glass	34
1.3	The change in energy required to form a nucleus of radius $r$	42
1.4	Effect of temperature on rates of nucleation and crystal growth	45
1.5	Heterogeneous nucleation	46
1.6	(a) Hypothetical phase diagram showing immiscible region and spinodal decomposition (b) Free energy of mixing at temperature $T_1$	49
1.7	Free energy diagram for the attachment process at the crystal-melt interface	53
1.8	Variation of growth rate with temperature	55
1.9	Time-temperature schedule for making a glass-ceramic	58
1.10	Energy band diagram for an insulator	64
1.11	Energy band diagram for intrinsic silicon semiconductor	64
1.12	Schematic density-of-states diagrams for a semiconducting glass (a) An "Ideal" glass (b) A glass with defect states (c) The Cohen-Fritzsche-Ovshinsky model	72
1.13	Davis and Mott Model	73
1.14	Potential wells on a pair of Ions a and b during the hopping process (i) before hopping (ii) thermally activated state when electrons can move	78
1.15	Equilibrium phase diagram for the system $TiO_2-Nb_2O_5$	85
2.1	Schematic representation of D.C. conductivity cell with measuring apparatus	91

<u>FIGURES CONTINUED</u>		<u>Page</u>
3.1	Variation in growth rate of TiO <sub>2</sub> needles with temperature for J1 glass	109
3.2	Plot of log <sub>10</sub> resistivity against 1000/temp for partially crystalline samples of J1 glass	118
3.3	Plot of log <sub>10</sub> resistivity against 1000/temp for partially crystalline samples of J1 glass	119
3.4	Plot of log <sub>10</sub> resistivity against 1000/temp for partially crystalline samples of J2 glass	123
3.5	Plot of log <sub>10</sub> resistivity against 1000/temp for partially crystalline samples of J3 glass	126
3.6	Plot of log <sub>10</sub> resistivity against 1000/temp for partially crystalline samples of J4 glass	129
3.7	Plot of log <sub>10</sub> resistivity against 1000/temp for partially crystalline samples of J8 glass	135
3.8	Plot of log <sub>10</sub> resistivity against 1000/temp for partially crystalline samples of J9 glass	138
3.9	Plot of log <sub>10</sub> resistivity against 1000/temp for partially crystalline samples of J10 glass	141
3.10	Plot of log <sub>10</sub> resistivity against 1000/temp for partially crystalline samples of J11 glass	144
3.11	Plot of log <sub>10</sub> resistivity against 1000/temp for partially crystalline samples of J12 glass	147
3.12	Plot of log <sub>10</sub> resistivity against 1000/temp for partially crystalline samples of J13 glass	150
3.13	Plot of log <sub>10</sub> resistivity against 1000/temp for partially crystalline samples of JS11 glass	153

<u>FIGURES CONTINUED</u>		<u>Page</u>
3.14	Room temperature resistivity of crystallised J3 glass as a function of length of rutile needles. All samples, except J3/7, phase separated prior to crystallisation	154
3.15	(a) Plot of lattice parameter " $a_0$ " against $f(\theta)$ for pure rutile, $TiO_2$	161
	(b) Plot of lattice parameter " $c_0$ " against $f(\theta)$ for pure rutile	161
3.16	(a) Plot of lattice parameter " $a_0$ " against $f(\theta)$ for rutile doped with 1.9 mole% $Nb_2O_5$	164
	(b) Plot of lattice parameter " $c_0$ " against $f(\theta)$ for rutile doped with 1.9 mole% $Nb_2O_5$	164
3.17	Variation in the lattice parameter " $a_0$ " of rutile with mole% addition of $Nb_2O_5$	166
3.18	Variation in the lattice parameter " $c_0$ " of rutile with mole% addition of $Nb_2O_5$	167
3.19	Relationship between the $TiO_2/NaCl$ peak height ratio and the wt% crystalline $TiO_2$ in a glass/ $TiO_2$ mixture	169
4.1	The structure of rutile, $TiO_2$	182
4.2	An overall view of rutile emphasising the arrangement of the octahedral chains and showing the relation to Figure 4.1	182
4.3	Variation between the minimum value in $\log \rho$ at $25^\circ C$ and the ratio of wt% $Nb_2O_5$ to wt% $TiO_2$ for a) 10 wt% $TiO_2$ glasses b) 15 wt% $TiO_2$ glasses	196
4.4	Increase in length, $\Delta L$ , against temperature, $T$	202

LIST OF PLATES

		<u>Page</u>
3.1-3.2	Scanning Electron Micrographs of Selected Crystallised Glasses	
3.1	J3 heat treated for 0.5 hours at 1000°C	105
3.2	J3 heat treated for 3 hours at 800°C followed by 0.5 hours at 1000°C	106
3.3-3.4	Transmission Electron Micrographs of Phase Separated Glasses	
3.3	J3 glass heat treated for 3 hours at 800°C	107
3.4	J3 glass heat treated for 3 hours at 800°C	108

## CHAPTER 1

### 1.1 Introduction

This thesis describes the work which has been performed in an attempt to produce an improved semiconducting glaze for the coating of high voltage electrical insulators.

Since the 1940's various attempts have been made to reduce the interference produced by electrical discharge and flashover on overhead power lines. High voltage insulators as used in the UK are predominantly of electrical porcelain coated with a ceramic glaze to provide a non-porous surface. In polluted and damp conditions electrical discharge can readily occur. Improvements have centred on producing a glaze with semiconducting properties which would provide a more uniform voltage distribution, and at the same time, through the leakage of a small amount of current to earth provide a surface which would dry more readily.

Glazes containing conducting metal oxides, produced by the application of mechanically milled glass powder and oxides applied as a slurry and then fired onto the surface of the porcelain, have shown that the appropriate electrical properties may be achieved. However, the long term benefits have not materialised since electrolytic action within the glaze and corrosion problems have lead to failure of these coatings after several years in service.

The most promising semiconducting glaze to date has contained a dispersion of fine SnO<sub>2</sub> crystals doped with

$\text{Sb}_2\text{O}_5$  or  $\text{Sb}_2\text{O}_3$ . However the difficulty in producing a uniform dispersion of  $\text{SnO}_2$  particles with the traditional mechanical mixing methods led to some areas of the glaze being more resistive than others, which enhanced degradation of the glaze.

In the present study an extremely fine and uniform distribution of doped  $\text{TiO}_2$  crystals within a glassy matrix has been achieved by controlled heat treatments of an initial homogeneous glass. With the appropriate treatment the phase separation of the homogeneous glass into regions rich in  $\text{TiO}_2$  and those rich in  $\text{SiO}_2$  was achieved, followed by the crystallisation of the  $\text{TiO}_2$  rich regions to rutile ( $\text{TiO}_2$ ).

The glazes have been rendered semiconducting by the addition of a few weight per cent of  $\text{Nb}_2\text{O}_5$  to the initial glass. During heat treatment the  $\text{Nb}^{5+}$  ions associate with the  $\text{TiO}_2$  to give a defect crystalline structure with the semiconducting properties.

The thesis describes the way in which the semiconducting properties have been optimised by the amount of  $\text{TiO}_2$  added, the ratio of  $\text{TiO}_2$  to  $\text{Nb}_2\text{O}_5$ , and the heat treatment of the glass. The conduction mechanism and the applicability of the semiconducting glaze for coating insulators is discussed.

## 1.2 History Of Semiconducting Glazes

Forrest (1942)<sup>1</sup> pointed out that a new type of high voltage insulator was needed with a controlled leakage of

current to earth. He suggested that in the presence of moisture, a pollution layer of relatively low resistance was deposited on the surface of porcelain insulators, and under these conditions a considerable leakage current may flow across the surface. Layers of pollution will dry out where the current density is high, to leave behind dry bands of relatively high resistance. If the voltage gradient across a dry band is greater than that required for the ionisation of air, then flashover occurs. This can have the effect of drying out regions immediately on either side of the dry bands, and thus making them grow, and in extreme cases complete flashover of the insulator can occur. Forrest's original suggestion was to prevent these excessive voltage drops by shunting each unit with a standard 10 megohms resistor. However, this approach was dropped on the grounds that the long-term stability of fixed resistances was unknown.

Forrest suggested an alternative approach was to coat the surface of the insulator with a semiconducting glaze having the required surface resistivity of about 10 megohms. This would provide a leakage path parallel to the pollution layer and thus prevent the build up of large voltage drops across dry bands. The small leakage current would also have the effect of heating up the surface of the insulator and thus keeping the pollution layer dry and non-conducting.

#### 1.2.1 Iron oxide based glazes

The earliest coatings were based on  $Fe_2O_3$  with added

oxides which formed glazes containing a continuous network of crystals of complex spinel structure, the simplest being  $\text{Fe}_3\text{O}_4$ .

Bradburn and Rigby<sup>2</sup> had measured the conductivity of spinels such as ferrites, aluminates and chromites, and concluded that the ferrites had the highest electrical properties. They noticed a marked increase in conductivity for  $\text{Fe}_3\text{O}_4$  which contained an equal number of  $\text{Fe}^{2+}$  and  $\text{Fe}^{3+}$  ions in octahedral sites. However, the resistance increased when the Fe in  $\text{Fe}_3\text{O}_4$  was replaced by other metal ions as in the complex spinels. When ions of similar valency are present in equivalent lattice sites then the introduction or removal of an electron is required before conduction can take place ie a defect must be introduced.

Glazes containing spinel crystals performed well under polluted conditions but long term trials showed that they deteriorated within a year. A further suggestion at the time was to coat the glaze layer with grease to prevent adsorption of moisture; this proved futile. Lucas (1952)<sup>3</sup> suggested that the deterioration of the spinels was due to the poor electrical contact between the semiconducting glaze and the Portland cement which led to sparking. However, as deterioration occurred remote from the junction this led Lucas to believe that electrolytic corrosion of the glaze might be occurring. With the aid of an electrolytic cell, Lucas showed that resultant attack occurred with both d.c. and a.c. and he went on to propose that electrolytic



corrosion occurred at the edge of dry bands. This was where the current transferred from the glaze to the more conducting wet pollution film (electrolyte) and vice-versa.

Smith (1959)<sup>4</sup> passed a known amount of current through a corrosion cell, similar to that used by Lucas, and determined the quantity and type of elements in the electrolyte. His work showed that the more complex the spinel then the lower its corrosion resistance. Even the simple spinels such as barium ferrite and zinc ferrite and  $\text{Fe}_3\text{O}_4$  were prone to electrolytic corrosion. The single phase oxide used for Smith's corrosion experiments was a barium ferrite ( $\text{BaO} \cdot 6\text{Fe}_2\text{O}_3$ ) with a minimum of 4% ZnO added. The barium ferrite decomposed to give haematite and a spinel, which Smith reported to be magnetite. He noticed that if ZnO was not added then  $\text{Fe}_2\text{O}_3$  was produced and the glaze did not have the required conductivity. There was no investigation of the phases present in the complex spinels and so one must assume that there was a spread in composition in any one glaze.

Binns<sup>5</sup> investigated the glazes based on  $\text{BaO} \cdot 6\text{Fe}_2\text{O}_3$  with the additions of ZnO and successfully identified the spinel formed after firing as zinc ferrite. He pointed out that the replacement of Ba by Zn occurred at around  $1000^\circ\text{C}$  by solid state diffusion.

Binns also looked at the  $\text{Fe}_2\text{O}_3$  - ZnO glazes and noted that the conductivity increased with increasing zinc ferrite content.

Binns believed that a continuous network of conducting crystals was required for conduction. Using iron powder in a glass, at 11-14% by volume of iron there was a marked increase in conductivity corresponding to point-to-point contact of iron particles. However, for the iron oxide glaze this sharp increase in conductivity was noticed for only 8-11% by volume of the conducting phase. Observations under the microscope revealed the glazes to have a very uneven distribution of needle shaped crystals. He proposed less than 11-14% by volume was possible for a continuous network in the iron powder/glass system if the iron particles were distributed less evenly.

The iron oxide glazes were unsuitable because of their high temperature coefficients of resistance [ie a large increase in conductivity with increasing temperature], so while keeping the surface of the insulator dry, this could lead to failure of the glaze due to overheating. Another contributing factor was the rather high coefficient of thermal expansion of the spinels which would lead to the glaze being under tension rather than compression which would in turn increase the chance of crazing. With all these problems the production of spinel glazes was stopped in the mid-sixties.

#### 1.2.2 Reduced-titania glazes

Parallel with the development of the spinel based glazes the Steatite and Porcelain Company developed a semiconducting glaze based on reduced  $TiO_2$ . Clark, Turner

and Powell (1961)<sup>6</sup> prepared reduced TiO<sub>2</sub> glazes; the glazes were comprised of an engobe which had a base composition similar to porcelain but with added TiO<sub>2</sub>, and a cover glaze. Firstly, the engobe was applied to the insulator followed by the cover glaze and the whole system was then fired. The cover glaze was specially formulated to allow the reducing gases access to the engobe at high temperature but to protect the engobe from oxidising conditions during the cooling cycle. The partially reduced titania contained Ti<sup>3+</sup> ions which are associated with oxygen vacancies and conduction arises by electron transfer from Ti<sup>3+</sup> to Ti<sup>4+</sup>. These glazes had characteristic blue colours due to Ti<sup>3+</sup> ions as opposed to the white colour of the stoichiometric TiO<sub>2</sub>. The conductivities of the glaze depend upon the amount of TiO<sub>2</sub>, peak firing temperature and the oxygen partial pressure in the kiln. The increase in conductivity with increase in peak firing temperature surprised the authors at first but microscopic analysis showed this seemed to be associated with the growth of TiO<sub>2</sub> needles from the glaze, joining together isolated areas.

Another reason for the increase in conductivity would be the greater rate of oxygen diffusion through the cover glaze at higher temperatures, giving rise to a greater concentration of oxygen vacancies. The authors reported non-linear V-I characteristics of the form  $I = kE^n$ , where  $n$  is approximately 1.6, and suggested this non-linearity was a property of the engobe. The conductivity was permanently

altered by applying voltage stresses of about 3kV/cm or more. However, a voltage gradient high enough to produce surface flashover in air ( $\approx 10\text{kV/cm}$ ) caused about a 40% permanent increase in conductivity. Small holes were visible on the surface of the cover glaze and thought to be due to electrical discharges between the surface and engobe when sufficiently high voltages developed. The formation of these holes would imply that the engobe was open to the atmosphere for re-oxidation and thus rendered it non-conducting. However, the increase in conductivity remains unexplained.

The reduced titania glazes had very good corrosion resistant properties as reported by Smith ( $0.2\text{--}2\ \mu\text{g/C}$  as opposed to about  $4\ \mu\text{g/C}$  for the simple spinel glazes). The values reported arise from the concentration of ions in the electrolyte per coulomb of charge passed. The glazes also had low thermal expansion coefficients in accordance with the requirements for the porcelain. The temperature coefficient of resistance was about half that for the spinel based glazes and so the likelihood of thermal damage was reduced. Smith quoted  $T_{\frac{1}{2}}$  values, ie the temperature rise needed to double the conductivity, as about  $60^\circ\text{C}$  for the titania-conducting glaze as opposed to about  $30^\circ\text{C}$  for iron oxide based glaze.

Clark (1964)<sup>7</sup> quoted  $T_{\frac{1}{2}}$  values of between  $50$  and  $75^\circ\text{C}$  while Powell (1973)<sup>8</sup> gave  $50^\circ\text{C}$ . Powell reported that the glazes operated successfully for about 2 years after which

time the blue non-stoichiometric oxide was oxidised to the white stoichiometric form by spark discharges thus rendering them non-conducting.

### 1.2.3 Tin oxide based glazes

Verwey et al (1950)<sup>9</sup> looked at valency controlled semiconductors and suggested that the material to be incorporated in the glaze must have a resistivity of about  $10^2 \text{ohm.cm}$ . During the early sixties the British Ceramic Research Association (B.C.R.A.) did much experimental work and of the compounds investigated only the following had the right values:  $\text{Sb}_2\text{O}_3/\text{Sb}_2\text{O}_5\text{-SnO}_2$ ,  $\text{TiO}_2\text{-ZnO}$ ,  $\text{NiO-Li}_2\text{O}$ ,  $\text{CuO-Li}_2\text{O}$ .

However, the latter three pairs reacted with the glaze to produce non-conducting systems. This investigation heralded the beginning of the tin oxide semiconducting glazes, although Smith (1959) had previously shown their resilience to electrolytic corrosion [ $0.5 \mu\text{g/C}$ ]. Binns<sup>10</sup> (1973) gave details of the glazes and showed that the conductivity depended on such factors as:

- a) the calcination temperature of the  $\text{SnO}_2/\text{Sb}_2\text{O}_5$  mixture;
- b) the firing temperature of the glaze;
- c) the proportion of Sb in Sb-doped  $\text{SnO}_2$ ;
- d) the proportion of semiconducting oxide added to the glaze;
- e) the glaze composition.

The Royal Doulton Company began experimenting with the  $\text{SnO}_2$  semiconducting glazes in 1964 with results which were

similar to those reported by Binns. However they went on further to suggest that the resistance was dependent on glaze thickness and the method of preparation (eg ball milling or stirrer mixing of the glaze formulation).

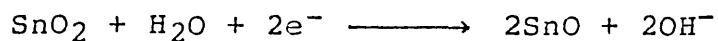
Taylor & Tunnicliff (1965) showed that additions such as ZnO or B<sub>2</sub>O<sub>3</sub> which lowered the viscosity of the melt, also lowered the resistivity. This meant that less SnO<sub>2</sub>/Sb<sub>2</sub>O<sub>5</sub> was required in the glaze body to achieve the same conductivity and showed the significance of base glaze composition on glaze resistance. At about the same time Doulton ran into problems regarding the Sb<sub>2</sub>O<sub>5</sub> purity and switched to using Sb<sub>2</sub>O<sub>3</sub> instead. The Steatite and Porcelain Company, after the failure of the reduced titania glazes, changed over to the SnO<sub>2</sub> semiconducting glazes and confirmed the possibility of using Sb<sub>2</sub>O<sub>3</sub>. Furthermore, their work indicated that the kiln atmosphere also played a significant role.

Nigol et al (1973)<sup>11</sup> covered almost all of the earlier ground confirming all of the factors affecting resistance, and also showed that glazes containing about 1% ZnO had much improved T<sub>1/2</sub> values (120-160°C).

The semiconducting glazes based on doped SnO<sub>2</sub> had surface resistivities of about 10<sup>7</sup> Ohm cm.cm<sup>-1</sup> (at room temperature) and so had good electrical properties for application on high voltage insulators; unfortunately as with previous coatings, these too deteriorated after a period of about 2½-3 years in service [Bourgsdorf<sup>12</sup>]

depending upon the severity of the atmospheric pollution.

The Electrical Research Association suggested a primary cause of deterioration was electrolytic in nature and involved the reduction of tin (IV):



thus rendering the glaze non-conducting.

The British Ceramic Research Association showed that a secondary cause of deterioration was spark erosion which led to electrical puncturing. They showed that the semiconducting crystals were the targets of sparks and the surrounding areas frequently showed signs of thermal shock. The tin oxide volatilised leaving holes in the glassy matrix and an uneven deposit of tin oxide on the surrounding surface.

Using S.E.M. and E.P.M.A. techniques Taylor<sup>13</sup> showed the existence of relatively conducting and relatively insulating areas in the glaze. The conducting areas contained clusters of rounded crystallites of doped SnO<sub>2</sub> [about 0.3 μm diameter] but point-to-point contact was not apparent.

Taylor suggested that electrical conductivity occurred through the overlapping of solubility rims around the doped SnO<sub>2</sub> crystals. As the Sn and Sb solubilities in the glaze are low, he argued that the conduction in these rims was akin to activated conduction brought about by non-stoichiometry in pure SnO<sub>2</sub> as it was difficult to

envisage a close association of Sn and Sb atoms in the rims. Taylor also reported the diffusion of Ca from the glaze to porcelain and a slight amount of diffusion of Na, K and Al from porcelain to glaze. The solubility rims were shown by Taylor, Allinson and Barry<sup>14</sup> to be only a few tenths of a micron thick. The uniformity in size and shape of the SnO<sub>2</sub> crystallites indicated that the small SnO<sub>2</sub> particles in the original powder went into solution on firing and recrystallised on cooling on surviving crystals.

Morgan et al<sup>15</sup> studied the electrical properties of alumino-silicate glasses containing SnO<sub>2</sub>/Sb<sub>2</sub>O<sub>5</sub>. They observed that at high temperatures the samples displayed ionic conduction, with loss in conductivity with time from polarisation of the glass, presumably due to migration of Na<sup>+</sup> ions. A band model was introduced for the electronic conduction in SnO<sub>2</sub> and this will be discussed later<sup>(16)</sup>.

#### 1.2.4 Criteria for selection of a semiconducting crystalline phase for a semiconducting glaze.

##### A. Compatibility with the glaze

- (i) The semiconducting crystalline phase must be stable in the glaze throughout the firing schedule and should not react chemically with the glaze to impair its appearance. For example, the addition of SiC produces blisters. TiO<sub>2</sub>-ZnO is a semiconducting compound but reacts with the glaze to make it effectively non-conducting. Special firing atmospheres are required for reduced titania glazes and the presence of



oxidising gases renders these glazes non-conducting.

(ii) The coefficient of thermal expansion of the conducting phase should produce a glaze with an overall thermal expansion which is compatible with the ceramic substrate. Ideally, it should have a lower value as this puts the glaze under compressive stress which minimises the possibility of crack formation and enhances mechanical properties. This is probably one of the most serious restrictions to influence the choice of a semiconducting phase; though if it is present in low proportions the thermal expansion is relatively less important.

- B. The conducting phase should have a resistivity below 100 Ohm cm to obtain surface resistivities of about  $10^6$  Ohms/cm<sup>2</sup> at reasonable concentrations of the conducting phase.
- C. The conducting phase should have good corrosion resistance.
- D. The conducting phase should have a small negative or even positive temperature coefficient of resistivity.
- E. The conducting phase should be a valence-controlled-semiconductor since non-stoichiometric semiconductors can be rendered non-conducting by electrolysis and minor electrical discharges.

The composition of the glaze is important in determining its final properties and the requirements for glass formation and crystal growth in oxide systems should

be clearly understood.

### 1.3 Glass Formation And Crystallisation

#### 1.3.1 Glass formation

Most inorganic elements and compounds (eg Na, LiCl) melt to form liquids with similar viscosities ( $10^{-2}$  poise). On cooling these liquids, rapid crystallisation takes place at, or just below, the melting point.

However, certain materials melt to give very viscous liquids (eg  $\text{SiO}_2$ - $10^6$  poise) and on cooling these below their melting points the viscosity increases without crystallisation, as the temperature is reduced until the viscosity is so high that the material is effectively a solid. This material is called a glass. The American Society for Testing Materials proposed the following definition of glass: "Glass is an inorganic product of fusion which has cooled to a rigid condition without crystallisation". In addition certain organic compounds, such as glycerol form glasses, and the use of novel techniques such as vapour phase deposition can be used to prepare glasses from materials which cannot be made as glasses using traditional methods [Table 1.1].

The two principle characteristics of the amorphous state are:

- a) the absence of long range order, although a high degree of short range order may be preserved;
- b) an excess of free energy, frozen into the system, compared to the thermodynamically stable phase(s) of

TABLE 1.1

Preparation of non-crystalline materials from solid, liquid and gaseous phases

Starting phase	Technique	Examples of materials prepared by the technique
Gas	Vapour phase hydrolysis	Synthetic high purity fused silica.  Also used to control the refractive index gradient of optical fibres by ion doping.
	Glow discharge decomposition	Amorphous films of Si and Ge from their respective hydrides. Can also be used to dope amorphous semiconductors.
	Thermal evaporation	Most classes of amorphous semiconductors, Si, Ge and chalcogenide glasses.
	Sputtering	Some chalcogenides, amorphous V <sub>2</sub> O <sub>5</sub> .
Liquid	Splat cooling	Glassy metals
	Chemical reaction and precipitation	Amorphous As <sub>2</sub> S <sub>3</sub> by passing H <sub>2</sub> S gas through a solution of As <sub>2</sub> O <sub>3</sub> in HCl.
	Electrolytic Deposition	Ge from electrolysis of GeCl <sub>4</sub> in glycol.
Solid	Neutron or ion bombardment	Silica
	Shock wave bombardment	Silica

the same composition.

Amorphous materials are therefore in a state of metastable equilibrium and will tend to transform to a form of stable state given a sufficient period of time. The transformation is, for many silicate glasses, maybe a few minutes or many hundreds of years.

### 1.3.2 Theories of glass formation

The theories of glass formation fall into three main groups: structural, thermodynamic and kinetic.

#### 1.3.2.1 Structural theories

Structural theories emphasise some feature of the structure of the glass-forming material, eg the geometrical arrangement of the constituent atoms. Structural theories will be mentioned first since they were the first ideas to be developed. Historically, the greatest debate about the structure of glass has been between supporters of the rival "crystallite" and "random network" theories. The crystallite hypothesis originated by Lebedoff<sup>17</sup> and propagated through the Russian school, held that glass consisted of very small, randomly arranged, crystallites which probably contained other substances in solid solution and that the function of annealing was merely to attain complete polymorphic equilibrium. Multicomponent glasses such as those in the present study would have different kinds of crystallites corresponding to different compounds in the phase diagram and would thus be a heterogeneous material. The opposite view, proposed by

Zachariasen<sup>18</sup>(1932), came about primarily as the result of some work done by V M Goldschmidt<sup>19</sup>(1926). Goldschmidt looked at some simple oxides of the general formula  $A_mO_n$  and concluded that, for the system to be glass-forming, the ionic radius ratio  $R_a/R_o$  must be between 0.2-0.4. At that time it was known that the ionic radius ratio of cation to anion in ionic crystals determines the number of anions around each cation, and that a value of 0.2-0.4 indicates four anions tetrahedrally arranged around a cation. This therefore prompted Goldschmidt to state that, for glass formation to occur, it is necessary to have a tetrahedral arrangement of oxygen ions around the cation A.

Zachariasen was not completely happy with Goldschmidt's work as certain oxides such as  $BeO$ , which were in the range 0.2-0.4, did not form glasses. He approached the problem by assuming that the inter-atomic forces in oxide glasses must be similar to those in the corresponding crystals, on the grounds that their mechanical properties were similar. Glass has a 3-D network but, allowing for the diffuseness of the x-ray diffraction pattern, the network is not symmetrical or periodic as is a crystalline lattice. This led to the statement that "the glass network is an infinitely large unit cell with an infinite number of atoms, no two of which are structurally equivalent." Thus it was now possible to explain why glasses do not have a sharp melting point as do ionic crystals, but instead gradually decrease in viscosity over a wide temperature by assuming

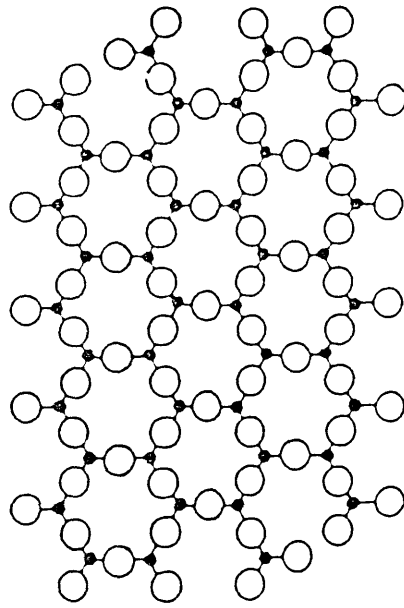
that there is a range of A-O bond strengths and, on heating, an increasing proportion of these bonds are broken.

As glass is a thermodynamically metastable substance, Zachariasen concluded that glass has a higher internal energy than the crystalline state, but not so large that devitrification occurs. Morey<sup>20</sup>(1934) was not convinced that the stability of glasses could be assessed by how much the internal energy of the glass exceeded that of the corresponding crystal and suggested heats of fusion as being more indicative of stability.

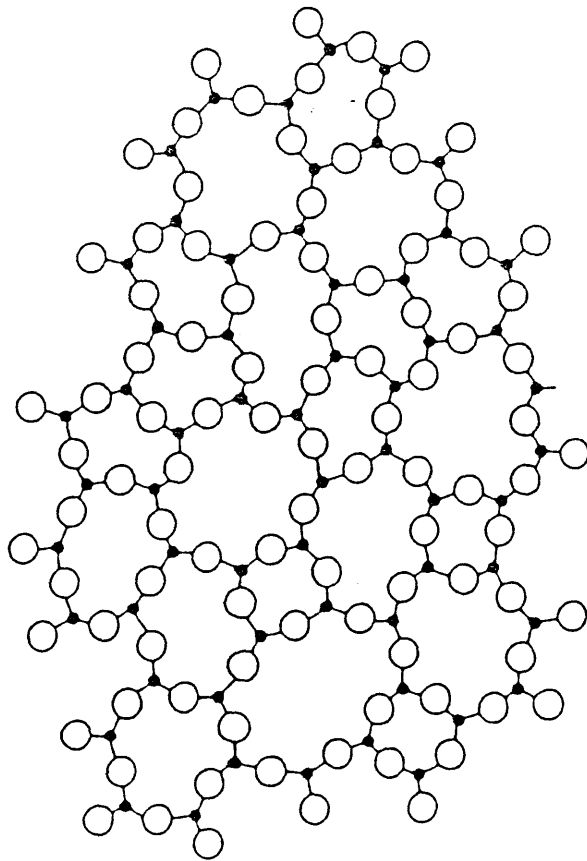
As crystalline oxides are discussed in terms of oxygen polyhedra and the way they are joined together, where the nature of the polyhedra depends on the number of oxygen atoms around the cation, there is no reason why glasses could not be described in a similar way; eg crystalline silica consists of  $\text{SiO}_4$  tetrahedra joined at the corners, whereas vitreous silica also consists of  $\text{SiO}_4$  tetrahedra joined at the corners but the relative orientation of the adjacent tetrahedra is variable. This is demonstrated by the structure of the hypothetical two dimensional compound  $\text{X}_2\text{O}_3$  as shown in figure 1.1.

Using structural considerations, Zachariasen formulated a number of rules which an oxide must obey to be a glass-former:

1. No oxygen atom may be linked to more than two atoms A.
2. The number of oxygen atoms surrounding atoms A must be small.



(a)



(b)

Fig 1.1 Structure of the compound  $X_2O$ , in (a) the crystalline and (b) the glassy form.

3. The oxygen polyhedra share corners with each other, not edges or faces.
4. At least three corners in each polyhedron must be shared.

Thus  $A_2O$  and  $AO$  should not form glasses as they do not satisfy these rules. Oxides which satisfy the rules 1, 2 and 3 are:

- a)  $A_2O_3$ , only if there exists a triangular arrangement of oxygen around A;
- b)  $AO_2$ ,  $A_2O_5$ , only if there exists a tetrahedral arrangement of oxygen around A;
- c)  $AO_3$ ,  $A_2O_7$ ,  $AO_4$ , only if there exists an octahedral arrangement of oxygen around A.

Zachariasen did not know of any glass-forming oxides in c) at the time and so modified rule 2 as follows, "the number of oxygens surrounding A must be 3 or 4."

The simple glass-forming oxides known at the time fitted in nicely with the Zachariasen rules, eg  $SiO_2$ ,  $GeO_2$ ,  $P_2O_5$  which consist of  $AO_4$  tetrahedra while  $B_2O_3$  and  $As_2O_3$  consist of  $AO_3$  triangles. The glass-forming  $BeF_2$  could also be explained on the grounds that it consisted of  $BeF_4$  tetrahedra and so here the word oxygen is replaced by fluorine in Zachariasen's rules.

For complex glasses containing more than one oxide, Zachariasen added another rule which stated that for a glass to be formed, the sample must contain a high percentage of oxygen triangles or tetrahedra around the cations.



Appreciable amounts of glass-forming cations must be present, eg  $\text{Si}^{4+}$ , but other cations which can isomorphically replace these are also possible, eg  $\text{Al}^{3+}$  for  $\text{Si}^{4+}$ . However, an  $\text{Na}^+$  ion must be introduced to maintain the total positive charge.

Thus we now have a distinction between "network-formers" such as  $\text{Si}^{4+}$  which provide the vitreous framework, and "network-modifiers" such as  $\text{Na}^+$  which disrupt the framework. Zachariasen suggested that the network modifiers were large ions with low charge, eg  $\text{Na}^+$ ,  $\text{K}^+$ ,  $\text{Ca}^{2+}$ ,  $\text{Ba}^{2+}$  and  $\text{Zn}^{2+}$  and that these fitted into relatively large holes in the network. This requires that at least three corners of a tetrahedron are shared with other tetrahedra for the network to be 3-dimensional. From x-ray diffraction data, Warren et al<sup>21</sup> agreed with the structure of silica proposed by Zachariasen.

They looked at sodium silicate glasses and noted the presence of non-bridging oxygens due to the addition of  $\text{Na}_2\text{O}$  to the silica network (figure 1.2). Also apparent was that the modifying cation  $\text{Na}^+$  fitted randomly into large holes in the framework and thus the O/Si ratio becomes greater than 2.

Structural theories do not give any insight into the relative ease of glass formation. For estimates of this it is necessary to consider the nature of the bonds between the constituent atoms, energy and entropy. These come under the main heading of thermodynamic theories.

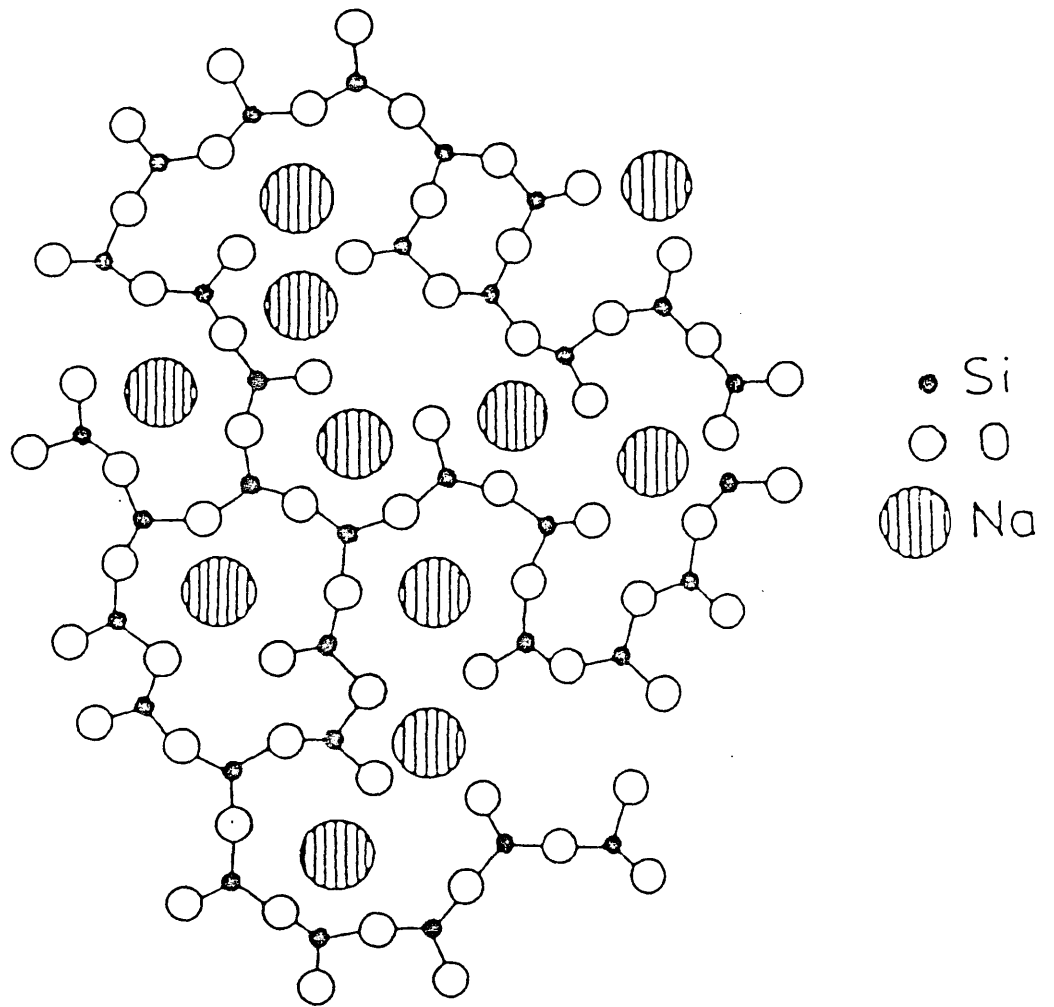


Fig 1.2 Structure of a  $\text{Na}_2\text{O-SiO}_2$  glass.

### 1.3.2.2 Thermodynamic Theories

Many theories have attempted to relate bond strength to the ease of glass formation. Smekal<sup>22</sup>(1951) proposed that "mixed chemical bonds" and not purely ionic, covalent or metallic bonds were a necessity for glass formation. He went on further to suggest three classes of glass-formers with mixed bonding.

- i) Inorganic compounds, eg  $\text{SiO}_2$ ,  $\text{B}_2\text{O}_3$ , where the A-O bonds are partly ionic and partly covalent.
- ii) Elements, eg S, Se, which have chain structures with covalent bonding within the chains and Van der Waals interactions between the chains.
- iii) Organic compounds containing large molecules with covalent bonds within the molecules and Van der Waals forces between them.

Stanworth<sup>23</sup>(1946, 48,52) pointed out that there is a correlation between the Pauling (1945) electronegativity value of an element and its glass-forming capability. He predicted that as Te and P have similar electronegativity values then one would expect  $\text{TeO}_2$  to be as good a glass-former as  $\text{P}_2\text{O}_5$ .  $\text{TeO}_2$  alone is not a glass-former but it is commonly found as a component in binary systems, eg the  $\text{Al}_2\text{O}_3$ - $\text{TeO}_2$  and  $\text{BaO}$ - $\text{TeO}_2$  systems. The correlation is not very reliable when considering the whole range of inorganic substances, let alone the field of oxide glasses. For example, Sb has the same electronegativity value as Si and so one would expect  $\text{Sb}_2\text{O}_3$  to be as good a glass-former as

silica but this is not the case.

Winter<sup>24</sup>(1955) suggested that glass-forming capability was related to the number of outer shell "p" electrons per atom, the favourable number being four, but 2-4 being possible. Clearly, this was wrong as O, S, Se and Te all have four outer shell "p" electrons but do not have the same glass-forming capability.

Sun<sup>25</sup>(1947) proposed that glass-forming potential went hand in hand with high single bond strength values. He noticed that three groups emerged from a study of single bond strengths of various inorganic oxides: these were glass-formers, intermediates and modifiers. However, the theory failed when it was applied to materials containing more than one type of bonding, eg CO<sub>2</sub> which has strong covalent bonding within molecules but weak Van der Waals interactions between molecules and so does not form a glass. Another exception was V<sub>2</sub>O<sub>5</sub> which would be expected to form a glass because of its high single bond strength but does not, possibly as Sun suggested, because of "small ring formation" in the melt leading to ease of crystallisation.

Rawson<sup>26</sup>(1956) agreed with Sun but suggested that it was also necessary to consider the thermal energy available at the melting point or liquidus temperature to break the bonds. He proposed the ratio (single bond strengths):(mpt in °K) as indicative of glass-forming potential but this too fails when applied to examples such as CO<sub>2</sub> and V<sub>2</sub>O<sub>5</sub>. Rawson also pointed out the existence of binary systems

which formed glasses but where the individual oxides did not, for instance  $V_2O_5$ - $PbO$ . He suggested that this occurred at a special composition where the liquidus temperature was low and he called this the "liquidus temperature effect". Rawson thought that the role of the second oxide was to lower the liquidus temperature and so the thermal energy available to break bonds and, as a result, increase the glass-forming tendency. Thus one would expect the  $SiO_2$  rich eutectic compositions to be likely to form glasses.

Gibbs<sup>27</sup> had a novel approach and proposed that the configurational entropy in a liquid decreases with temperature which leads to a decrease in mobility. At the freezing point, crystallisation would lead to zero configurational entropy but a supercooled liquid, however, at the glass transition temperature,  $T_g$ , would have a small excess entropy. This approach can be criticised in that it does not predict the relative glass-forming tendency.

#### 1.3.2.3 Kinetic Theories

It has long been known that it is possible to produce a glass by cooling a melt below the glass transformation temperature. Another consequence of cooling a melt is crystallisation. Thus, for glass formation, it is necessary to prevent crystallisation by suppressing both nucleation and crystal growth rates (these will be discussed later). Both these rates go through maxima at temperatures below the liquidus temperature. If the melt is cooled quickly it is possible to by-pass these maxima and obtain a glass at a low

enough temperature to render atomic rearrangements unlikely. Kinetic theories therefore attempt to calculate the minimum cooling rates which are necessary for glass formation.

Dietzel and Wickert<sup>28</sup> proposed that "glassiness" was the reciprocal of crystal growth rate and then went on to relate this to melt properties such as high viscosity, low liquidus temperature and a large change in composition on crystallisation. A direct relationship was postulated between critical cooling rate and composition for alkali-silicate glasses.

Havermans, Stevels and Stein<sup>29</sup> used critical cooling rate (CCR), ie minimum cooling rate required to form a glass, and its variation as a function of composition in alkali-silicate systems. They noticed an increased glass formation tendency on going from the lithium to sodium to potassium-silicate system possibly in line with Rawson's idea of an increased glass formation tendency with a lowering of the eutectic temperature. However, minima in critical cooling rates were obtained for the lithium and sodium systems close to the compositions  $\text{Li}_2\text{O} \cdot 2\text{SiO}_2$  and  $\text{Na}_2\text{O} \cdot 2\text{SiO}_2$ . This was not the case for potassium which revealed a small maximum near the composition  $\text{K}_2\text{O} \cdot 2\text{SiO}_2$ . This tends to suggest that the phenomenon is rather more complicated than Dietzel and Wickert suggested.

Turnbull<sup>30</sup> thought that nucleation rates were important and argued that a single nucleation event in a low-viscosity liquid would lead to crystallisation. This approach was

adequate to explain the easy crystallisation of metallic melts because of their low viscosities ( $10^{-2}$  poise) but oxide melts, which had higher viscosities, could tolerate more than one nucleation event without crystallisation taking place.

Sarjeant and Roy<sup>31</sup> assumed that the critical cooling rate (CCR) for glass formation depends directly on the melting point and molecular mobility at the melting point. Their estimated value of CCR for  $\text{SiO}_2$  was several orders of magnitude out from the rate at which glassy  $\text{SiO}_2$  can be obtained experimentally. Thus they came to the conclusion that the two factors already mentioned were important qualities but insufficient for specifying the CCR. Uhlmann<sup>32</sup> proposed a minimum volume fraction ( $V_c/V$ ) of crystals equivalent to  $10^{-6}$  as being just discernable. Therefore, a criterion for the vitreous state would be  $V_c/V < 10^{-6}$ . The cooling rate required to avoid this minimum volume fraction can be estimated by constructing time-temperature-transformation (T-T-T) curves. These curves are constructed by calculating the time required for a given  $V_c/V$  to form at a particular temperature and repeating at different temperatures. The critical cooling rate is given by the cooling rate which just by-passes the nose of the curve. The CCR do not depend significantly on the value assumed for the barely detectable degree of crystallinity. The treatment assumes uniform homogeneous nucleation. Some factors affecting glass formation were

determined using this model:

- i) a high viscosity at the liquidus temperature;
- ii) a viscosity which increases strongly with falling temperature below the liquidus temperature.

For materials with similar viscosity-temperature relationships glass formation is favoured by:

- iii) a low liquidus temperature,

and in complex systems by:

- iv) a large redistribution of material being required for crystallisation.

Hruby<sup>33</sup> studied glass-forming potentials of materials by quenching well below the glass transition temperature ( $T_g$ ) and then reheating at a slower rate to obtain the temperature ( $T_{cr}$ ) of the crystallisation exotherm using differential thermal analysis. He suggested a parameter  $K_{gl}$  as a measure of glass-forming potential:

$$K_{gl} = \frac{T_{cr} - T_g}{T_m - T_{cr}} \quad (1.1)$$

Hruby assumed that the stability of glass is in direct proportion to the ease with which it forms and that all glasses at  $T_g$  are in a comparable state. Thornburg<sup>34</sup> pointed out that  $K_{gl}$  depends strongly on the heating rate.

Davies et al<sup>35</sup> predicted that systems with high  $T_g/T_m$  ratios, eg metallic systems where  $T_g/T_m > 0.7$ , required cooling rates of the order of  $10^6$  degrees per second for forming glasses. Table 1.1 shows various methods available for the formation of non-crystalline materials.



#### 1.4 Crystallisation of glasses

The cooling of a liquid below its freezing point will tend to produce the crystalline state. This transformation is neither instantaneous nor homogeneous as the crystals grow at a finite rate from a finite number of nuclei. Two mechanisms of nucleation are considered: homogeneous and heterogeneous. In the former, the nuclei are generated within the melt itself and in the latter the nuclei consist of impurity particles, minute fragments of undissolved materials and even the walls of containers may act as possible nucleation sites.

##### 1.4.1 Homogeneous nucleation

There is a decrease in free energy of  $\Delta G$  per mole associated with the crystallisation of a liquid. If we assume a spherical crystalline region of radius  $r$  being formed, then the corresponding decrease in free energy is given by:

$$W = 4\pi r^3 \Delta G/3V_m \quad (1.2)$$

where  $V_m$  is molar volume. However, there is also a contribution of the surface energy of the interface between the crystal and surrounding liquid denoted by  $\sigma$  (per unit area). Thus the overall free energy change is given by:

$$W = 4\pi r^3 \Delta G/3V_m + 4\pi r^2 \sigma \quad (1.3)$$

The variation of  $W$  with  $r$  is shown in figure 1.3. Below  $r^*$ ,  $W$  increases as  $r$  increases; however if the crystal remelts then the free energy of the system decreases. Those particles with  $r$  less than  $r^*$  are called embryos and arise

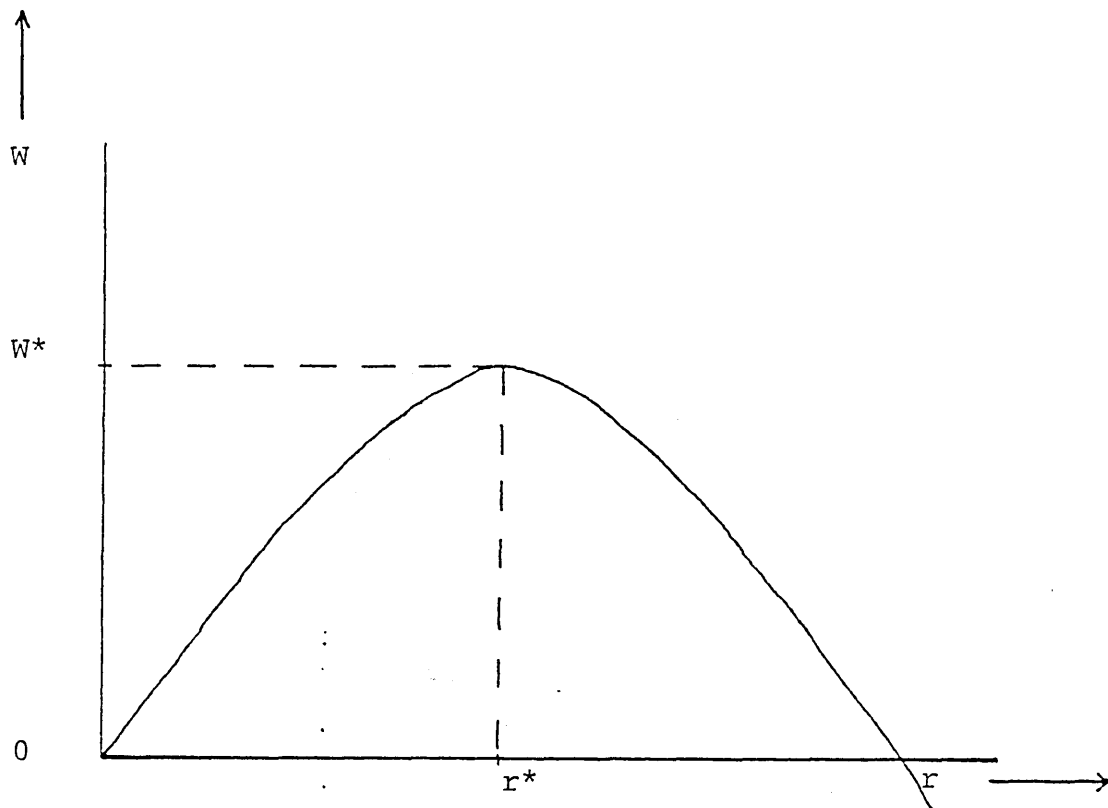


Fig 1.3 The change in energy required to form a nucleus of radius  $r$ .

as a result of random fluctuations in the melt and disappear very quickly. Stable embryos are formed if a fluctuation produces a crystalline region of radius greater than  $r^*$ , and therefore the value of the critical radius  $r^*$  for which the free energy is a maximum (ie  $W^*$ ), occurs at:

$$\frac{\delta W}{\delta r} = 0 \quad (1.4)$$

This leads to:

$$r^* = -2 \sigma V_m / \Delta G \quad (1.5)$$

which in turn gives the maximum free energy change  $W^*$ :

$$W^* = 16 \pi \sigma^3 V_m^2 / 3 \Delta G^2 \quad (1.6)$$

It is quite obvious that the formation of a nucleus of radius  $<r^*$  is not favourable since this transformation leads to an increase in free energy. However, a nucleus  $>r^*$  is a stable entity because on further growth a decrease in free energy of the system occurs.

Statistical thermodynamics can be used to show that the probability of a thermal fluctuation leading to a free energy change equal to or greater than  $W^*$  is given by the Boltzmann equation:

$$p(W^*) = \exp (-W^*/KT) \quad (1.7)$$

The nucleation rate must therefore be proportional to  $p(W^*)$ . Hence,

$$I = A \exp(-W^*/KT) \quad (1.8)$$

where  $I$  is the nucleation rate. At the melting point,  $T_m$ ,  $\Delta G$  is zero and therefore using equation (1.6),  $W^*$  must be infinitely high. This implies that  $p(W^*)$  is zero which

leads one to conclude that the nucleation rate must also be zero at the melting point.

It is evident that enough thermal energy is required for the atoms and molecules to overcome the energy barrier ( $\Delta G_D$ ) for structural rearrangement from the liquid to crystalline state by diffusion across the interface. This creates a kinetic barrier represented by "A" in equation (1.7):

$$A = n \nu \exp(-\Delta G_D/KT) \quad (1.9)$$

and overall, the nucleation rate can be expressed by:

$$I = n \nu \exp(-\Delta G_D/KT) \exp(-W^*/KT) \quad (1.10)$$

where "n" is the number of molecules/cm<sup>3</sup> and  $\nu = KT/h$  and is the molecular jump frequency. The kinetic barrier to nucleation increases with increasing undercooling as the diffusivities of the components decrease, whilst the thermodynamic barrier decreases (Figure 1.4).

For a multicomponent system equation (1.10) must be modified in the following ways:

- (i) The mole fraction of the nucleating component must be included.
- (ii) The free energy change on crystallisation,  $\Delta G$ , will depend on the composition of the nucleating component.
- (iii) The dependence of the interfacial energy on the chemical composition gradient.
- (iv) The kinetic term must take into account the long range diffusion of the nucleating component to replenish the surrounding liquid.

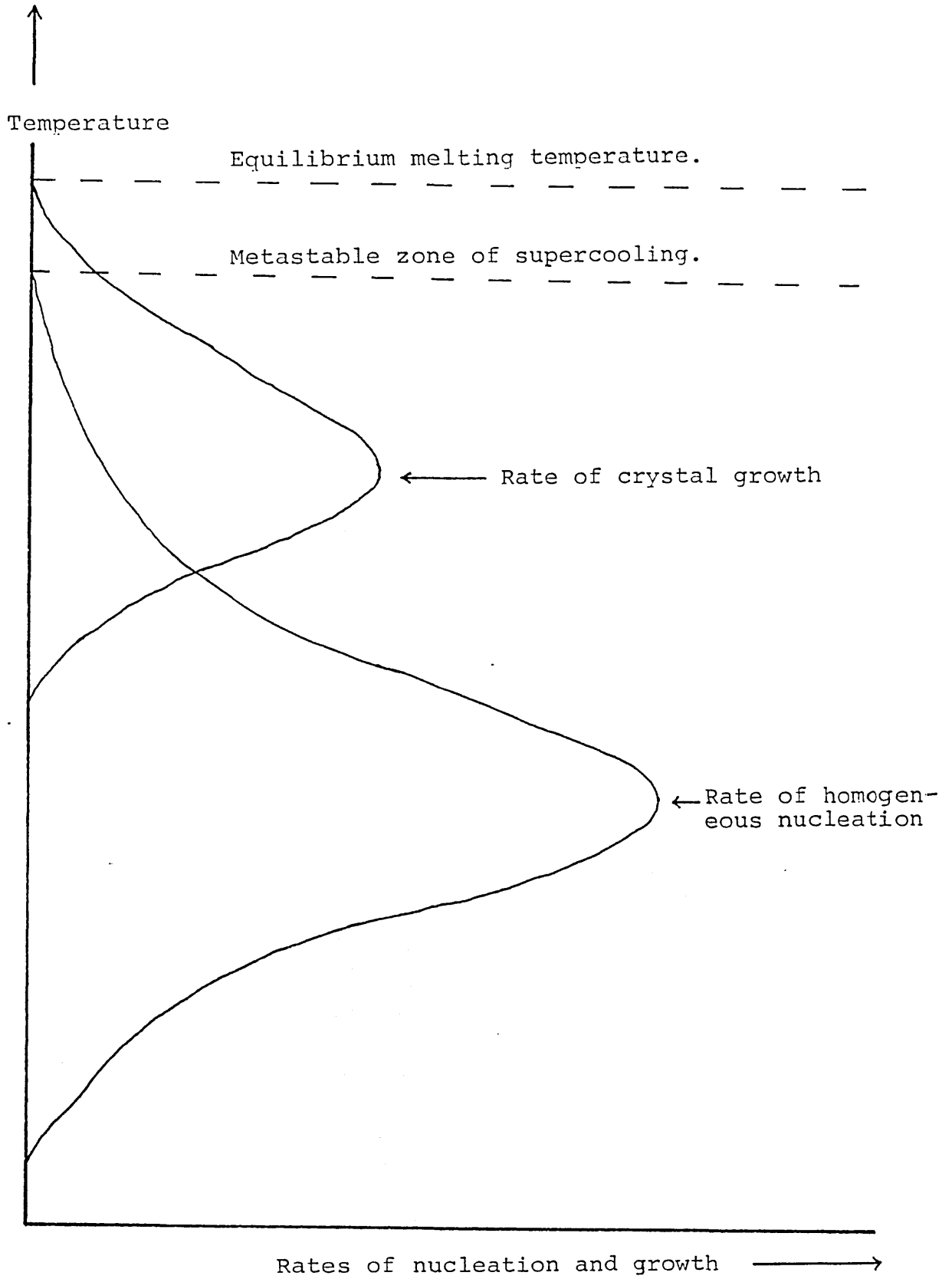


Fig 1.4 Effect of temperature on rates of nucleation and crystal growth.

1.4.2 Heterogeneous Nucleation

In heterogeneous nucleation, the nuclei consist of impurity particles, undissolved crystals and even walls of containers. The thermodynamic barrier to nucleation is lowered in proportion to the degree of wetting of the substrate. Thus the activation energy becomes:

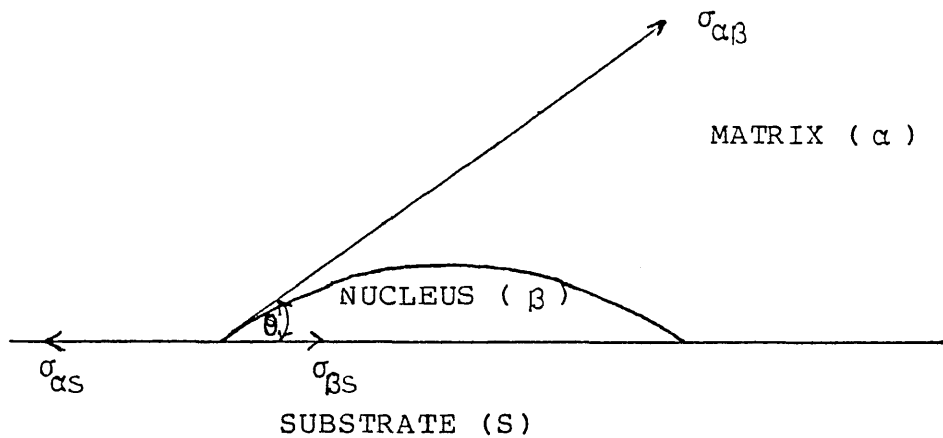
$$\Delta G^*(het) = \Delta G^*(hom) \times f(\theta) \quad (1.11)$$

where  $f(\theta) = (2 + \cos \theta)(1 - \cos \theta)^2/4$  (1.12)

$\theta$  represents the contact angle and

$$\cos \theta = (\sigma_{\alpha s} - \sigma_{\beta s})/\sigma_{\alpha\beta} \quad (1.13)$$

Figure 1.5



It can be seen from the diagram that a low value of  $\theta$  is desirable for good wetting of the substrate. The complete expression for heterogeneous nucleation,  $I_S$ , must take into account the effective area of the substrate with suitable sites for nucleation:

$$I_S = K_S \exp \left\{ -(\Delta G_D + \Delta G^*(het))/KT \right\} \quad (1.14)$$

where  $K_S$  contains parameters such as vibrational frequency and the number of molecules per unit volume and may be

difficult to calculate in practice.

Another approach relates the nucleating potential of a site to the degree of similarity between its crystal structure and that of the phase to be crystallised. This is termed epitaxial growth since the growth of the crystal takes place in a favoured orientation around the nucleus. Generally, the discrepancy of similar low index planes for both nucleus and precipitating crystalline phase should not exceed 20%, though for effective nucleation the value should be under 15%. As mismatch increases, a greater degree of super cooling is required.

A further modification to the nucleation process becomes necessary when liquid/liquid phase separation occurs as below.

#### 1.4.3 Liquid-liquid phase separation

In many silicate and borate melts, two-liquid phase formation is observed. Immiscibility in these systems can occur above or below the liquidus. The latter is called sub-liquidus or metastable immiscibility. Common binary silicate systems which exhibit stable immiscibility above the liquidus usually contain divalent metal oxides such as SrO, CaO, FeO, ZnO or MgO. Sub-liquidus immiscibility is often found in silicate melts containing oxides such as K<sub>2</sub>O, Na<sub>2</sub>O and Li<sub>2</sub>O. The competition for a local environment of oxygen atoms which arises between different cations such as Na<sup>+</sup> and Si<sup>4+</sup> gives rise to phase separation.

The invention of the electron microscope in the early

1950's proved useful in observing glass structures. Replica and transmission electron microscopy (TEM)<sup>36</sup> were used to show segregation in many glass-forming systems which had been previously thought to be homogeneous eg B<sub>2</sub>O<sub>3</sub> - SiO<sub>2</sub> system. Objections were raised by many concerning the authenticity of the detected effects which they believed to be of secondary order.

Two kinds of phase separation are possible,

- a) nucleation and growth,
- b) spinodal decomposition.

The process of nucleation has already been mentioned.

A free energy diagram representing spinodal decomposition with the corresponding miscibility diagram for two components is shown in figure 1.6. Both a maximum and a minimum in the free energy curve exist with respect to variations in composition of the two components. Consider a composition at X where  $\delta^2 G / \delta c^2$  is positive. A small fluctuation in composition will tend to increase the free energy of the system and as this is not favourable, the system returns to its original state. However, it is possible to overcome this thermodynamic barrier by the formation of critical sized nuclei,  $r^*$ , which lower the free energy on subsequent growth (see section under nucleation).

When one looks at position Y, where  $\delta^2 G / \delta c^2$  is negative, small fluctuations in composition will tend to lower the free energy of the system with no thermodynamic barrier. As this is favourable, small fluctuations occur



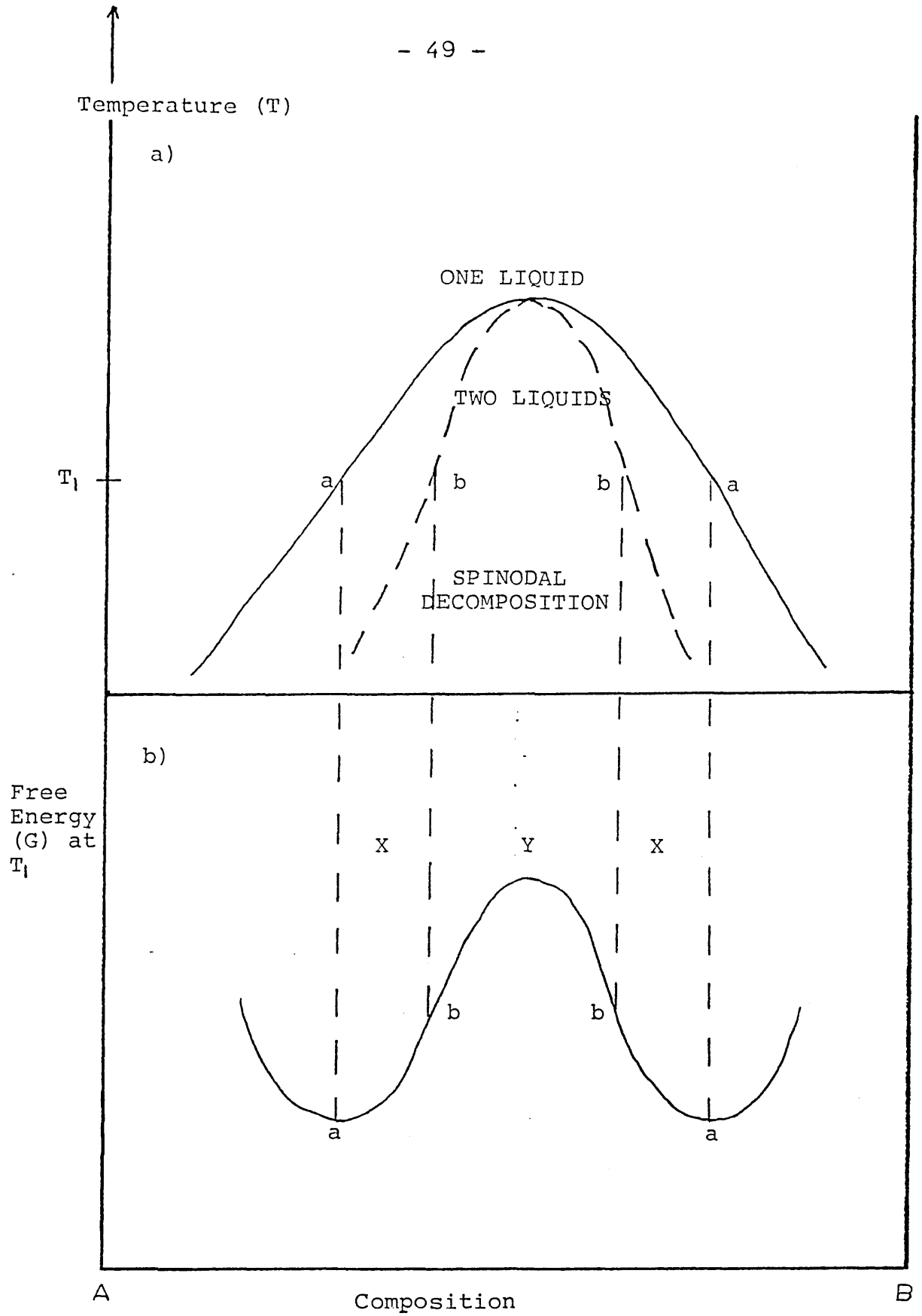


Fig 1.6(a) Hypothetical phase diagram showing immiscible region and spinodal decomposition.

Fig 1.6(b) Free energy of mixing at temperature  $T_1$ .

and subsequently grow. As they grow the distinction between the phases becomes clearer and well defined. Hence there exists in spinodal decomposition an interconnected morphology. However, it is possible to get a lowering of free energy by a coarsening process to leave a system retaining connectivity or one forming spheroids. In the nucleation and growth mechanism, random second-phase particles are formed initially, in which near neighbours may coalesce to form an interconnected morphology resembling that of spinodal decomposition. It would appear that caution should be exercised when interpreting electron micrographs of phase separated systems. In general, the tendency to phase separation in a two component system is dependent upon the difference in the field strength between the cations present, the interfacial energy between developing microzones of different composition and on the volume occupied by the different structural elements.

#### 1.4.4 Crystal growth

The process of crystal growth occurs when suitable nucleation sites are available; the rate of crystal growth being dependent upon three factors:

- i) Long range diffusion.
- ii) Removal of the latent heat of crystallisation.
- iii) Interfacial reaction.

The first factor is only rarely observed as a rate determining step, whereas factor (iii) is quite well known for its time dependency. The second factor is required

because the latent heat of crystallisation sets up a temperature gradient which could lead to a change in morphology. The classic approach to crystal growth assumes three types of mechanism possible for attachment of particles to the surface of nuclei, namely:

- i) Normal or continuous growth model.
- ii) Surface nucleation growth model.
- iii) Screw dislocation growth model.

The first of these is associated with a rough interface in the atomic order of magnitude and it is assumed that there are no large number of centres for accumulation and migration of atoms. The treatment is based on simple activated processes. The second model assumes a smooth surface and that growth is on steps provided by 2-dimensional nuclei at the interface. The third model is based on a smooth surface but one where growth only occurs by the addition of atoms at a screw dislocation at the interface.

Turnbull and Cohen (1958) showed that it is possible, assuming that a normal growth mechanism operates, to represent the number of species transferring from the liquid to the crystal phase per unit time by:

$$X_{1c} = s v_0 \exp (- \Delta G_D' / KT) \quad (1.15)$$

where  $\Delta G_D'$  is the kinetic barrier for an atom, molecule or structural unit to diffuse from the liquid to the growing interface, "s" is the number of molecules in the liquid facing the crystal at the interface and  $v_0$  is the jump

frequency.

However, for the reverse process to occur:

$$X_{c1} = s v_0 \exp \{-(\Delta G'_D + v \Delta G_V)/KT\} \quad (1.16)$$

where  $\Delta G_V$  is the free energy change per unit volume and "v" is the volume of the molecule, see figure 1.7.

This leads to a net transfer of material from liquid to crystal, given by:

$$X_{lc} - X_{c1} = s v_0 \exp(-\Delta G'_D/KT) \{1 - \exp(-v \Delta G_V/KT)\} \quad (1.18)$$

and a growth rate (U) where:

$$U = \lambda v_0 \exp(-\Delta G'_D/KT) \{1 - \exp(-v \Delta G_V/KT)\} \quad (1.18)$$

where  $\lambda$  is the jump distance.

The variation of crystal growth rate is shown alongside that for nucleation in figure 1.4. Experimental and theoretical values of growth rates will tend to vary, especially in multicomponent systems.

Turnbull and Hillig<sup>37</sup> defined a diffusion coefficient (D) for transport across the interface:

$$D = D_0 \exp(-\Delta G'_D/KT) = v_0 \lambda^2 \exp(-\Delta G'_D/KT) \quad (1.19)$$

and obtained an expression for the growth rate (U):

$$U = (D/\lambda) \{1 - \exp(-v \Delta G_V/KT)\} \cdot f \quad (1.20)$$

where f is the fraction of active sites. Hence, this approach assumes that the normal growth model is not applicable.

A value for D can be derived using the Stokes-Einstein equation if one assumes that the activation process for diffusion across the interface is similar to that for viscous flow:

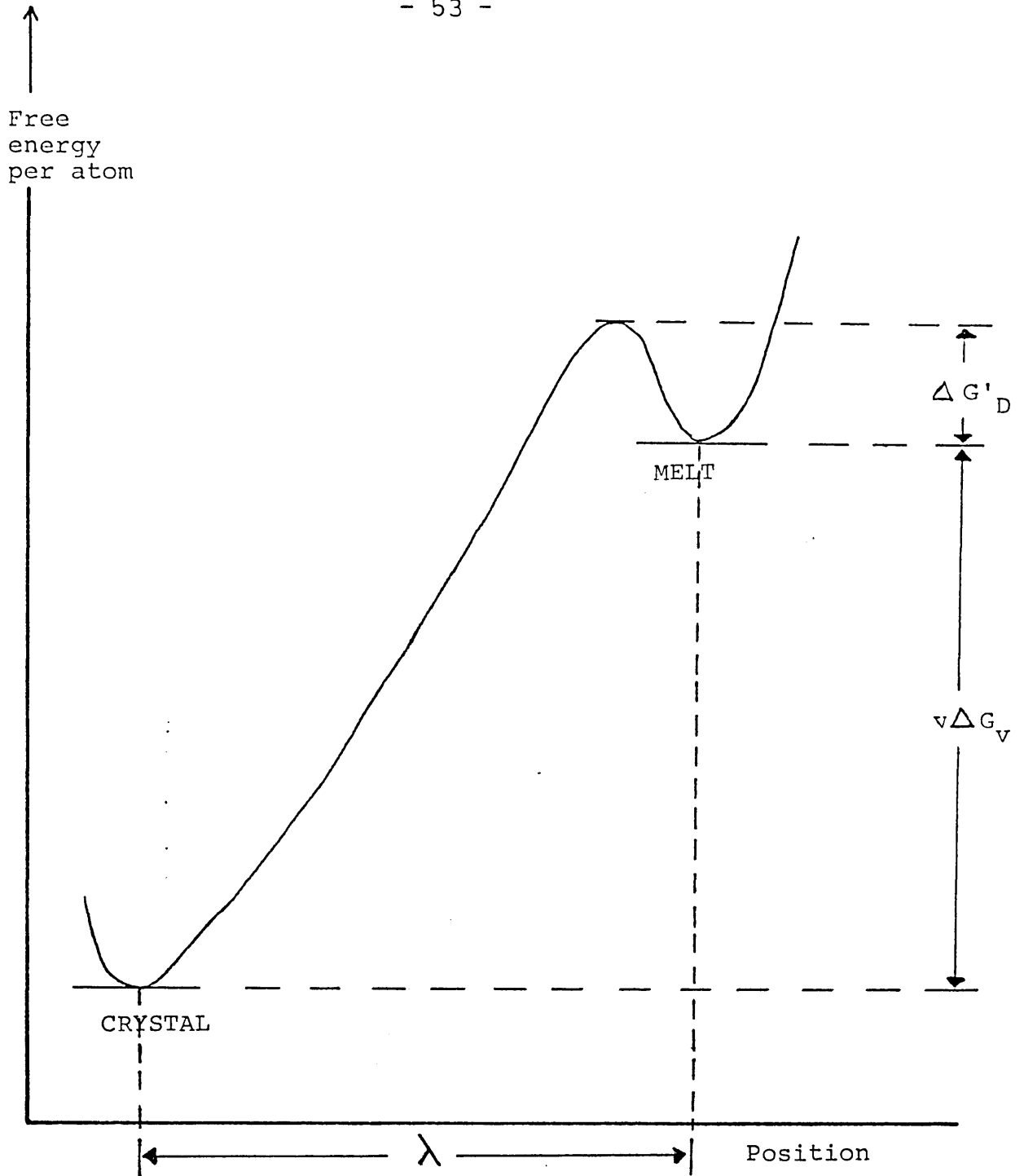


Fig 1.7 Free energy diagram for the attachment process at the crystal-melt interface.

$$D = \frac{KT}{3 \pi \lambda \eta} \quad (1.21)$$

where  $\eta$  is the viscosity.

Also, Wagstaff<sup>38</sup> made a further approximation to estimate  $\Delta G_V$  for simple glasses:

$$\Delta G_V \approx \Delta T \cdot \Delta S_V = \Delta T \cdot \Delta H_V / T_1 \quad (1.22)$$

where  $\Delta H_V$  is the latent heat of crystallisation per unit volume.

The two limiting cases are:

i) At small undercoolings when  $v \Delta G_V \ll KT$ , where:

$$\frac{v \Delta T \cdot \Delta H_V}{T_1} \ll KT \quad (1.23)$$

$$\text{and if } v \Delta G_V = \frac{\Delta G_m}{N} = \frac{\Delta H_m \Delta T}{T_1 N} \quad (1.24)$$

where m refers to molar quantities, then the growth rate is given by:

$$U = \frac{\Delta H_m f K}{3 \pi \lambda^2 T_1} \cdot \frac{1}{\eta} \cdot \Delta T = \frac{\text{constant}}{\eta} \cdot \Delta T \quad (1.25)$$

For small undercoolings, there is a linear dependence of growth rate on undercooling.

ii) For large undercoolings, where  $v \Delta G_V \gg KT$  then

$$\ln U \propto 1/T \quad (1.26)$$

See figure 1.8.

The mechanism of crystal growth can be deduced by calculating the reduced crystal growth rate ( $U_R$ ) and investigating its dependence on the undercooling,  $\Delta T$ :

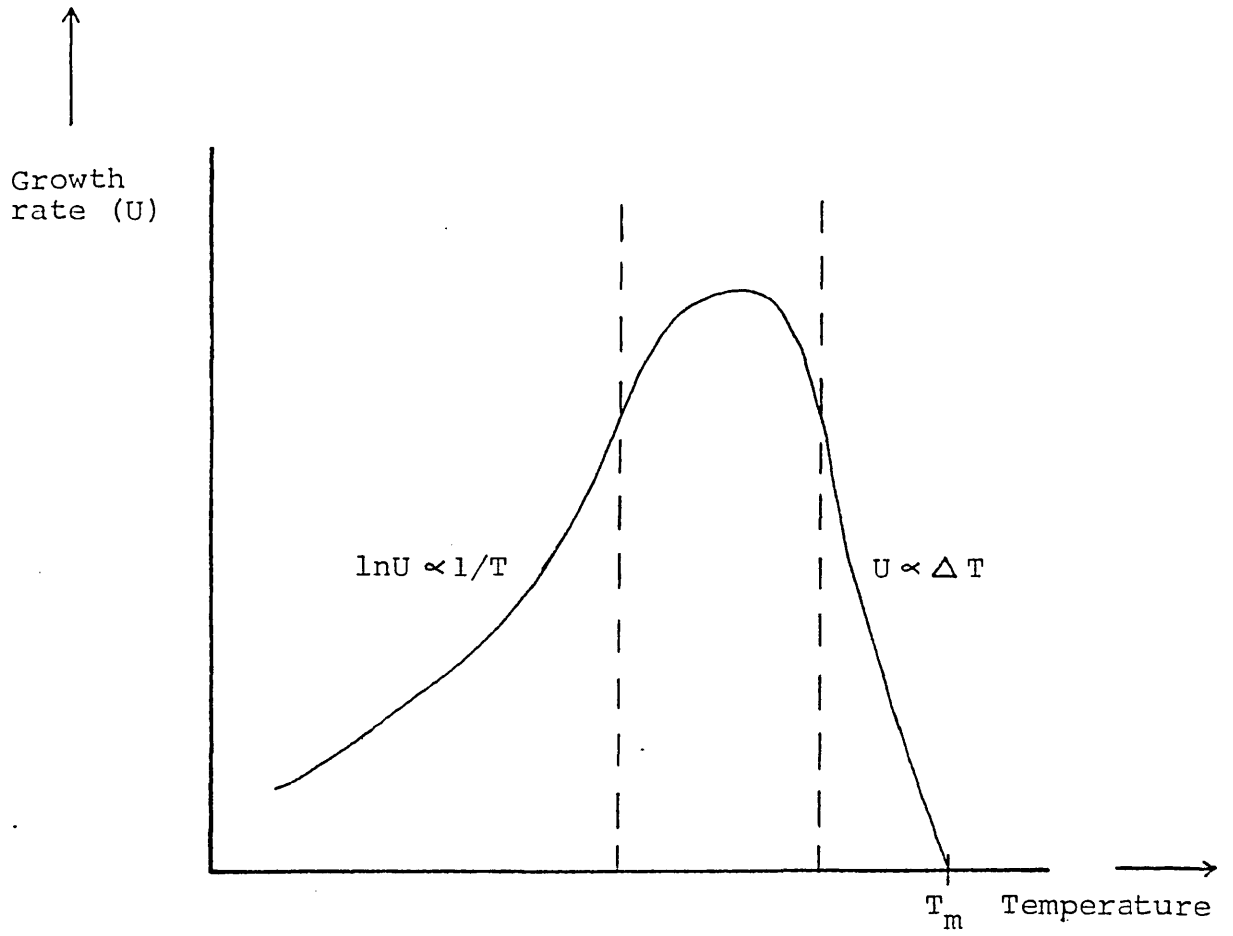


Fig 1.8 Variation of growth rate with temperature.

$$U_R = \frac{U \eta}{1 - \exp \left\{ \frac{-\Delta H_m \Delta T}{KNT_1 T} \right\}} = \frac{KT}{3 \pi \lambda^2} \cdot f \quad (1.27)$$

Kirkpatrick<sup>39</sup> showed that when only considering a normal growth model, a plot of  $U_R$  against  $\Delta T$  gives a straight line of zero slope. Only simple systems show this behaviour, such as  $\text{SiO}_2$ ,  $\text{GeO}_2$  and  $\text{Na}_2\text{O} \cdot \text{SiO}_2$ . However, for a surface nucleation model, a plot of  $\log U_R$  against  $\Delta T$  produces a straight line; an example being  $\text{CaMgSi}_2\text{O}_6$ , diopside. Finally a plot of  $U_R$  against  $\Delta T$  will produce a straight line for examples of the screw dislocation model such as sodium trisilicate.

The two most common crystal growth mechanisms are spherulitic and dendritic, the latter being of importance in the present study. The two growths are competitive processes but at relatively large undercoolings the predominant growth is spherulitic. Here, fibrous growths branch out at low angles to each other, the degree depending on the interference of the diffusion fields of adjacent branches, until eventually radial growth exists. At low undercoolings however, dendritic growth occurs because of favoured growth branching from the original fibre. It is then possible to get branching from the main branches which leads to parallel growth. The growth is anisotropic as the sides become depleted of crystallised material while favoured growth occurs at the tip of the fibre. Spherulitic and dendritic growths occur when the composition of the crystalline phase differs from that of matrix and there is a



diffusion dependency of the crystallising component to the interface.

### 1.5 Glass-ceramics

Conventional glass-ceramics are formed by a two-stage heat treatment (figure 1.9). The first low temperature treatment provides the nuclei on which the main crystalline phases grow at the higher temperature treatment. However, other processes have been developed<sup>40</sup> in which the nuclei are produced during the cooling of a silicate melt and so the need for reheating is eliminated. The aim of the first treatment is to produce a large number of nuclei for crystal growth, and is achieved by heating at the temperature corresponding to the maximum nucleation rate. The second treatment results in the growth of crystals of the required size depending on duration of treatment. The best mechanical properties are achieved with a fine dispersion of small crystals as large ones are liable to set up internal stresses within the matrix which may lead to cracking. The coefficient of thermal expansion of the crystalline phase should be quite low, as that of the residual glassy matrix will generally be so.

Internal nucleation is controlled by the addition of nucleating agents to the glass. Examples of such nucleating agents include sulphides, fluorides, oxides and metals. The effect of these additives is to change the interfacial tension of the phase in which the additives concentrate or to change the glass structure. For example in the addition

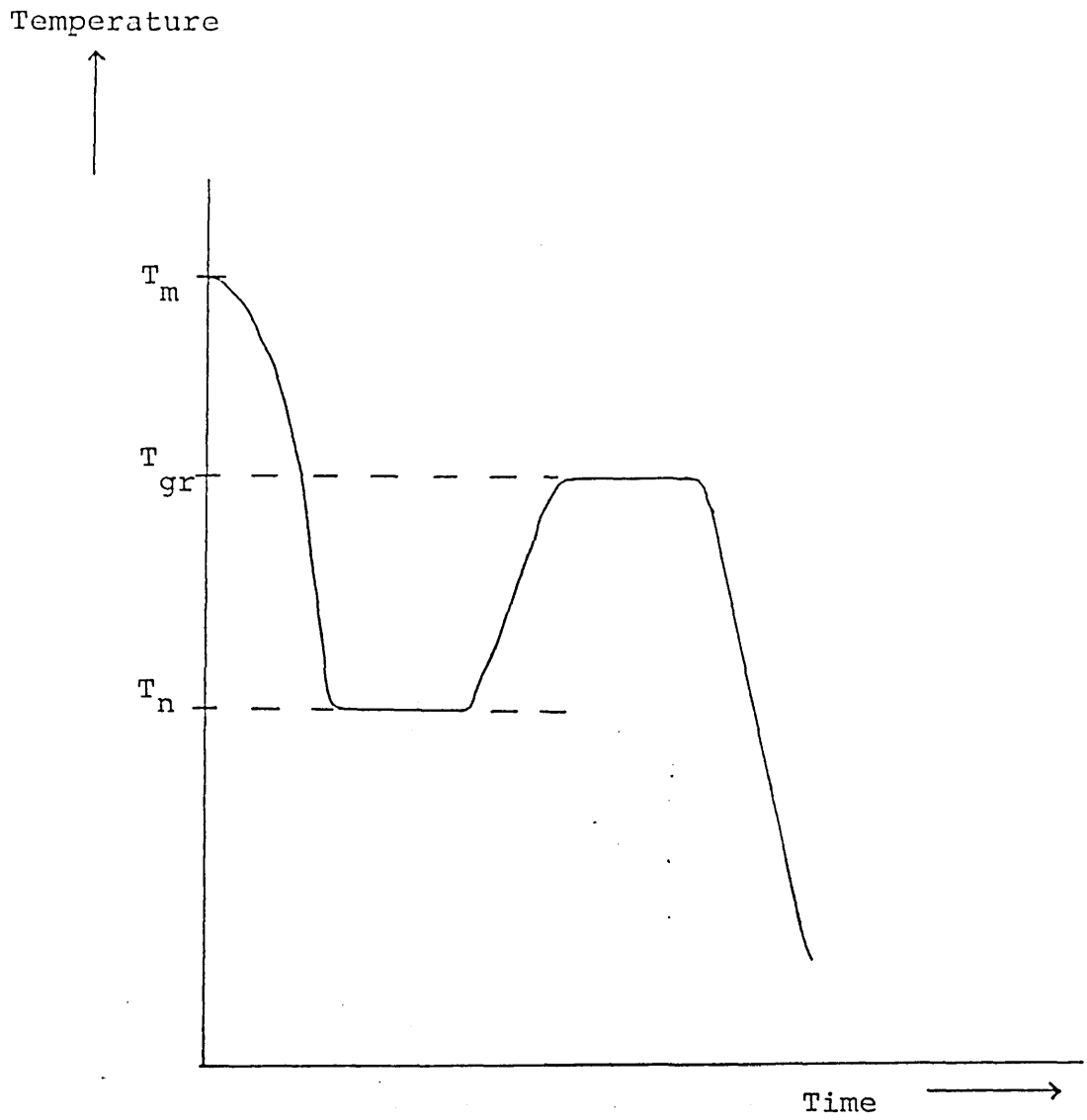


Fig 1.9 Time-temperature schedule for making a glass-ceramic.

of fluorides to oxide glasses, it is assumed that the fluoride ions replace bridging oxygens. This leads to a lowering of the viscosity of the system and, as a result, the diffusion rates of mobile ions increase which in turn leads to a greater degree of phase separation. On the other hand, ions like  $\text{Cl}^-$ ,  $\text{Br}^-$ ,  $\text{I}^-$  and  $\text{SO}_4^{2-}$  will expand the size of the network, rather than replacing bridging oxygens, which leads to an increased mobility of the network modifiers resulting in a higher degree of segregation.

The addition of metallic compounds is such that a uniform, colloidal, dispersion of particles is obtained which aggregate to facilitate heteronucleation of the crystalline phase. Metals such as Pt, Au and Cu are prime examples and are usually added in the form of chlorides or oxides which dissociate easily in the presence of a reducing agent or during melting. For example, copper may be added as  $\text{Cu}_2\text{O}$  in the presence of  $\text{SnO}$ , a reducing agent. On quenching and reheating, copper crystals are obtained which facilitate heteronucleation. This process is known as "striking" and also occurs with the addition of sulphides such as  $\text{CdS}$  and  $\text{CdS} + \text{CdSe}$ .

The most common nucleating agents for oxide glasses are  $\text{TiO}_2$  and  $\text{P}_2\text{O}_5$ . The latter is known to cause phase separation in certain systems by precipitation of metallic phosphates or surface energy effects leading to increased nucleation rates. It was originally thought<sup>41</sup> that  $\text{TiO}_2$  containing glasses precipitated rutile crystals on cooling,

and that crystallisation occurred on these nuclei, but this theory was not completely satisfactory as rutile does not always appear as a crystalline phase, and even when it does it may not be detected until after the precipitation of other crystalline phases. Ohlberg et al<sup>42</sup> showed that rutile speeded up the phase separation and crystallisation processes of a magnesium aluminosilicate glass but the nuclei were not considered to be crystalline  $\text{TiO}_2$  as rutile was the last phase to crystallise out. They believed that a two stage mechanism was operating where initially phase separation occurred due to the presence of minute quantities of the  $\text{TiO}_2$  and that secondly, these grew to a critical size of about  $0.4 \mu\text{m}$  which could facilitate heterogeneous nucleation.

Vogel and Gerth<sup>43</sup> suggested that  $\text{TiO}_2$  enhanced phase separation because  $\text{Ti}^{4+}$  had a high charge density but believed that  $\text{TiO}_2$  may itself become separated into its different crystalline forms. Maurer<sup>44</sup> studied magnesium-aluminosilicate glasses and proposed that the presence of  $\text{TiO}_2$  produced emulsions. Thus  $\text{TiO}_2$  was considered to lower the activation energy for nucleus formation.

Bobovich<sup>45</sup> suggested that a lithium aluminosilicate glass containing  $\text{TiO}_2$  consisted of  $\text{TiO}_4$  tetrahedra. However, on heat treatment, the  $\text{TiO}_4$  tetrahedra rearrange to  $\text{TiO}_6$  octahedra whose corners are shared. Further heating results in partial linking of the octahedra by ribs to produce crystallites similar to or more complicated than

rutile. He stated that these acted as nuclei but added that it was also possible to have crystallites of the composition  $m\text{Al}_2\text{O}_3.n\text{TiO}_2$  as nuclei. G T Petrovski et al<sup>46</sup> confirmed the rearrangement of  $\text{TiO}_4$  tetrahedra to  $\text{TiO}_6$  octahedra in the lithium aluminosilicate system and suggested that an energy barrier existed as the rearrangement process resulted in a weakening of the aluminium-oxygen interaction. Pudushko and Kozlova<sup>47</sup> studied the lithium aluminosilicate system with additions of  $\text{TiO}_2$  varying from 2-11%. They came to the conclusion that  $\text{TiO}_2$  led to structural changes such as phase separation and cracking, on which nuclei would appear whose composition corresponded to that of the fundamental crystalline phase. Unlike Pudushko and Kozlova, Barry<sup>48</sup> found no evidence of phase separation but suggested that  $\text{TiO}_2$  lowered the surface energy between liquid and crystalline phases and so increased the nucleation rate.

Hillig<sup>49</sup> studied the  $\text{BaO-SiO}_2\text{-TiO}_2$  system and observed  $\alpha\text{-BaO.2SiO}_2$  as the nucleating phase, suggesting that  $\text{TiO}_2$  did in fact have an influence on the free energy of the system at the interface surfaces.

## 1.6 Electrical Conduction In Crystalline Solids

Metals such as sodium contain a three dimensional array of nuclei so that each nucleus acts as a potential well for electrons. If the well is infinitely deep, assuming the nuclei are far apart, then the electrons will fall into fixed positions. However, it is possible to get overlap of the outer levels which leads to splitting. The energy

difference between the splitting is trivial and so the levels broaden. In the presence of an electric field, the innermost electrons cannot move since the upper levels are filled. The uppermost 3s valence band is only partially filled and overlap with 3s levels of other atoms results in the bonding. However, the empty 3p levels also broaden by splitting and form the conduction band which actually overlaps the 3s level. Thus in metals overlap occurs between the partially filled valence band and the empty conduction band, but for conduction to occur there must be available both energy states which are occupied and others which are empty. Here, no thermal excitation is required for conduction. Resistance arises due to interaction between mobile electrons and metal ions and is termed scattering and results from:

- i) Thermal motion of the atoms (phonon scattering);
- ii) the presence of substitutional atoms (impurity scattering);
- iii) the presence of defects such as dislocations, vacancies and interstitial atoms.

Unlike metals, semiconducting crystalline solids have filled valence bands which are separated from the next empty upper level by a gap. The two classic types of semiconductors are described as intrinsic and extrinsic semiconductors.

Elemental semiconductors such as Si and Ge are characteristic intrinsic semiconductors. For Si there is an

energy gap of about 1eV between the full 3s3p hybrid valence band and the empty 4s conduction band. There is not enough energy available at room temperature to excite electrons into the conduction band. Hence thermal excitement at higher temperatures raises electrons from the valence band into the conduction band and these electrons can then move through the crystal under an applied field. The hole left behind in the valence band can be filled by an electron in an adjacent valence level and this leads to movement of the hole in the opposite direction to the electron. Equal numbers of conduction electrons and valence holes are formed in intrinsic semiconductors and the conductivity is given by:

$$\sigma = |e| (n_e \mu_e + n_h \mu_h) \quad (1.28)$$

where  $\mu_e$ ,  $\mu_h$  are electron and hole mobilities and  $n_e$ ,  $n_h$  are the numbers of electrons and holes.

Figures 1.10 and 1.11 show representations of the energy band diagram for an insulator and an intrinsic semiconductor such as Si. The number of pairs of electrons and holes rise with temperature and so does the conductivity.

The intrinsic conductivity of most oxides is quite low and so the electrical properties are highly dependent upon the defect structure of the crystals. These materials are called extrinsic semiconductors and show significant conduction below the intrinsic conduction temperature. The energy levels associated with the defects may lie within the band gap between valence and conduction band and as a result

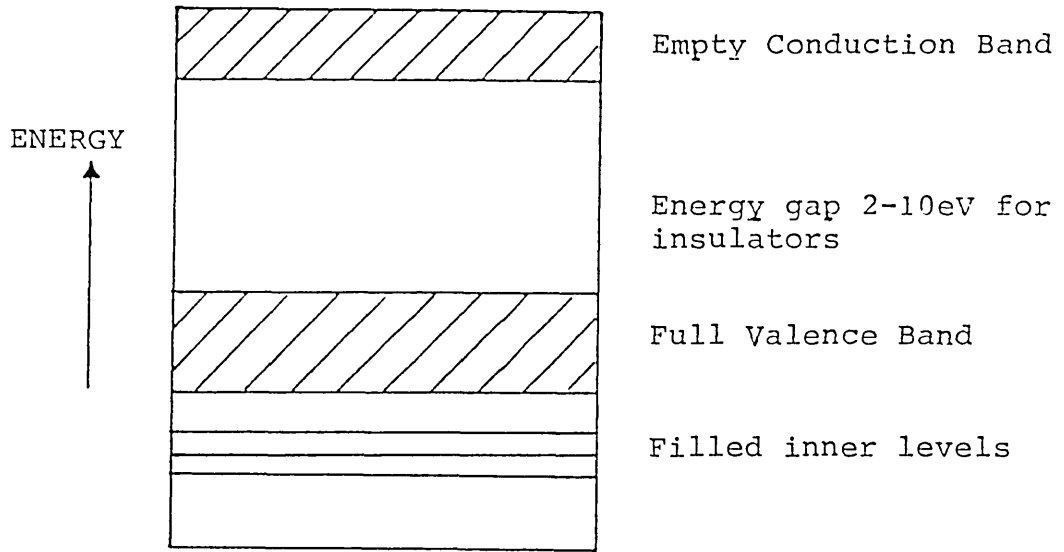


Fig 1.10 Energy band diagram for an insulator.

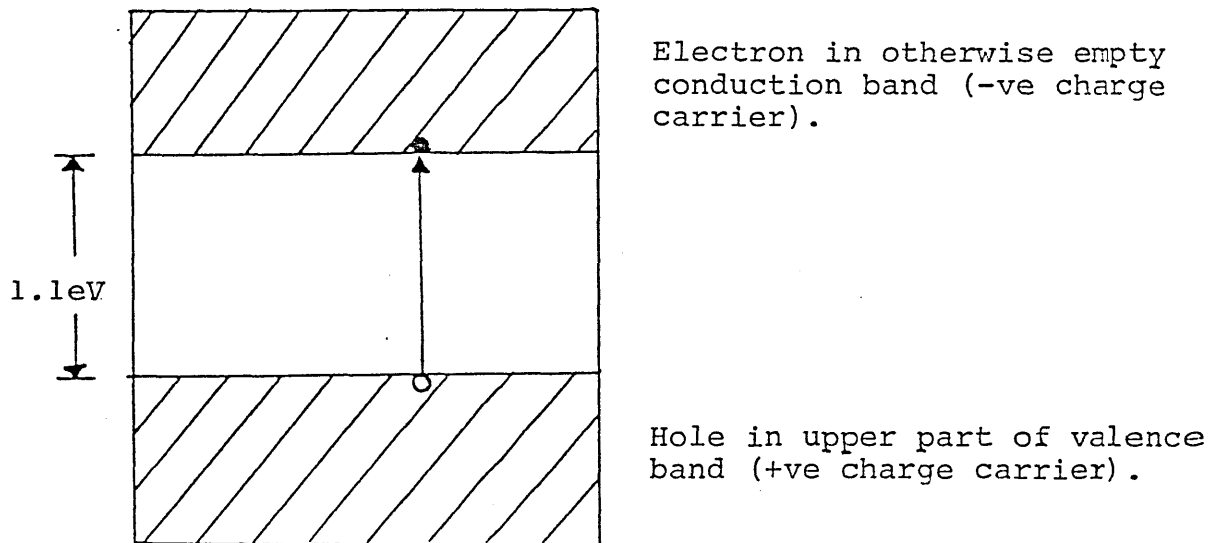


Fig 1.11 Energy band diagram for intrinsic silicon semiconductor.



may act as donors of electrons from the valence band. The former are described as N-type semiconductors while the latter as P-type semiconductors. It is apparent that in N-type semiconduction there exists an excess of electrons in comparison to holes (cf intrinsic semiconductors). The main ways of giving the oxide crystal the required conductivity are:

i) Non-stoichiometry

If the composition of the oxide is non-stoichiometric, then either p-type or n-type semiconduction can occur.

If we consider the non-stoichiometric oxide  $M_2O$  (eg  $Cu_2O$ ) then p-type semiconduction can arise as a result of metal vacancies [or oxygen interstitials, though these are unlikely in a close packed lattice]. It is possible for the metal vacancy to accept an electron from an adjacent oxygen ion. As the valence band arises from the filled oxygen 2p level then a positive hole is left behind as the metal vacancy accepts an electron and conduction is therefore p-type. Conductivity will increase with increase in oxygen pressure as this will determine the number of positive holes in the valence band.

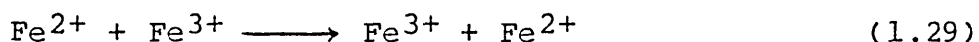
In a similar way N-type semiconduction can occur by anion vacancies or cation interstitials. If an oxygen vacancy is formed, the electrons formerly associated with the anion will remain in the vicinity of the vacancy, and can be excited into the conduction band, which implies that the anion vacancy behaves as a donor level. However, the

electron need not always be released into the conduction band but may in fact be trapped by another ion, eg with partially reduced titania. Here, the electron combines with  $Ti^{4+}$  to give  $Ti^{3+}$ . The relative concentrations of free electrons and  $Ti^{3+}$  ions depend on the relative energy levels of the conduction band and  $Ti^{4+}$  acceptor levels. Though, in this case most electrons are associated with  $Ti^{3+}$  centres and consequently have a much lower mobility. For cation interstitials eg ZnO interstitial zinc atoms act as donor impurities and donate electrons into the empty conduction band, which arises from the empty 4s level of  $Zn^{2+}$ . In this case, there is an activation energy of about only 0.05 eV for the donor electrons and so thermal excitations can easily occur. Here, conductivity will increase with lowering the oxygen pressure.

It is evident that the conduction will depend on such things as atmosphere, temperature and the individual energy levels in the particular material. Included in the non-stoichiometric semiconductors are many transition metal oxides and the normal spinels.

ii) Conduction in inverse spinels( $B[AB]O_4$ )

A good example here is magnetite,  $Fe_3O_4$  which has the following structure  $Fe^{3+}(Fe^{2+}Fe^{3+})O_4$ . Equal amounts of  $Fe^{2+}$  and  $Fe^{3+}$  ions occupy octahedral lattice sites and conduction proceeds by electron transfer between adjacent atoms as shown:



The number of electrons taking part is high and the electronic activity likewise. Any deviations from stoichiometry will tend to reduce the conductivity as the  $\text{Fe}^{2+}/\text{Fe}^{3+}$  ratio will change from unity (ie in the octahedral sites). Mention of these has already been made under the section titled "History of Semiconducting Glazes".

iii) Valency controlled semiconductors

The conductivity of the oxide can be controlled by the addition of appreciable amounts of another component which substitutionally replaces host metal ions and has a fixed valency and therefore provides for more uniform properties. The cation of the doping oxide must have an ionic radius similar to that of the host cation, and a higher or lower valency. The doping cation can either provide the donor or acceptor levels needed for semiconduction, or cause a change in valency of some of the host cations (eg  $\text{Li}^+$  in  $\text{NiO}$ ), and these ions are then the defect sites which are donors or acceptors. Consider pure  $\text{SnO}_2$  which has a band gap of 3.7eV and is an insulator. In naturally occurring  $\text{SnO}_2$ , extrinsic semiconductivity is provided by non-stoichiometry and arises from oxygen vacancies or tin interstitials giving rise to a donor defect level about 0.15eV from the Sn 5s conduction band. However, for much more controlled properties  $\text{Sb}_2\text{O}_5$  is added, where  $\text{Sb}^{5+}$  substitutionally replaces  $\text{Sn}^{4+}$  and provides an electron for excitation into the conduction band thus giving rise to n-type semiconduction. The conductivity of the doped oxide increases with addition of  $\text{Sb}_2\text{O}_5$  until

the solubility limit of  $\text{Sb}_2\text{O}_5$  in  $\text{SnO}_2$  is reached and any further addition of dopant will reduce the conductivity through dilution of the semiconducting material. Gress et al<sup>50</sup> showed a decrease in resistivity as antimony was added for up to about 4 at % Sb, above which the resistivity rose again.

## 1.7 Electrical conduction in oxide glasses

### 1.7.1 Ionic conduction in glasses

It has long been known that the presence of alkali ions in glasses results in ionic conductivity at elevated temperatures. Unlike crystalline materials, there is no single energy barrier to conduction in a glass as it varies from point to point within the material. On applying a potential, there is an immediate current due to the movement of randomly distributed alkali ions. The mobile alkali ions may come up against potential barriers and as a result the current falls off to an equilibrium value. However, on removing the potential, the ions migrate back to a random distribution. The movement of alkali ions occurs by jumps between holes in the network and so the time taken to reach equilibrium can take anything from a few minutes to a few hours depending on the position of the potential barriers. As the temperature is increased the time taken for the mobile ions to reach the potential barriers shortens due to increased mobility.

In the presence of an applied field the alkali ions, eg  $\text{Na}^+$ , migrate towards the cathode electrode, but if there is

no replenishment of  $\text{Na}^+$  at the anode, then electrode polarisation occurs and the conductivity will fall off to zero. One way of overcoming this is to use a sodium amalgam or molten sodium nitrate as the anode.

At high enough temperatures, usually above  $300^\circ\text{C}$ , the electrode polarisation is so rapid that the absorption current is not easily detected.

The ionic conductivity of a glass can be represented by an Arrhenius equation such that:

$$\log \sigma = A - \frac{B}{T} \quad (1.30)$$

where  $\sigma$  is the conductivity,  $A$  a constant and  $B$  a measure of the activation energy for ionic conduction.

A similar approach by Stevels proposed that:

$$\ln \sigma = \ln \left( \nu e^2 \lambda^2 n / 2KT \right) - \Delta H_{dc} / RT \quad (1.31)$$

where  $n$  is the number of carriers,  $\lambda$  the distance between sites and  $\nu$  is the vibrational frequency of the ions. He showed that experimental data fitted both  $\ln \sigma T$  or  $\ln \sigma$  against  $1/T$  and that the result was a straight line whose gradient gave the value of  $\Delta H_{dc}$ .

The ionic conductivity can be expressed as being diffusion dependent, so that:

$$\sigma = Dnz^2e^2/KT \quad (1.32)$$

where  $n$  is the concentration of the mobile ion,  $z$  its charge and  $D$  the diffusion constant.

For tight networks which have predominantly bridging oxygens, only the smallest ions such as  $\text{Li}^+$  will be able to

move. However, for open networks where there are a great number of non-bridging oxygen ions, the larger ions such as  $K^+$  have the greatest mobility because of their lower charge density. A way of reducing the ionic conductivity of glasses containing alkali ions is the mixed alkali effect. In this case the presence of two alkali cations in equimolar proportions gives a higher resistance than an equivalent amount of only one of the cations. An alternative way of reducing ionic conductivity is by utilising the blocking effect of divalent cations such as  $Ca^{2+}$ .

Conduction due to an ionic transport mechanism is only briefly reviewed here as the current research project was aimed at investigating the electronic properties and so alkali ions were deliberately not added to the glasses.

#### 1.7.2 Electronic conduction in glasses

It was proposed by Mott and Davis<sup>51</sup> that as the density-of-states is mainly dependent on the first coordination number, then, as there is not much variation of this between the crystalline and glassy material, no major change in the density of states is likely except that due to changes in specific volume. Although the band edges are no longer clearly defined, it is possible to define extended states (non-localised states).

Anderson<sup>52</sup> originally suggested the presence of localised states at the band edge as a consequence of the lack of long range order in the amorphous state. An electron placed on such a potential well at  $0^\circ C$  would not be

able to diffuse away, but would instead be localised. Hence, a definition for localisation can be that the mobility of an electron at such a site must be zero at  $0^{\circ}\text{K}$ . This localisation is a feature of an "ideal glass" (figure 1.12a) in which a fully connected yet disordered network with no dangling bonds is present. However, in real glasses with structural defects such as broken or dangling bonds, vacancies or chain ends give rise to deeper states within the gap (figure 1.12b). The distribution of charge in the defect states largely determines the position of the Fermi level, and so the defect structure has a large influence on the electronic properties.

Cohen, Fritzsche and Ovshinsky<sup>53</sup> suggested that the valence and conduction band tails of localised states extend into the gap and overlap near the centre. Hence, electrons from the top of the valence band can transfer into states at the bottom of the conduction band thus placing the Fermi level in the region of overlap (figure 1.12c). However, it is generally accepted that the model in figure 1.12b is more realistic than that of Cohen, Fritzsche and Ovshinsky.

A band model proposed by Davis and Mott suggested that the defect states within the gap form tails but of insufficient density to pin the Fermi level. A band of compensated levels was thought to lie near the gap centre in order to pin the Fermi level (figure 1.13). However it was suggested by Mott that this central band of localised levels may be split into a donor band and an acceptor band.

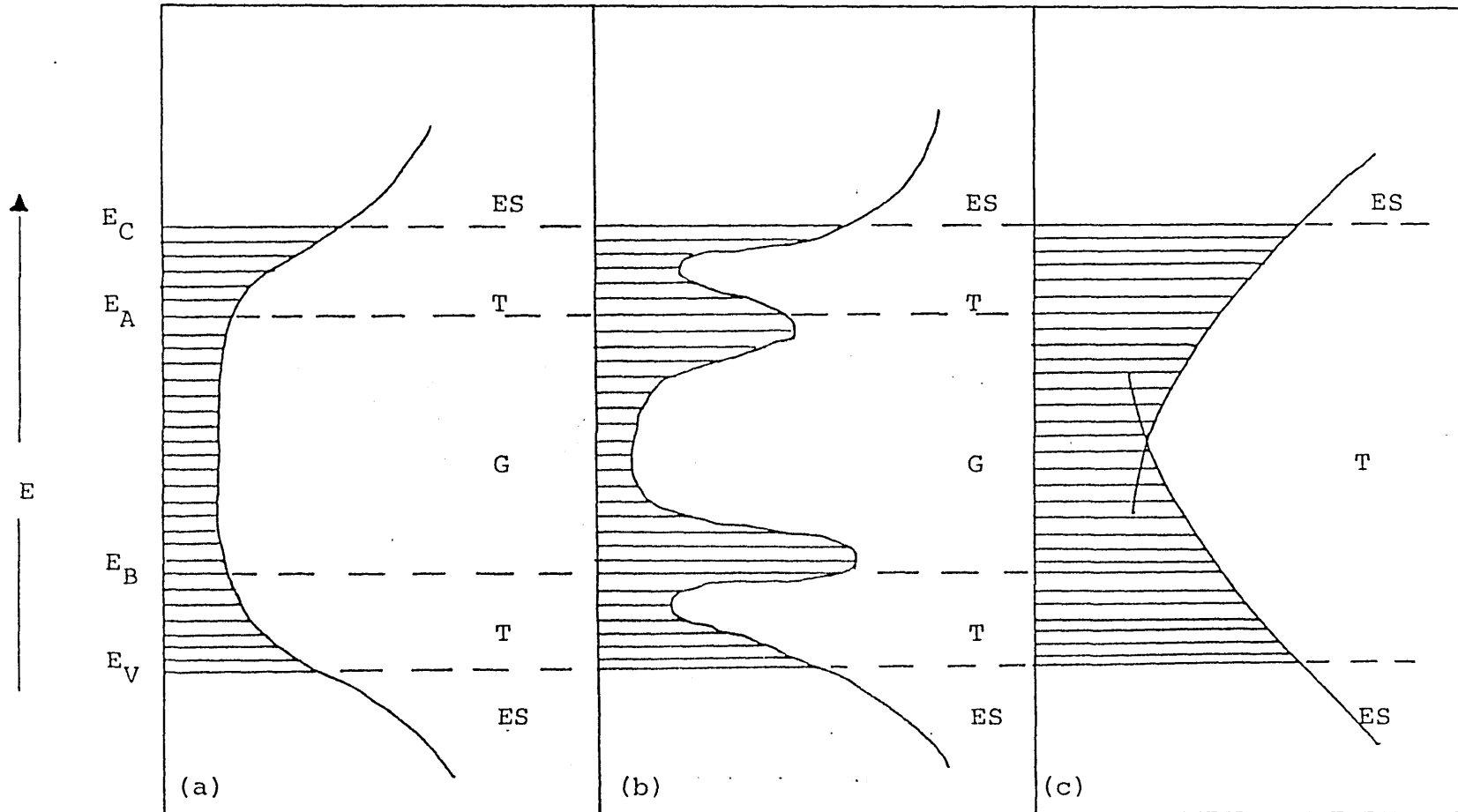


Fig 1.12 Schematic density-of-states diagrams for a semiconducting glass  
 (a) An "Ideal" glass  
 (b) A glass with defect states  
 (c) The Cohen-Fritzsche-Ovshinsky model.



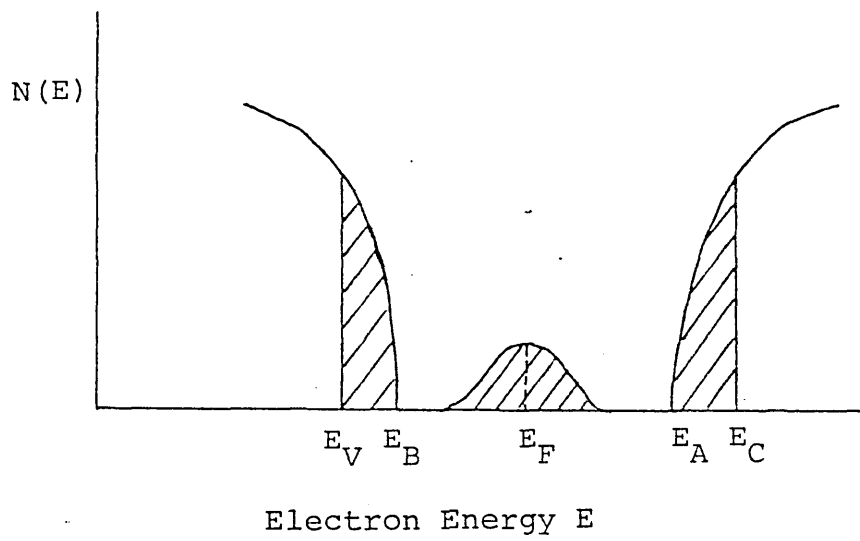


Fig 1.13 Davis and Mott Model.

In the extended states region, the effects of random potentials and of fluctuation in the inter-atomic distances begin to dominate the electronic transport mechanism, as the mean free path of the electrons approaches the interatomic separation.

Cohen<sup>54</sup> pointed out that the transport of electrons was a diffusive process, rather like that of Brownian motion, with the electron jumping from site to site without thermal activation. The electron mobility ( $\mu$ ) is estimated to be about  $10 \text{ cm}^2\text{V}^{-1}\text{s}^{-1}$  but Cohen suggested a lower limit of about  $10^{-2} \text{ cm}^2\text{V}^{-1}\text{s}^{-1}$  for diffusive mobility.

Below the energy  $E_C$  or above  $E_V$  (figure 1.12) there is a sudden change in transport mechanism as localisation sets in. The mechanism for conduction now becomes phonon assisted hopping of electrons between localised sites, where the mobility of electrons is expected to be about  $10^{-2} \text{ cm}^2\text{V}^{-1}\text{s}^{-1}$ , or less. Hence, this drop in mobility from diffusive to phonon assisted hopping defines the mobility gap. It was shown by Mott and Davies that if the Fermi level lies in the localised states, then at low temperature it is energetically favourable for variable range hopping to occur. In this situation, the carrier moves from site to site until it reaches a site of similar energy to its initial state. Thus the conductivity and temperature are related as follows:

$$\sigma \propto T^{1/4} \quad (1.33)$$

## 1.8 Temperature Dependence of D C Conductivity

Mott and Davis suggested that there are three main contributions to conductivity: band conduction, thermally assisted tunnelling and tunnelling conduction near  $E_F$ .

### 1.8.1 Band conduction

This arises due to carriers excited into the non-localised states, with the conductivity being given by:

$$\sigma = \sigma_0 \exp\{-(E_C - E_F)/KT\} \quad (1.34)$$

for electrons being excited into the conduction band. A similar approach can be used for conductivity via holes in the valence band.

### 1.8.2 Thermally assisted tunnelling

This occurs in the localised states near the band edge and arises from nearest neighbour jumps to unoccupied sites. Since there is likely to be a small energy difference between the two sites, the process is termed "elastic" ie it results in the absorption or emission of a phonon. Hence, there is a hopping energy,  $\Delta W_1$  associated with the excitation of an electron to  $E_A$ :

$$\sigma = \sigma_1 \exp[-(E_A - E_F + \Delta W_1)/KT] \quad (1.35)$$

### 1.8.3 Tunnelling conduction near $E_F$

This occurs between localised states near the Fermi energy and is given by:

$$\sigma = \sigma_2 \exp[-\Delta W_2/KT] \quad (1.36)$$

where  $\Delta W_2$  is the hopping energy of half the width of the defect band shown in figure 1.13.

A straight line is expected for  $\ln \sigma$  against  $1/T$  if

the mechanism is nearest neighbour hopping but at lower temperatures, it is possible for the carrier to seek centres of similar energy which are not nearest neighbours. Mott<sup>55</sup> showed that the conductivity was given by:

$$\sigma = B \exp [ -(T_0/T)^{1/4} ] \quad (1.37)$$

where B and  $T_0$  are constants.

#### 1.8.4 Polaron Hopping Conduction

When considering transition metal oxide glasses a pre-requisite for electronic conduction is the presence of the transition metal in at least two of its valence states. Conduction occurs by the transfer of an electron from a reduced to a more oxidised ion eg  $V^{4+} \rightarrow V^{5+}$ . The conductivity,  $\sigma$ , is given by:

$$\sigma = ne\mu \quad (1.38)$$

where n is the number of carriers and  $\mu$  the drift mobility.

Even for glasses with the greatest conductivities, the drift mobility,  $\mu$ , is still only small ( $< 10^{-4} \text{ cm}^2\text{V}^{-1}\text{s}^{-1}$ ), which suggests that electrons move slowly and interact strongly with the network. The charge transfer occurs through the partially filled d-orbitals but as the band width is small and the electron wavelength is of the order of a lattice spacing, the electron can be thought of as being localised and trapped. It is possible for the oxygen ions around the T M ion containing the extra electron, to be polarised to form a polaron. As the electron moves slowly through the lattice, the surrounding oxygens have sufficient time to relax into appropriate positions and so the

polarisation cloud moves with the electron; hence the two can be treated as a single particle. Two types of polaron are possible:

- i) Small polarons are those where the polaron radius,  $r_p$ , is less than the interionic distance and,
- ii) large polarons are those with  $r_p$  greater than the interionic distance.

It has been suggested<sup>56</sup> that in a glass, the disordered structure would inhibit the formation of large polarons. Hence small polaron formation is favoured in glasses.

Two regimes can be distinguished for polaron conduction:

- a) Adiabatic regime; where the electron makes many forward and backward transitions during excitation between two potential wells (figure 1.14) and the probability of transfer is unity. The jump rate,  $P$ , is given by:

$$P = p \exp(-W/KT) \quad (1.39)$$

where  $W$  is the activation energy and  $p$  is proportional to  $\nu_{ph}$  the phonon frequency ( $10^{12}$ - $10^{13}$  s<sup>-1</sup>).

- b) Non-adiabatic regime; where the probability of the electron moving from one site to another during the excitation is small (temperatures greater than  $\frac{1}{2} \theta_D$ ):

$$\mu = (eR^2/KT) \nu_{ph} \exp(-2\alpha R) \exp(-W/KT) \quad (1.40)$$

where  $R$  is the average hopping distance,  $\exp(-2\alpha R)$  describes the overlap of the wavefunctions on neighbouring hopping sites where  $\alpha$  represents the spatial decay of a localised wavefunction. The total

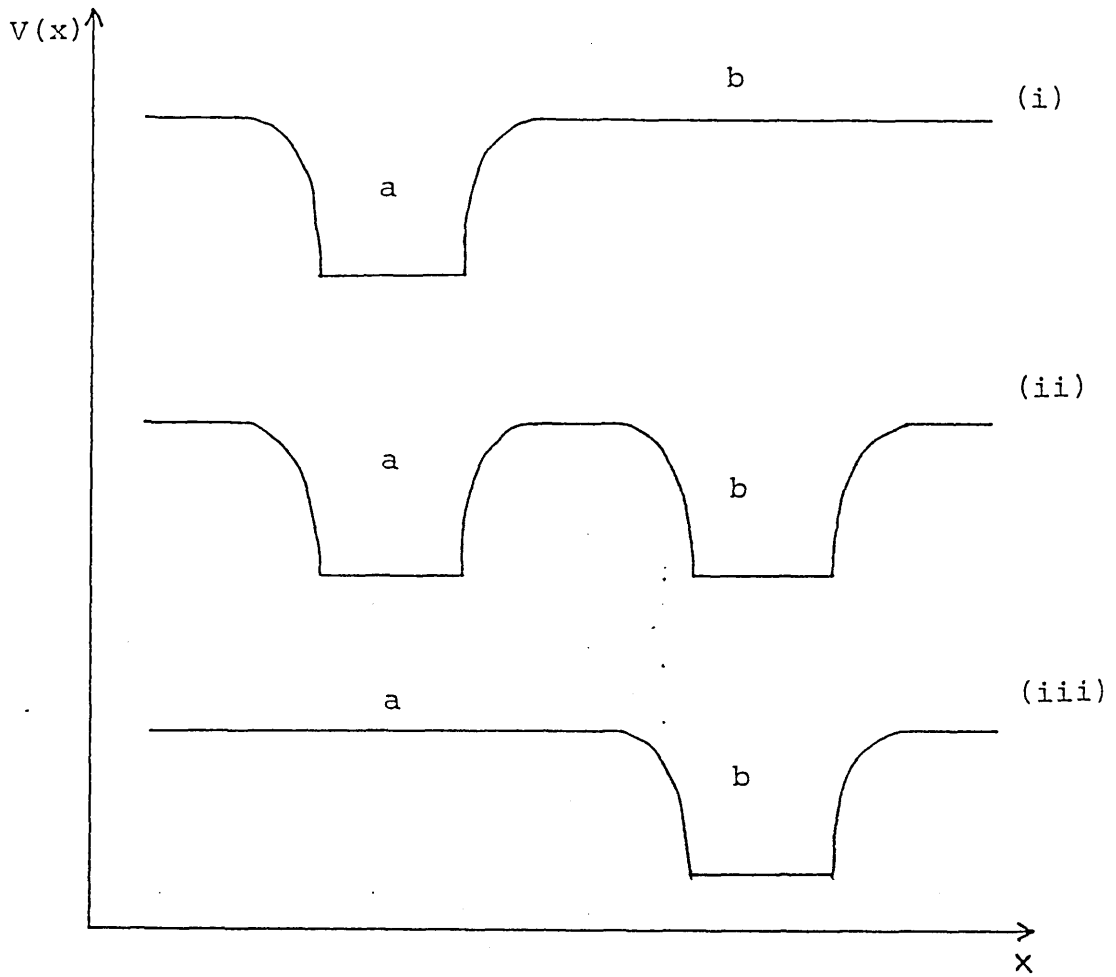


Fig 1.14 Potential wells on a pair of Ions a and b during the hopping process  
(i) before hopping  
(ii) thermally activated state when electrons can move  
(iii) after hopping.

activation energy for the hopping process,  $W$ , can be written as:

$$W = W_H + \frac{1}{2}W_D \quad (1.41)$$

where  $W_H$  is the polaron hopping energy [where  $W_H = \frac{1}{2}W_p$  and  $W_p$  is the polaron binding energy] and  $W_D$  the disorder energy. It was suggested by Mott that the disorder of a glass would lead to the T M sites being spread over an energy equal to  $W_D$ , where  $\frac{1}{2}W_D$  may be defined as the average energy between nearest neighbour sites.

Equation (1.41) only applies at temperatures greater than  $\frac{1}{3}\theta_D$  where  $\theta_D$  (the characteristic Debye temperature) is defined as:

$$K \theta_D = h \omega_0 \quad (1.42)$$

where  $\omega_0$  is the characteristic phonon frequency.

Emin suggested that  $W_H$  was constant down to  $(1/3)\theta_D$ , after which  $W_H \rightarrow h \omega_0$  rapidly as  $T$  drops further. At low temperatures ( $T < (1/4)\theta_D$ ), then:

$$W_H \rightarrow 0 \text{ as } T \rightarrow 0 \quad (1.43)$$

$$W = \frac{1}{2}W_D \quad (1.44)$$

Mott also suggested that at very low temperatures  $W_D \rightarrow 0$  because the polaron will prefer to hop to more distant sites with a smaller energy difference. This led to Mott's  $T^{1/4}$  rule for variable range hopping at low temperatures as previously mentioned (see equation 1.33).

So far it has been assumed that both T M ions are in identical coordination sites in the glass. However, it is

possible to have different environments present such as octahedral and tetrahedral. Austin<sup>57</sup> proposed the addition of another term,  $\Delta U$ , to account for these differences in structure. Therefore:

$$W = W_H + \frac{1}{2}W_D + \Delta U \quad (1.45)$$

Overall, the conductivity ( $\sigma$ ) for the non-adiabatic hopping mechanism can be represented by the following expression, based on 1.38 and 1.40:

$$\sigma = \frac{ne^2R^2}{KT} \cdot v_{ph} \exp(-2\alpha R)\exp(-W/KT) \quad (1.46)$$

However, a modification has to be made to the above expression to take into account the valence ratio of the T M ions:

$$\sigma = v_{ph}Nc(1-c)(e^2R^2/KT)\exp(-2\alpha R)\exp(-W/KT) \quad (1.47)$$

where  $N$  is the total number of transition metal ions per unit volume,  $c$  is the fraction of reduced T M ions (eg  $Fe^{2+}$ ) and  $(1-c)$  is the fraction of oxidised T M ions (eg  $Fe^{3+}$ ).

Equation 1.47 can be used to make a number of predictions:

- i) A plot of  $\log \sigma$  against  $1/T$  would produce a straight line of gradient  $(W_H + \frac{1}{2}W_D)/K$  at high temperatures. At lower temperatures the slope falls continuously to  $\frac{1}{2}W_D$  as  $T \rightarrow 0^\circ K$ .
- ii) The conductivity should increase as the TM ion spacing is decreased.
- iii) The conductivity versus redox ratio should exhibit a maximum value.

On rewriting equation 1.47 in terms of resistivity,  $\rho$ , and plotting  $\log(\rho/T)$  against  $1/T$ , it is possible, by making



a suitable substitution for  $v_{ph}$  (ie  $10^{13}s^{-1}$ ) to calculate  $\alpha$  from the intercept of the graph.

For the small polaron theory to apply Greaves<sup>58</sup> pointed out that the polaron radius,  $r_p$ , must satisfy the following condition:

$$\alpha^{-1} < r_p < R \quad (1.48)$$

where  $\alpha^{-1}$  is the reciprocal of the electronic decay component and is a measure of the radius of the ion on which the electron is localised, and  $R$  is the intersite distance.

A value for  $r_p$  can be obtained by using the equation given by Bogmolov et al<sup>59</sup>:

$$r_p = \frac{1}{2} \left[ \frac{\pi}{6} \right]^{1/3} . R \quad (1.50)$$

where  $R = N^{-1/3}$ .

Using simple electrostatics, Mott obtained the following relationship:

$$W_H = (e^2/16\pi \epsilon_0 \epsilon_p)(1/r_p - 1/R) \quad (1.51)$$

and Miller and Abrahams<sup>60</sup> went on to show:

$$W_D = Ke^2/4\pi \epsilon_0 \epsilon_s R \quad (1.52)$$

where  $\epsilon_p$  and  $\epsilon_s$  are the effective and static dielectric constants, respectively, and  $K$  is a constant, having the value of about 0.3 for T M ion containing glasses. Values obtained for  $W_D$  from this equation are typically  $\leq 0.1$  eV.

### 1.9 TiO<sub>2</sub>/Nb<sub>2</sub>O<sub>5</sub> System

Pure rutile, TiO<sub>2</sub>, is an electrical insulator with a band gap of about 3eV which indicates the onset of intrinsic semiconduction at high temperature. However, extrinsic

semiconductivity can be imparted by departures from stoichiometry, as suggested by Johnson<sup>61</sup>, by replacing an occasional  $Ti^{4+}$  ion with another cation having a charge greater than four. This was accomplished by the addition of 1 mole % of oxides such as  $Nb_2O_5$ ,  $Sb_2O_5$  and  $Ta_2O_5$ , though the highest conductivity reported was that for the addition of  $Nb_2O_5$ . Samples were prepared by heating the powdered mixtures at  $1200^\circ C$  for 4 hours. Conductivity measurements were recorded at  $250^\circ C$  and compared with those of rutile at  $250^\circ C$ . Johnson's results revealed that  $Nb_2O_5$  increased the conductivity of rutile by a factor of about  $5.5 \times 10^3$  to give a conductivity value of  $3.3 \times 10^{-4} \text{ Ohms}^{-1}\text{cm}^{-1}$ . Johnson noticed that the conductivity of the doped rutile increased with increasing additions of the  $Nb_2O_5$  until it reached a maximum value corresponding to a solid solution containing 0.5 mole %  $Nb_2O_5$ . This led Johnson to believe that 0.5 mole % was the upper limit of  $Nb_2O_5$  which would form a solid solution with  $TiO_2$  under the conditions used. He suggested that the solubility of  $Nb_2O_5$  in  $TiO_2$  increased with temperature but that the rate of cooling would determine the amount of  $Nb_2O_5$  which would separate from solid solution. His work also showed that a 0.5 mole %  $Nb_2O_5$  solid solution sample exhibited a change in slope in the conductivity vs temperature plot at around  $300^\circ C$ . Johnson suggested that oxidation of  $Ti_2O_3$  (ie oxygen vacancy filling) and exsolution of  $Nb_2O_5$  may play an important role in this region. Such a sample also showed voltage dependent

conductivity up to 400°C, whereas a sample doped with 1 mole % Nb<sub>2</sub>O<sub>5</sub> showed voltage dependent conductivity up to 300°C, after which the conductivity became constant for both samples. The electrical properties of the doped rutile could be impaired by incorporating into the lattice cations of a lower valency, such as Al<sup>3+</sup>, possibly due to a couple Nb<sup>5+</sup>Al<sup>3+</sup> taking the place of two Ti<sup>4+</sup> ions, and with the Al<sup>3+</sup> ions acting as potential wells for trapping the electrons.

Bogoroditskii et al<sup>62</sup> investigated rutile crystals doped with 0.005 - 1.0 wt % Nb. Samples were prepared by coprecipitation of titanium and niobium salts from solution and subsequent thermal decomposition. The specimens were annealed twice in air at 800°C for 3 hours and then allowed to cool slowly in order to eliminate mechanical stresses and minimise the number of oxygen vacancies. Conductivity measurements indicated that the effect of [Nb] on the numerical value of the conductivity had a pronounced tendency towards saturation. It was suggested that the results could be explained by the decrease in charge carrier mobility due to increased impurity scattering, the contribution of which varied with temperature. Activation energies at room temperature for samples with different Nb contents ranged between 0.03 - 0.12 eV. Measurements of the conductivities in directions parallel to both the "a<sub>0</sub>" and "c<sub>0</sub>" lattice parameters showed a slightly higher conductivity was obtained in the direction parallel to the "c<sub>0</sub>", for a

given wt% of Nb. It was suggested that this anisotropy was an intrinsic property of the structure. The values obtained for the anisotropy in conductivity ( $\sigma_c/\sigma_a$ ) at a given temperature, were similar for crystals with different Nb contents. It was further shown that the semiconducting properties of rutile prepared by doping were much more stable toward changes in oxygen pressure at elevated temperatures than those of reduced rutile.

Roth and Coughanour<sup>63</sup> investigated pressed discs prepared by mixing known quantities of  $TiO_2$  and  $Nb_2O_5$  with a binder of a 5% soluble starch solution. Initial treatment at  $1100^\circ C$  for 4 hours was followed by grinding and remixing of the specimen and further heat treatment of pressed discs at various temperatures for periods ranging from 4 to 24 hours. X-ray diffraction results indicated that solid solution formation occurred with  $Nb_2O_5$  concentrations as high as approximately 11 mole %  $Nb_2O_5$  at  $1450^\circ C$  (figure 1.15).

Error and Smyth<sup>64</sup> reported that between 4-5 mole%  $Nb_2O_5$  could be incorporated into the rutile lattice at  $1060^\circ C$  before a compound,  $TiNb_2O_7$  was formed.

Baumard and Tani<sup>65</sup> investigated rutile doped with 0.04 - 3 at %Nb (0.02 - 1.5 mole %  $Nb_2O_5$ ) in the temperature range  $1000 - 1350^\circ C$ . They showed that  $Nb^{5+}$  was substitutionally incorporated into the rutile lattice. At moderately low oxygen pressures they expected charge compensation by an extra electron:

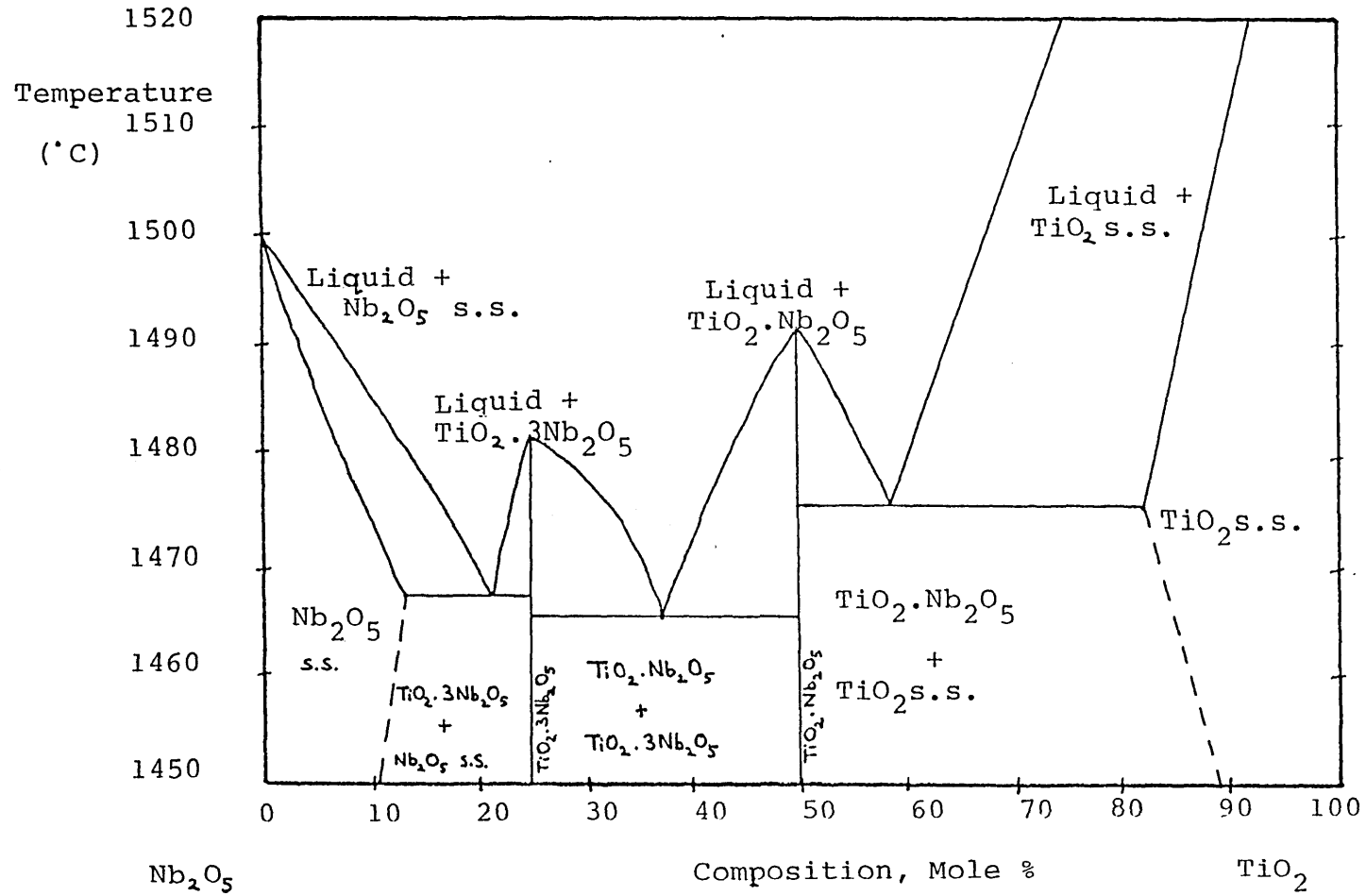
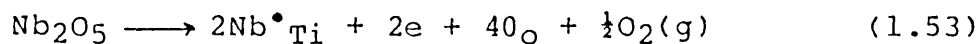


Fig 1.15 Equilibrium phase diagram for the system  $\text{TiO}_2$ - $\text{Nb}_2\text{O}_5$ .

s.s. - solid solution.



[using Kroger Vink notation<sup>66</sup>]. This would be representative of a "TiO - NbO<sub>2</sub>" solid solution. However, under oxidising conditions, they suggested that charge compensation occurred by a lattice defect, which could be a titanium vacancy or an oxygen interstitial. They argued that the latter was rather unlikely in the presence of an oxygen close-packed sub-lattice. The incorporation of Nb resulted in an overstoichiometric oxide of the type,  $\text{Nb}_y\text{Ti}_{1-y}^{4+}\text{O}_{2+y/2}$ . The authors proposed that the Fermi level lay in the upper part of the band gap, not too far from the conduction band. The high energy levels of the titanium vacancies were then occupied by electrons from the niobium levels. The authors reported an increased Nb solubility with temperature from 0.3 at % at 1000°C to 1at % at 1200°C and 2-3 at % at 1350°C.

May<sup>67</sup> stated that the conductivity of rutile was dependent on the concentration of charge carriers. Substitution of titanium ions with pentavalent ions such as Nb<sup>5+</sup> or Ta<sup>5+</sup> resulted in mobile electrons. However, May pointed out that the dopant (eg Nb<sup>5+</sup>) must be homogeneously dispersed to be effective. If so, he suggested that the electronic conductivity,  $\sigma$ , followed a close approximation to the Arrhenius relationship:

$$\sigma = K \exp (-E_a/RT) \quad (1.54)$$

where  $E_a$  is the activation energy for conduction.

## CHAPTER 2

### EXPERIMENTAL DETAILS

#### 2.1 Glass Preparation

It has long been known that alumino-silicate glasses exhibit superior chemical durability and mechanical properties which would make them strong contenders as glaze material for high tension insulators. The basic glass composition chosen was a calcium aluminosilicate glass as this had no mobile alkali ions which might impart ionic conduction, but at the same time would readily dissolve the transition metal oxides. The semiconducting properties were imparted by the addition of  $TiO_2$  doped with  $Nb_2O_5$  and  $ZnO$  was added to lower the melting temperature and the viscosity of the glass.  $CaO$  was actually added in the form of  $CaCO_3$  - allowance being made for loss of  $CO_2$  during melting.

The dried raw materials [Analar grade  $CaCO_3$ ,  $Al_2O_3$  and  $ZnO$ ;  $SiO_2$  as crushed Angolan quartz supplied by Thermal Syndicate;  $TiO_2$  (99.8%) supplied by Ventron;  $Nb_2O_5$  supplied by Koch Light Laboratories Limited) were thoroughly mixed in an agate mortar and pestle to give 100g of glass and melted at  $1500^\circ C$  in a Pt-5%Au crucible in an electric muffle furnace under an air atmosphere. During the preparation of the glass the melts were quenched and remelted three times to improve the homogeneity. In all, the melts were kept at  $1500^\circ C$  for approximately 3 hours. Each melt was then poured onto a large brass plate to produce a large circular sample of glass which was subsequently annealed overnight from

700°C. The compositions of the glasses are shown in Table 3.1.

The glass samples were cut up into individual pieces, 1-2 cms square, and heat treatments performed in electric muffle furnaces with a thermocouple placed alongside the specimens. The preliminary set of heat treatments were aimed at observing the conditions required for phase separation and crystal growth. This information then used to produce semiconducting glasses with the desired microstructure and electrical properties.

## 2.2 Optical Microscopy

The crystallinity of all the heat treated samples was observed directly using a Reichert Optical Microscope. Polished specimens were prepared by mounting the samples onto glass slides with Lakeside cement, and then thinned down using 800 grade carborundrum paper. It was possible to thin the samples down to about 30  $\mu\text{m}$  before they broke away from the glass slide. The samples were viewed in transmission; the maximum resolution was about 1  $\mu\text{m}$ .

## 2.3 X-ray Powder Diffraction Analysis

The two particular instruments used in this research project were the Guinier de Wolff focussing camera using cobalt  $K_{\alpha}$  radiation and the Philips Diffractometer with copper  $K_{\alpha}$  radiation.

In both cases, samples were ground to a fine powder using an agate mortar and pestle, prior to preparing the specimens. Up to four samples at a time were placed in the



sample holder and exposed for 3 hours in the Guinier De Wolff focussing camera. Any crystalline phase having less than 1-2% of the total volume of sample would not be detected.

The Guinier camera was generally used for the identification of crystalline phases present, while accurate lattice parameters were determined for measurements made with a Philips diffractometer.

#### 2.4 Transmission Electron Microscopy

The Jeol Transmission Electron Microscope (JEM 120CX) was used to show that the original glasses did not exhibit phase separation but that selective heat treated samples showed the presence of phase separation.

Samples were prepared by polishing one side down to a 1  $\mu\text{m}$  diamond finish and then cementing this face to a glass slide with Lakeside cement. The other side was then thinned down as far as possible using 800 grade carborundum paper and followed by a final diamond polish to give a 1  $\mu\text{m}$  finish. The sample was removed from the glass slide, by dissolving the Lakeside cement in acetone, and then stuck down with Durafix between two 3mm, single hole, copper electron microscope grids. The sample was thinned down further using a Technics argon ion beam thinner, until a small hole appeared in the centre of the specimen. The angle of incidence of the beam was about  $15^\circ$  to the surface of the sample which resulted in a removal rate of about 1-2  $\mu\text{m/hr}$ . The samples were coated with evaporated carbon

to prevent charging of the specimen under the electron beam.

## 2.5 Scanning Electron Microscopy

The morphology of the samples was examined using a JSM T200 scanning electron microscope. Samples with fractured surfaces were etched in a 1% HF/1% HCl solution for about ten seconds, to preferentially dissolve the glass between the crystalline regions to improve the contrast between glassy and crystalline phases. The samples were washed in an ultrasonic bath, dried, and then stuck down onto aluminium studs with Durafix. Specimens were coated with evaporated carbon to prevent charging of the samples, while silver dag was applied to ensure a good electrical contact across the Durafix film to the aluminium stud.

Photomicrographs were taken of representative samples and are presented in Chapter 3.

## 2.6 Electron Probe Microanalysis

The distribution of the metal ions within the samples can be detected using the EDAX facility on the T200 SEM. Samples were placed in a cold setting resin and polished down to a 1/4 $\mu$ m diamond finish. Thermally evaporated carbon was applied to prevent charging and selected areas were then scanned.

## 2.7 D C Conductivity Measurements

Using the techniques mentioned, samples were selected for d c conductivity measurements. Specimens were prepared by heat treating 2 x 2 cm pieces of glass at the appropriate temperature and for the required period of time. Samples

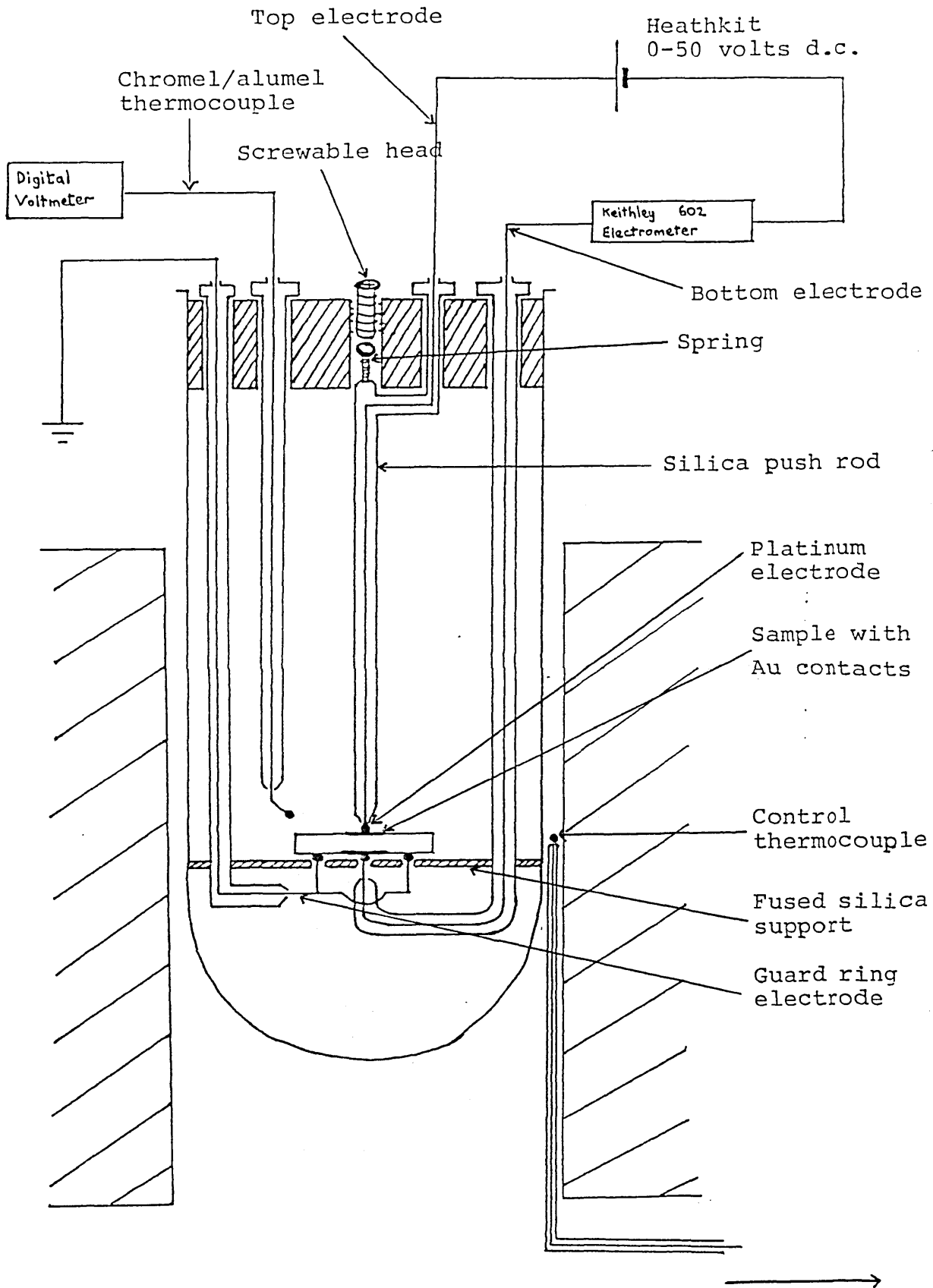


Fig 2.1 Schematic representation of D.C. conductivity cell with measuring apparatus.

To furnace controller

were then ground to a thickness of between 2-3.5 mm and given a final polish with 1200 grade carborundum paper. Gold contacts were applied by a d c sputtering technique to give a conventional three terminal guarded arrangement. The power was supplied by a Heathkit 1P 20U unit, for the range 5-40 volts, and the resulting current was measured by a Keithley 602 high impedance electrometer [figure 2.1]. Conductivity measurements were made from room temperature to 500°C with applied voltages from 5-40 V dc. The corresponding currents were measured and V-I plots obtained for different temperatures. The resistance values (Ohms) as obtained from the V-I plots were converted into resistivity,  $\rho$ , values (Ohms. cm) by using the following relationship:

$$\rho = \frac{V}{I} \frac{\pi (d/2)^2}{l} \quad \Omega \text{ cm} \quad (2.1)$$

where V is the applied voltage, I the current, d the diameter of the smaller electrode (cm) and l the thickness of the sample (cms).

Temperatures were accurately measured using a chromel/alumel thermocouple placed next to the specimen, while the temperature of the furnace was controlled by a Pt-Pt/13%Rh thermocouple connected to an Eurotherm controller.

## 2.8 TiO<sub>2</sub>/Nb<sub>2</sub>O<sub>5</sub> Solid Solution Formation

Various authors (as previously mentioned in section 1.8) have reported the presence of solid solution in the TiO<sub>2</sub>-Nb<sub>2</sub>O<sub>5</sub> system but no values have been reported for to the shift in the lattice parameters of rutile as a function

of Nb<sub>2</sub>O<sub>5</sub> content. The primary aim was to obtain a correlation between mole % Nb<sub>2</sub>O<sub>5</sub> and the "a" and "c" lattice parameters of rutile. It was hoped that this information would help in establishing the Nb<sub>2</sub>O<sub>5</sub> content of TiO<sub>2</sub> crystals in the partially crystallised glasses.

A series of solid state reactions were performed using mixtures of TiO<sub>2</sub> and Nb<sub>2</sub>O<sub>5</sub> with the same starting materials as those used for glass formation. The powdered oxides were thoroughly mixed and placed in alumina crucibles. The heat treatment consisted of a period of one week at 1450°C with regular grinding of the samples during this period. The samples were then analysed using a Guinier De Wolff focussing camera, from which it was possible to identify the crystalline phases present but not detect the shifts in the lines. Hence, it was decided to use the Philips diffractometer, as this would be more sensitive to small changes in the lattice parameters.

## 2.9 Determination of the wt% crystalline TiO<sub>2</sub> present in partially crystalline glass samples

The wt% crystalline TiO<sub>2</sub> was quantitatively analysed by x-ray diffraction using an internal standard method<sup>68</sup>. In this method, a diffraction line from the phase being determined is compared with a line from a standard substance mixed with the sample in known amounts.

If one wishes to determine the amount of phase "a" present in a mixture a,b,c,... where the relative amounts of the other phases can vary from sample to sample, then it is

necessary for a composite sample to be made with a standard, "s". The amounts of "a" and "s" used in the composite are known. Let the volume fraction of "a" in the sample and composite be  $V_a$  and  $V_{a'}$ , respectively, and the volume fraction of "s" in the composite be  $V_{s'}$ .

Then the intensity of a particular diffraction line from "a" in the composite sample is given by:

$$I_a = \frac{K_1 V_{a'}}{\mu_m} \quad (2.2)$$

where  $K_1$  is a constant and  $\mu_m$  the linear absorption coefficient of the mixture. Similarly, the intensity of a particular diffraction line from "s" is given by:

$$I_s = \frac{k_2 V_{s'}}{\mu_m} \quad (2.3)$$

where  $k_2$  is a constant.

It is possible to remove the unknown term,  $\mu_m$ , by dividing equation (2.2) by (2.3):

$$\frac{I_a}{I_s} = k_3 \left( \frac{V_{a'}}{V_{s'}} \right) \quad (2.4)$$

where  $k_3$  is a constant.

$$\text{Using, } V_{a'} = \frac{\text{Vol a in composite}}{\text{total Vol of composite}} \quad (2.5)$$

$$= \frac{\text{Vol a}'}{\text{Vol a}' + \text{Vol b}' + \text{Vol c}' + \dots \text{Vol s}'} \quad (2.6)$$

$$\text{where Vol a}' = \frac{\text{mass a}'}{\text{density a}'} = \frac{m_{a'}}{\rho_{a'}} \quad (2.7)$$

Then for the composite sample, we have:

$$V_{a'} = \frac{m_{a'} / \rho_{a'}}{m_{a'} / \rho_{a'} + m_{b'} / \rho_{b'} + \dots m_{s'} / \rho_{s'}} \quad (2.8)$$

and similarly for  $V_s$  :

$$V_{s'} = \frac{m_{s'} / \rho_{s'}}{m_{a'} / \rho_{a'} + m_{b'} / \rho_{b'} + \dots m_{s'} / \rho_{s'}} \quad (2.9)$$

Thus dividing equation (2.8) by (2.9):

$$\frac{V_{a'}}{V_{s'}} = \frac{m_{a'} / \rho_{a'}}{m_{s'} / \rho_{s'}} \quad (2.10)$$

Substitution of equation (2.10) into (2.4) gives:

$$\frac{I_a}{I_s} = k_3 \left( \frac{m_{a'} / \rho_{a'}}{m_{s'} / \rho_{s'}} \right) \quad (2.11)$$

As  $m_{s'}$  is kept constant for all the composite samples and  $\rho_{a'}$  and  $\rho_{s'}$  are also constant:

$$\frac{I_a}{I_s} = k_4 m_{a'} \quad (2.12)$$

The relationship between the weight fraction of "a" in the original sample ( $m_a$ ) and composite sample ( $m_{a'}$ ) is given by:

$$m_a = \frac{m_{a'}}{(1 - m_{s'})} \quad (2.13)$$

A calibration curve can be established by measuring the  $I_a/I_s$  ratio for a range of values of  $m_{a'}$  but keeping  $m_{s'}$  constant.

Mechanical mixtures were prepared containing known quantities of  $TiO_2$  (rutile), glass and NaCl as an internal standard. NaCl was chosen since its diffraction pattern contained relatively few lines with no interference with the

TiO<sub>2</sub> pattern. The weight percent of NaCl was originally varied until the peak height of the chosen line was of comparable size to the chosen rutile peak. Hence the amount of NaCl was kept constant at 10 wt % for each mixture. The ratio of the strongest peak for rutile and NaCl (3.25 Å and 2.82 Å, respectively<sup>69</sup>) led to a calibration plot of (TiO<sub>2</sub> peak height)/(NaCl peak height) against wt%. TiO<sub>2</sub> added to the glass.

The first series of mixtures were prepared by hand in an agate mortar with pestle. However, it was later found that mixing the samples in a vibration ball mill for a few hours produced a more homogeneous mixture. The vibration mill consisted of an agate tube with two small agate balls into which the powders were placed. The tube had a metallic strip attached to it and the application of an electromagnet resulted in the vibration of the tube containing the agate balls thus providing a thorough mixing.

Similarly, the wt % of crystalline TiO<sub>2</sub> in various crystallised glasses was determined by mixing powdered partially crystalline glass and 10 wt % NaCl in the vibration ball mill. The peak height ratio, TiO<sub>2</sub>/NaCl, was evaluated from x-ray diffraction data and, by using the calibration graph, an estimate obtained for the wt % of crystalline TiO<sub>2</sub> in the crystallised samples.

It was hoped that the volume % of crystalline TiO<sub>2</sub> could be determined in order to ascertain the effect of volume % crystalline TiO<sub>2</sub> on the conductivity of partially



crystalline glasses.

2.10 Determination Of The Coefficient Of Linear Expansion,  $\alpha$

The objective of the study was to assess the suitability of the semiconducting material as a glaze for coating insulators.

Rectangular specimens, approximately 10 x 5 x 3 mm, were heated in a silica glass dilatometer in which a change in dimension is converted via a linear variable differential transformer to an electrical signal. Expansion coefficients over the temperature range, room temperature to 850°C were measured and are reported in Chapter 3.

### CHAPTER 3

#### EXPERIMENTAL RESULTS

##### 3.1 Composition of the Glasses

The composition of the glasses investigated is shown in Table 3.1. All the glasses were made in batches of 100g and therefore the values in Table 3.1 indicate the weight percent of each component in the glass formulation. The annealed glasses were obtained as typically pale straw coloured although J10, 11 and 12 exhibited a very faint blue tinge. J13 glass was also straw coloured with a blue tinge but its base contained a white deposit. The white deposit was cut away and x-ray diffraction analysis revealed the presence of crystalline  $\text{TiO}_2$ , thus suggesting its solubility limit in the glass had been exceeded at  $1500^\circ\text{C}$ .

The annealing treatment had proved successful as the glasses did not shatter or show signs of cracking when being cut into individual pieces, 1-2 cms square.

X-ray diffraction analysis of the powdered glasses did not detect the presence of any crystalline phases. However, as this method is not sensitive for less than about 1% crystallinity then observations made on the optical microscope in the transmission mode of thin sectioned, polished samples revealed that all the base glasses were entirely vitreous. Homogeneity of the glasses was assessed by the uniformity of colour throughout the thin sections. Transmission electron microscopic evidence revealed that the glasses were homogeneous and not phase separated or crystalline.

Table 3.1

Composition of the glasses (wt%)

Glass Code	Composition (wt%)					
	SiO <sub>2</sub>	Al <sub>2</sub> O <sub>3</sub>	CaO	ZnO	TiO <sub>2</sub>	Nb <sub>2</sub> O <sub>5</sub>
J0	52.0	16.4	16.4	5.1	10	0
J1	51.9	16.3	16.3	5.1	10	0.5
J2	51.6	16.2	16.2	5.1	10	1.0
J3	51.0	16.0	16.0	5.0	10	2.0
J4	50.4	15.8	15.8	4.9	10	3.0
J5	50.1	15.7	15.7	4.9	10	3.5
J6	49.8	15.6	15.6	4.9	10	4.0
J7	48.7	15.3	15.3	4.8	10	6.0
J8	49.1	15.4	15.4	4.8	15	0.22
J9	49.0	15.4	15.4	4.8	15	0.5
J10	48.7	15.3	15.3	4.7	15	1.0
J11	47.5	14.9	14.9	4.7	15	3.0
J12	47.9	15.0	15.0	4.7	13.3	4.0
J13	46.0	14.4	14.4	4.5	20	0.67

### 3.2 Initial Heat Treatment Study

Preliminary heat treatments were performed on J0 and J3 glasses. Optical microscopy, scanning electron microscopy and x-ray diffraction analysis of various heat treated samples is shown in Table 3.2. Heat treatments performed on glass J0 gave results very similar to the corresponding J3 samples and so for the sake of brevity, results for J0 glass have not been reported.

As primary interest was in the bulk properties of the glasses, surface devitrification was always ground off on a diamond lapping wheel prior to x-ray diffraction analysis or before electrical measurements were made.

Plates 3.1 and 3.2 show the contrast in structure between a sample of J3 glass having a one stage crystallisation treatment and that having a two stage heat treatment, respectively. The sample treated for  $\frac{1}{2}$  hour at  $1000^{\circ}\text{C}$  (Plate 3.1) shows a wide distribution of crystalline  $\text{TiO}_2$  needle sizes present in a glassy background matrix; whereas the sample which has undergone a prior heat treatment at  $800^{\circ}\text{C}$  for 3 hours followed by  $\frac{1}{2}$  hour at  $1000^{\circ}\text{C}$  (Plate 3.2) displays a much finer and more uniform dispersion of  $\text{TiO}_2$  needles in a glassy matrix.

The initial treatment of 3 hours at  $800^{\circ}\text{C}$  produced samples which exhibited a light scattering phenomenon in so much as visibly they appeared blue in reflected light and orange/red under transmitted light. This would suggest that the particles within the glass, which had been shown to be

vitreous by x-ray diffraction analysis, must be of the same order of magnitude as the wavelength of visible light, 0.4-0.7  $\mu\text{m}$ . Plates 3.3 and 3.4 represent transmission electron micrographs of J3 glass heat treated for 3 hours at 800°C to induce phase separation prior to the crystallisation treatment at 1000°C. The micrographs show the existence of phase separation, in which the darker, droplet type regions represent a titania rich phase dispersed in a silica rich matrix. The droplet sizes ranged between 0.2-0.5  $\mu\text{m}$  which are comparable with the wavelength of visible light.

On closer examination, especially Plate 3.3B, a few minute needles are clearly visible in a background rather depleted in the  $\text{TiO}_2$  rich separated phase. As the initial glass was clear, then presumably  $\text{TiO}_2$  crystals must have grown from the titania rich droplets thus accounting for the lighter background; though it must be pointed out that x-ray diffraction analysis did not reveal the presence of any crystalline phases.

For glass J1, the growth rate ( $\mu\text{m}/\text{min}$ ) of rutile needles at various temperatures was determined from measurements of needle lengths using reflectance microscopy of polished specimens. A light etch, 1-2 seconds in 1% $\text{HF}/1\% \text{HCl}$  solution, was used to enhance the contrast between glassy and crystalline regions. The growth rate is not representative of the initial rate but is in fact an average over a 15 minute period as samples were held for 15

minutes at the selected temperatures and the corresponding lengths of rutile needles measured. A plot of growth rate against temperature is shown in figure 3.1.

Table 3.2

Preliminary heat treatments performed on J0 and J3 glasses

<u>Temp</u> (°C)	<u>Time (hours)</u>	<u>Observation</u>	<u>X.R.D</u>
750	3	Straw coloured glass	NDCP
	18	Slightly phase separated	NDCP
780	18	Phase separated	NDCP
800	3	Phase separated	NDCP
	18	Phase separated	NDCP
	68	Phase separated and small needles	Rutile
850	1	Phase separated	NDCP
900	1	Signs of crystallisation	Rutile + An
938	3	Surface and volume crystallisation	Rutile + An
	18	Surface and volume crystallisation	Rutile + An
1000	0.25	Surface and volume crystallisation, randomly sized and dispersed needles/dendrites	Rutile + trace An
	0.5		Rutile + trace An
	1	Rutile + An	
	3	Rutile + An + trace Ti	
	6	Rutile + An + trace Ti	
	10	Rutile + An + trace Ti	
	15	More surface and volume crystallisation	Rutile + An + trace Ti
	18		Rutile + An + trace Ti

Table 3.2 continued

<u>Temp</u> <u>(°C)</u>	<u>Time (hours)</u>	<u>Observation</u>	<u>X.R.D</u>
1038	0.5	Surface and volume crystallisation	Rutile + trace An,Ti
	6	More surface and volume crystallisation	Rutile + An + Ti
	18	Much coarser structure	Rutile + An + Ti
1105	0.5	Surface and volume crystallisation	Rutile + trace An,Ti
	6	Highly crystalline	Rutile + An + Ti
	18	Very coarse structure	Rutile + An + Ti
1146	0.5	Highly crystalline	Rutile + An
	6	Highly crystalline	Rutile + An + trace Ti
	18	Highly crystalline and coarse structure	Rutile + An + Ti
3hrs800°C + ½hr1000°C		Highly and finely crystalline	Rutile
18hrs800°C + ½hr1000°C		Highly and finely crystalline	Rutile

Rutile = TiO<sub>2</sub>

An = Anorthite CaO.Al<sub>2</sub>O<sub>3</sub>.2SiO<sub>2</sub>

Ti = Titanite CaO.TiO<sub>2</sub>.SiO<sub>2</sub>

NDCP = No Detectable Crystalline Phase



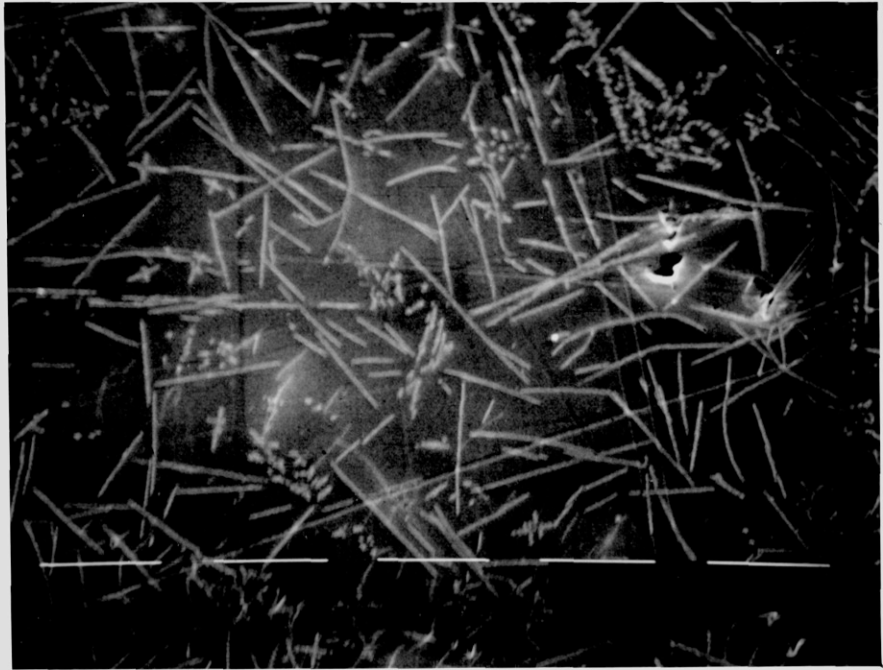


Plate 3.1

Scanning electron micrograph of J3 glass heat treated for 0.5 hour at 1000°C. Randomly sized rutile needles are evident in a glassy matrix.

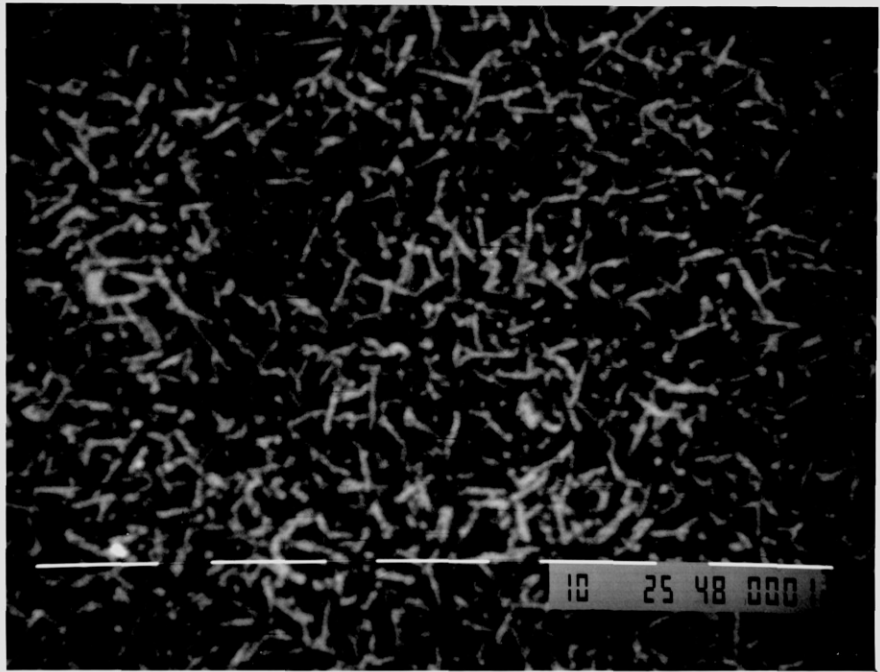
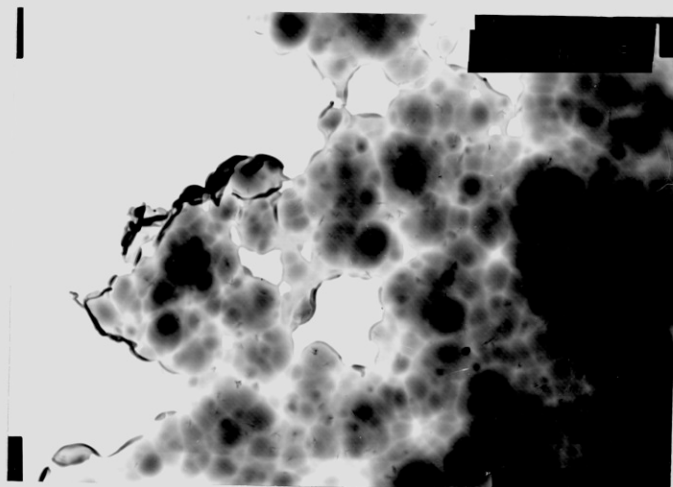
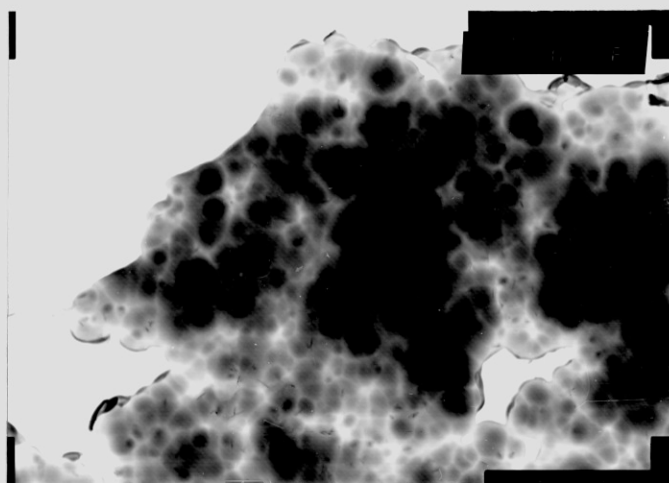


Plate 3.2

Scanning electron micrograph of J3 glass heat treated for 3 hours at 800°C followed by 0.5 hours at 1000°C. A fine dispersion of rutile needles is present in a glassy matrix.



(A)

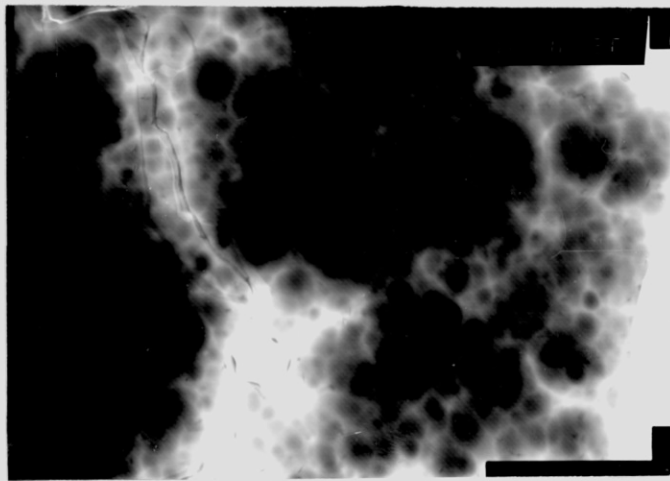


(B)

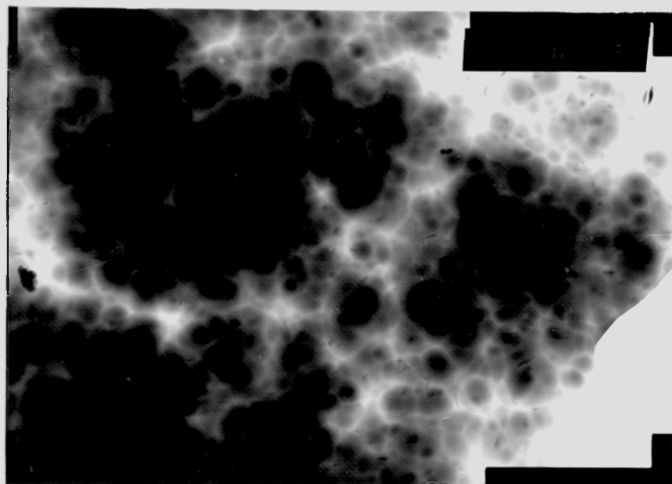
Plate 3.3

Transmission electron micrographs of J3 glass heat treated for 3 hours at 800°C. The dark, mottled regions represent a titania rich phase dispersed in a silica rich phase.

X 10,000



(A)



(B)

Plate 3.4

Transmission electron micrographs showing titania rich droplets dispersed in a silica rich matrix. Same sample as in Plate 3.3.

X 10,000

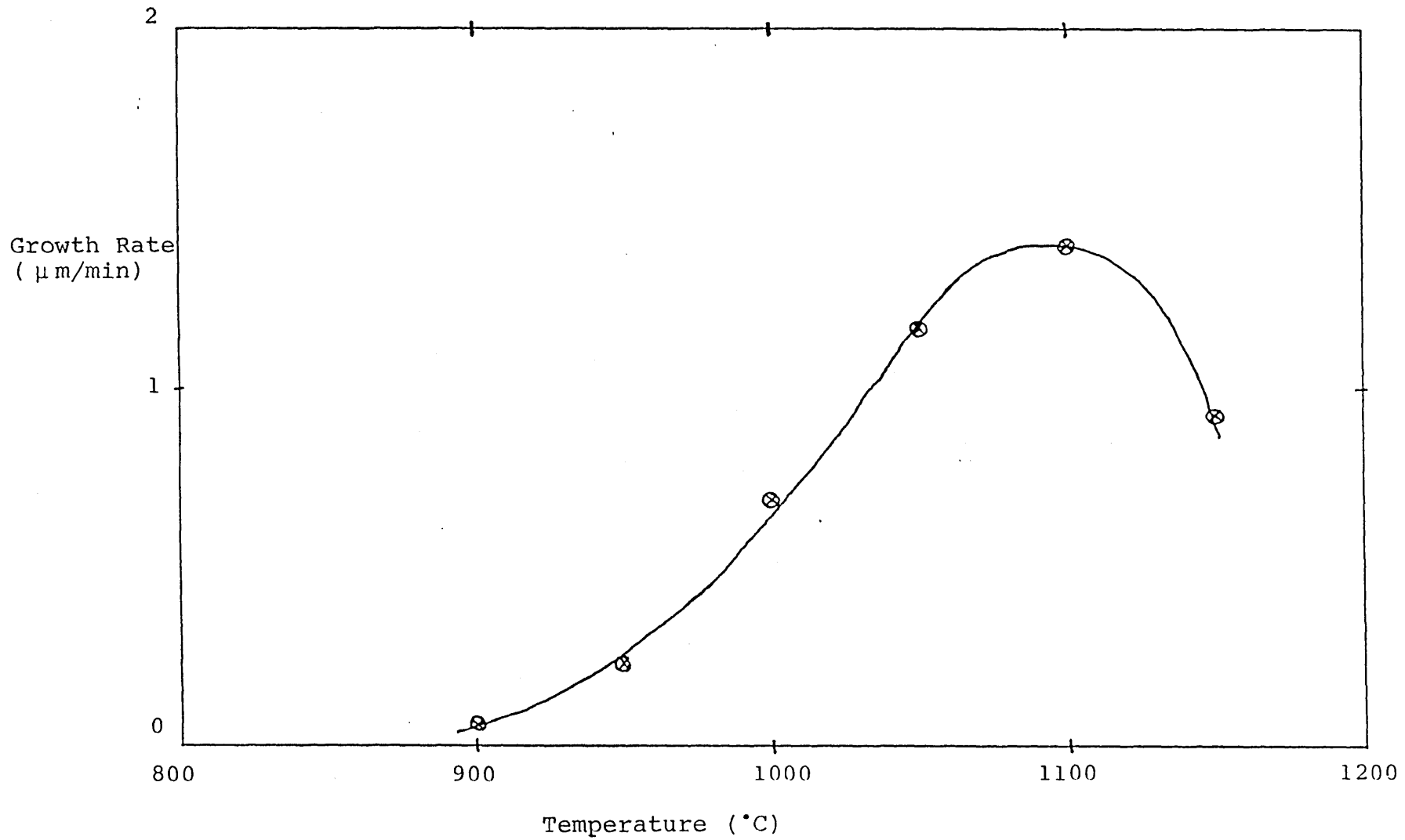


Figure 3.1 Variation in growth rate of  $\text{TiO}_2$  needles with temperature for J1 glass.

### 3.3 Electron Probe Microanalysis (EPMA) Results

EPMA was performed on selected partially crystalline samples in an attempt to show that niobium was predominantly associated with the rutile needles.

Table 3.3 shows such an analysis, with the numerical values representative of the relative peak intensities in arbitrary units. The data refers to the sample shown in Plate 3.2 which has undergone a phase separation treatment of 3 hours at 800°C followed by crystallisation at 1000°C for  $\frac{1}{2}$  hour.

Regions 3 and 4 represent scans attempted on rutile needles, whilst the remainder represent the glassy matrix. Analysis of the needles revealed the presence of both Ti and Nb but it is evident from the data that no direct relationship was found. As the resolution of the electron beam is 4-5  $\mu\text{m}$  then clearly with needles less than 1  $\mu\text{m}$  across the analysis will be representative of both the crystalline regions and the surrounding glassy matrix.

Table 3.3

EPMA analysis of partially crystalline J3 glass heat treated  
at 3 hours 800°C + 0.5 hours 1000°C

Region	Si	Al	Ca	Zn	Ti	Nb	Si/Ti	Si/Nb
1	28.4	10.1	13.9	1.0	5.8	1.1	4.9	25.8
2	55.1	19.3	23.8	1.0	9.5	1.5	5.8	36.7
3	71.2	24.8	34.8	1.0	14.9	2.3	4.8	31.0
4	67.5	23.5	34.7	1.0	14.8	1.9	4.6	35.5
5	47.3	14.9	25.2	1.0	10.4	1.4	4.5	33.8
6	36.8	11.7	20.2	1.0	8.0	0.8	4.6	46.0
7	106.0	35.3	48.1	1.0	19.0	3.0	5.6	35.3

The numerical values in the table refer to relative peak intensities given in arbitrary units.

### 3.4 DC Resistivity Results

Bulk dc resistivity measurements were performed on both the parent glass and the subsequently phase separated glassy specimens but there was no detectable electronic conduction. However, selectively partially crystallised specimens did exhibit electronic conduction and the resistivity values and heat treatment schedules are reported in tables 3.4 - 3.30 while figures 3.2 - 3.13 show the variation of  $\log_{10}$  resistivity with  $1000/\text{Temperature}$ . The values of the activation energy for electrical conduction were obtained directly from the plots of  $\log \rho$  against  $1/T$  using the following relationship based on the Arrhenius equation:

$$\text{slope} = \frac{E_a}{2.303R} \quad (3.0)$$

where  $E_a$  is the activation energy for conduction (KJ/mole) and  $R$  is the Universal gas constant ( $8.314 \text{ J}/^\circ\text{K mole}$ ).

For various partially crystalline samples, the values for the resistivity as a function of temperature are seen to lie on two intersecting straight line curves. Both the high and low temperature activation energies were calculated and are reported in the following tables when applicable.

In figure 3.13, the glass JS11 has the same composition as that of glass J11, but the  $\text{TiO}_2$  and  $\text{Nb}_2\text{O}_5$  have been initially heat treated together at  $1450^\circ\text{C}$  for 1 week to produce a solid solution; and this was added to the base glass formulation for glass preparation in the usual way



(Chapter 2). Similar treatments were performed for JS0 and JS6 which are based on J0 and J6 compositions respectively. Partially crystalline samples of JS11 glass were found to be electronically conducting as reported in figure 3.13 but there was no electronic conduction exhibited by any of the partially crystalline samples of JS0 or JS6 while the microstructure and crystalline phases present were typical of J0 and J6, respectively.

A few conducting samples were selected at random and their thickness reduced by about 25%. It was noted that the maximum change in  $\log_{10}\rho$  at room temperature was about 0.3%, thus suggesting that the contribution to surface conductivity was negligible.

The room temperature resistivity of crystallised J3 glasses as a function of length of rutile needles, the lengths being measured from SEM micrographs, is shown in figure 3.14.

The results indicate that both the parent glasses and the phase separated glasses, of all the compositions studied were non-conducting, as was also the case for partially crystalline samples of J0 glass which contained no  $\text{Nb}_2\text{O}_5$ .

However, phase separation followed by subsequent crystallisation allowed a fine dispersion of rutile needles to grow and for many glass compositions this resulted in a rapid increase in conductivity.

With prolonged heat treatment, a secondary non-conducting, crystalline phase, namely anorthite

(CaO.Al<sub>2</sub>O<sub>3</sub>.2SiO<sub>2</sub>) started to grow and eventually the conductivity of the specimens fell as the amount of anorthite increased. For 15wt% TiO<sub>2</sub> containing glasses the effect of heat treatment on the activation energy for conduction, E<sub>a</sub>, had a pronounced tendency towards increasing E<sub>a</sub> with increasing anorthite content. The effect was less marked for the 10wt% TiO<sub>2</sub> additions.

It is evident that the conductivity was related to the heat treatment and the size of rutile needles. However, specimens which had not undergone phase separation prior to crystallisation (eg J3/7) displayed a higher resistivity, presumably in accordance with their non-uniform dispersion of crystals and sizes, ie their microstructure.

However, some compositions which did in fact contain Nb<sub>2</sub>O<sub>5</sub> showed no signs of electronic conduction when subjected to a wide range of crystallisation heat treatments. These were J5, J6 and J7 which represented glasses containing 10wt% TiO<sub>2</sub> and 3.5, 4, and 6 wt% Nb<sub>2</sub>O<sub>5</sub>, respectively.

Heat treatment of J0 glass

Table 3.4

Sample	Heat treatment		Optical observation	Crystalline phases
	Time (hrs) at 800°C	+ Time (hrs) at 1000°C		
J0/1	3	0.25	Well crystalline. Stubby needles.	Rutile
J0/2	3	0.5	Highly crystalline	Rutile
J0/3	3	1	Highly crystalline	Rutile + trace An
J0/4	3	3	Highly crystalline	Rutile + An

Rutile =  $\text{TiO}_2$

An = Anorthite =  $\text{CaO} \cdot \text{Al}_2\text{O}_3 \cdot 2\text{SiO}_2$

Heat treatment of J1 glass

Table 3.5

Sample	Heat treatment		Optical observation	Crystalline phase
	Time (hrs) at 800°C	+ Time (hrs) at 1000°C		
J1/1	3	0.25	Finely crystalline. Many needles in a glassy matrix  ↓	Rutile
J1/2	3	0.5		Rutile
J1/3	3	1		Rutile + trace An
J1/4	3	2		Rutile + An
J1/5	3	3		Rutile + An
Sample	Heat treatment		Optical observation	Crystalline phase
	Time (hrs) at 800°C	+ Time (hrs) at 975°C		
J1/6	3	0.25	Stubby needles	Rutile
J1/7	3	0.5	Stubby needles	Rutile
J1/8	3	1	Stubby needles	Rutile
J1/9	3	3	Stubby needles	Rutile + trace An

Table 3.6

Electrical properties of partially crystalline  
samples of J1 glass

Sample	Room temperature/25°C	Activation energy for conduction	
	$\text{Log}_{10} \rho$	KJ/mole	eV
J1/1	5.72	15.79	0.16
J1/2	6.68	16.85	0.17
J1/3	7.00	17.52	0.18
J1/4	7.03	18.48	0.19
J1/5	6.55	15.70	0.16

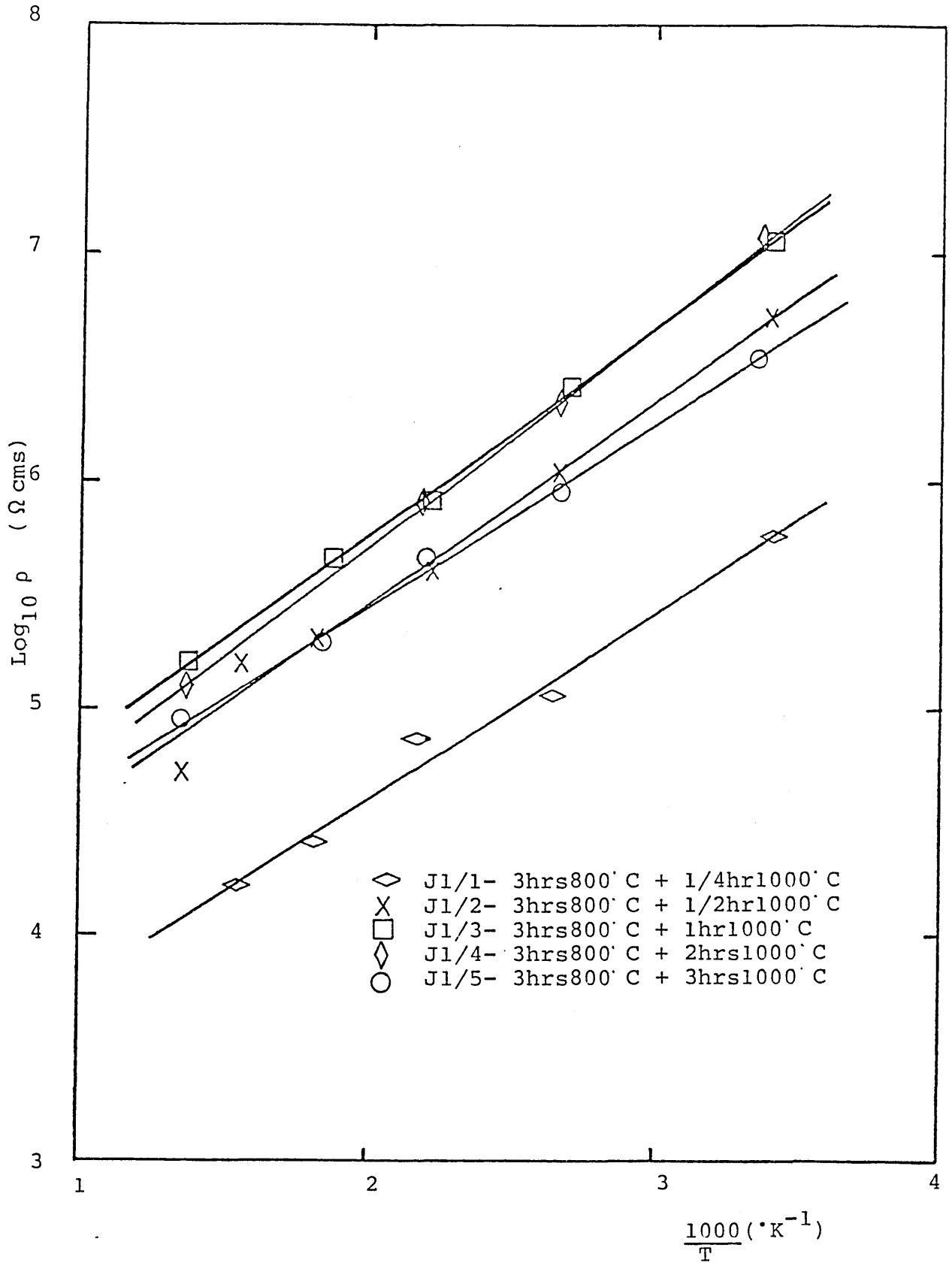


Figure 3.2 Plot of  $\log_{10}$  resistivity against  $1000/\text{temp.}$  for partially crystalline samples of J1 glass.

Table 3.7

Electrical properties of partially crystalline  
samples of J1 glass

Sample	Room temperature/25°C	Activation energy for conduction	
	Log <sub>10</sub> ρ	KJ/mole	eV
J1/6	-	-	-
J1/7	10.86	0.21	0.29
J1/8	9.18	0.21	0.21
J1/9	10.35	0.18	0.24

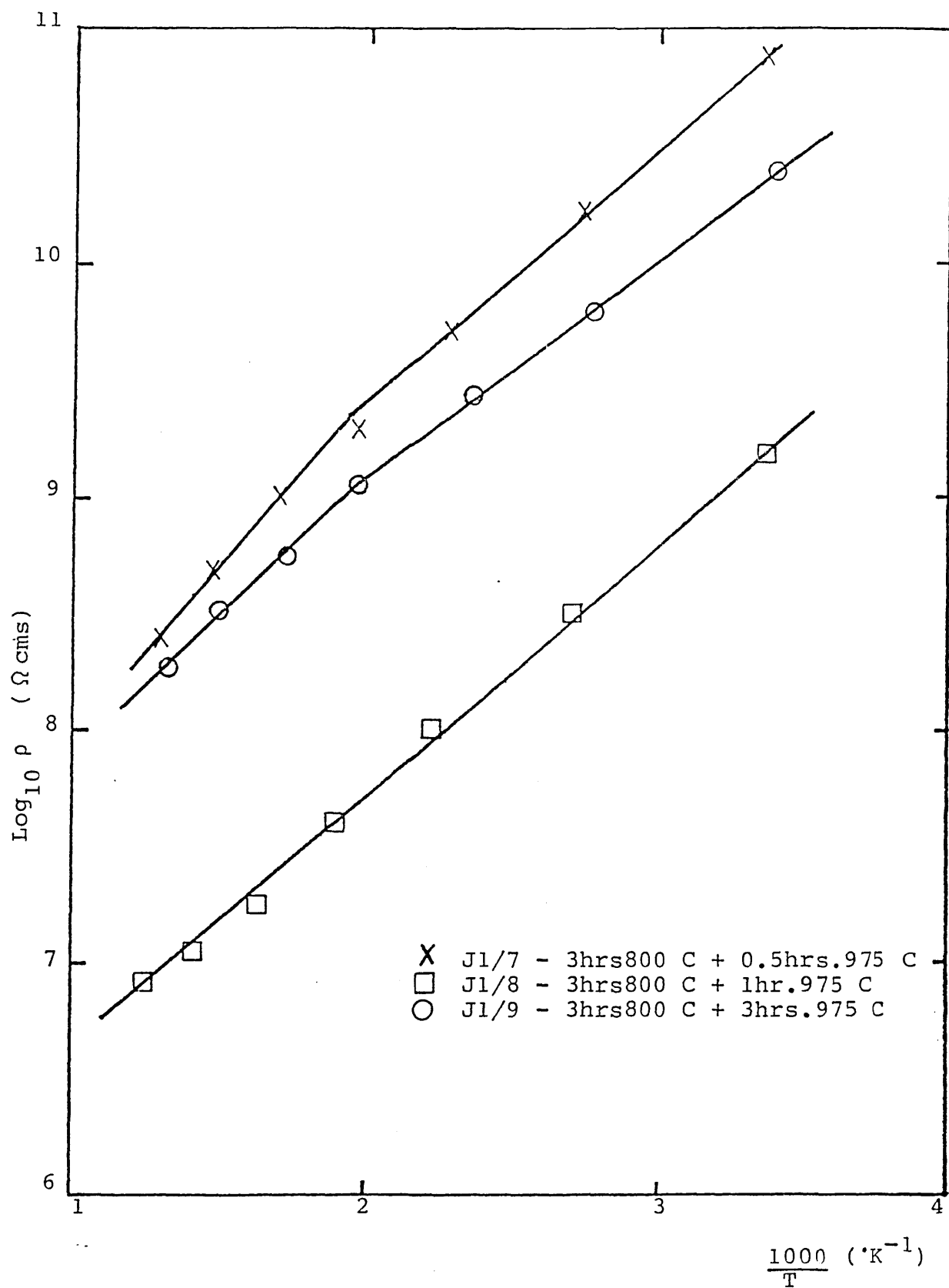


Figure 3.3 Plot of  $\log_{10}$  resistivity against  $1000/\text{temp}$  for partially crystalline samples of J1 glass.



Table 3.8

Heat treatment of J2 glass

Sample	Heat treatment		Optical observation	Crystalline phase
	Time (hrs) at 800°C	+ Time (hrs) at 1000°C		
J2/1	3	0.25	Fine dispersion of needles	Rutile
J2/2	3	0.5	Well crystalline	Rutile
J2/3	3	1	Well crystalline	Rutile + trace An
J2/4	3	3	Highly crystalline	Rutile + An

Table 3.9

Electrical properties of partially crystalline samples of J2 glass

Sample	Room temperature/ 25°C Log <sub>10</sub> ρ	Activation energy for conduction	
		Low temp slope (eV)	High temp slope (eV)
J2/1	-	-	-
J2/2	10.14	0.24	0.55
J2/3	8.06	0.13	0.49
J2/4	8.51	0.18	0.28

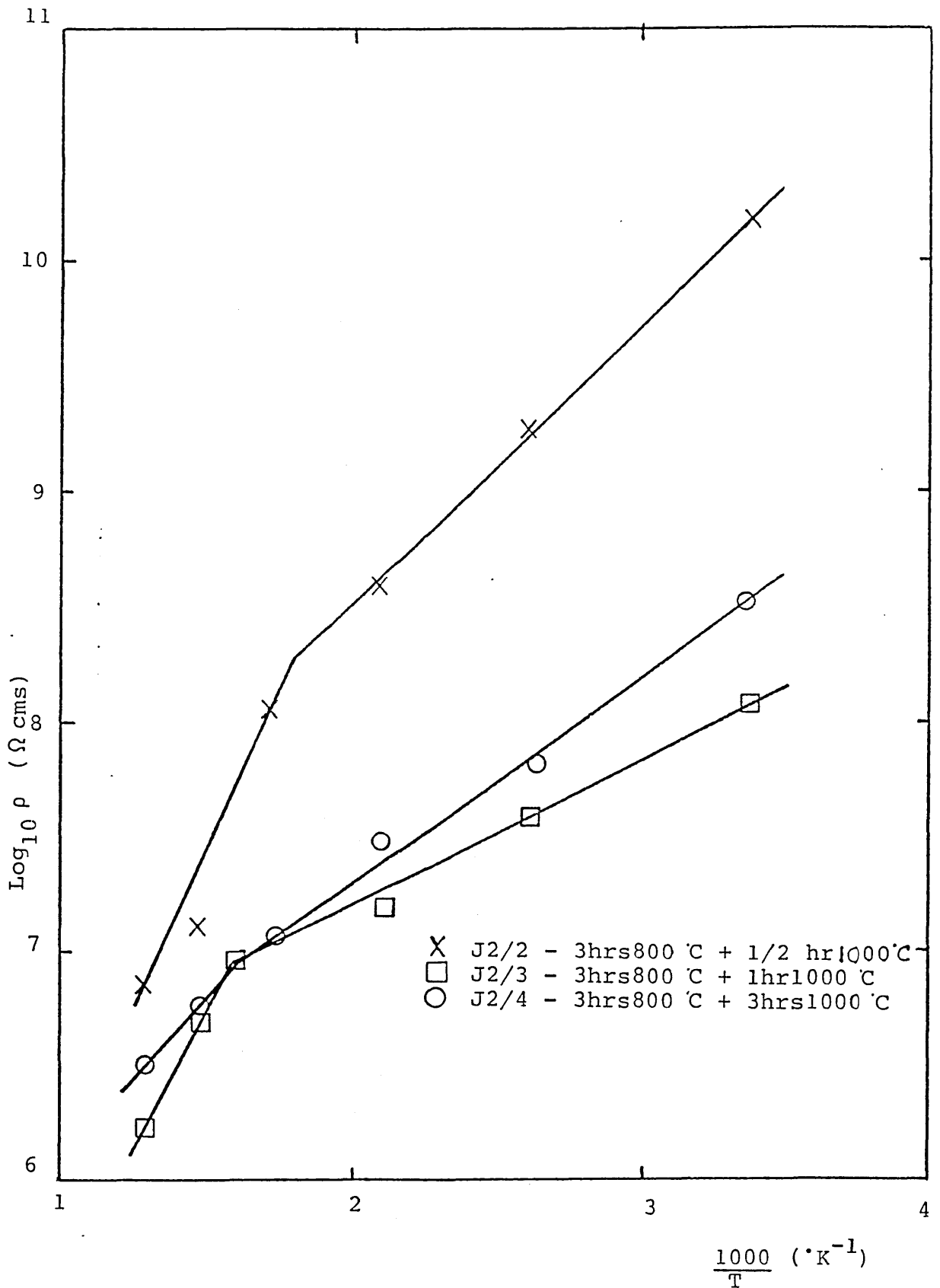


Figure 3.4 Plot of  $\log_{10}$  resistivity against  $1000/\text{temp}$  for partially crystalline samples of J2 glass.

Table 3.10

Heat treatment of J3 glass

Sample	Heat treatment		Optical observation	Crystalline phases
	Time (hrs) at 800°C	+ Time (hrs) at 1000°C		
J3/1	3	0.25	Fine crystalline structure	Rutile
J3/2	3	0.5	Finely crystalline	Rutile
J3/3	3	1	Well crystalline	Rutile + trace An
J3/4	3	3	Large needles	Rutile + An
J3/5	18	0.25	Fine, stubby needles	Rutile
J3/6	18	0.5	Finely crystalline	Rutile
J3/7	0	1	Large distribution of needle sizes	Rutile + trace An

Table 3.11

Electrical properties of partially crystalline samples  
of J3 glass

Sample	Room temperature/ 25°C Log <sub>10</sub> ρ	Activation energy for conduction	
		Low temp slope (eV)	High temp slope (eV)
J3/1	-	-	-
J3/2	8.72	0.18	0.39
J3/3	7.99	0.19	0.33
J3/4	6.17	0.19	0.31
J3/5	10.79	0.14	0.35
J3/6	8.45	0.26	0.26
J3/7	10.69	0.22	0.35

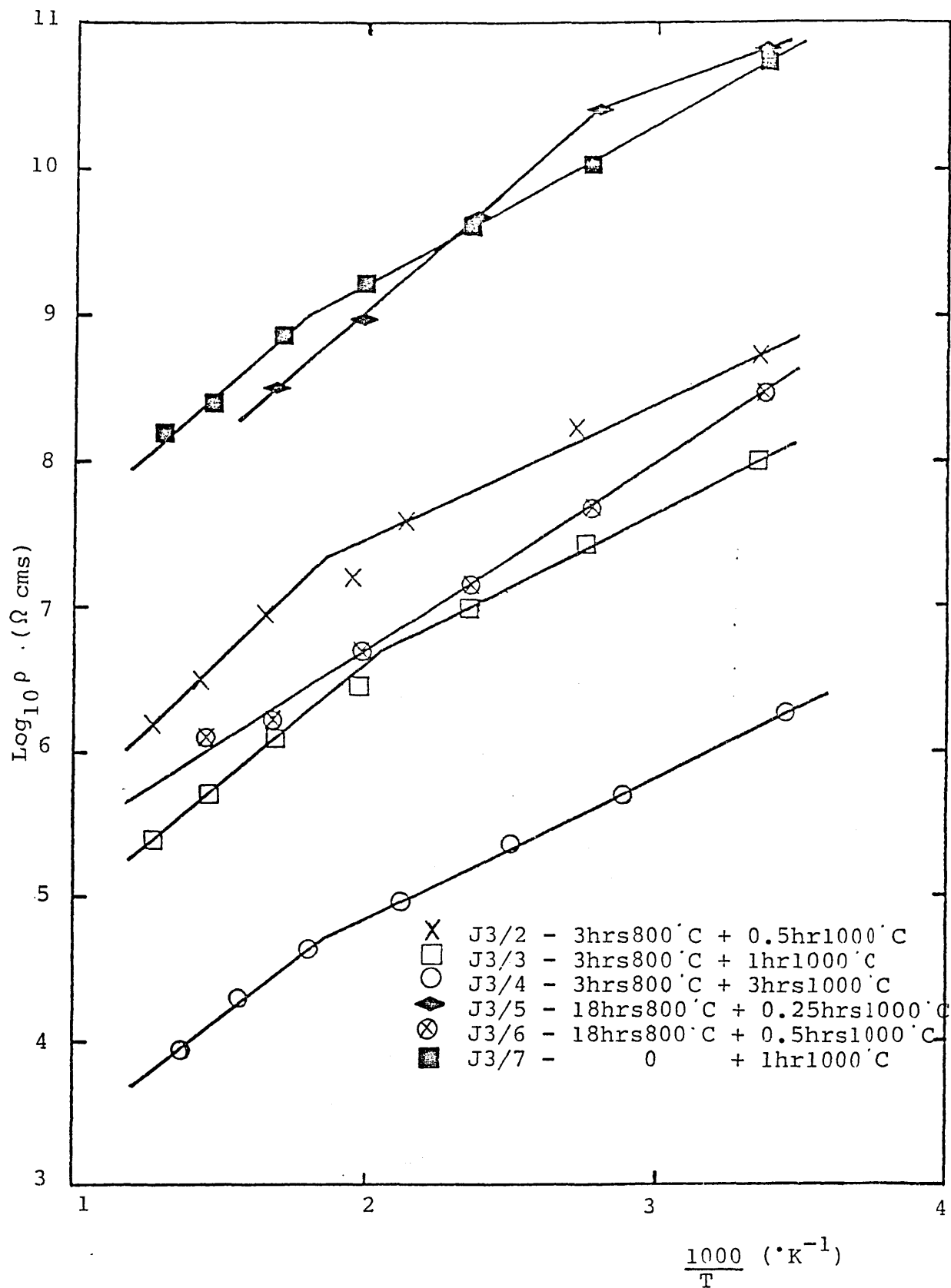


Figure 3.5 Plot of  $\log_{10}$  resistivity against  $1000/\text{temp}$  for partially crystalline samples of J3 glass.

Table 3.12            Heat treatment of J4 glass

Sample	Heat treatment		Optical observation	Crystalline phases
	Time (hrs) at 800°C	+ Time (hrs) at 1000°C		
J4/1	3	0.25	Fine needles	Rutile
J4/2	3	0.5	Fine needles	Rutile
J4/3	3	1	Fine needles	Rutile
J4/4	3	2	Fine needles	Rutile + trace An
J4/5	3	3	Fine needles	Rutile + trace An

Table 3.13

Electrical properties of partially crystalline samples  
of J4 glass

Sample	Room temperature/ 25°C Log <sub>10</sub> ρ	Activation energy for conduction	
		Low temp slope (eV)	High temp slope (eV)
J4/1	8.56	0.26	0.43
J4/2	9.70	0.26	0.45



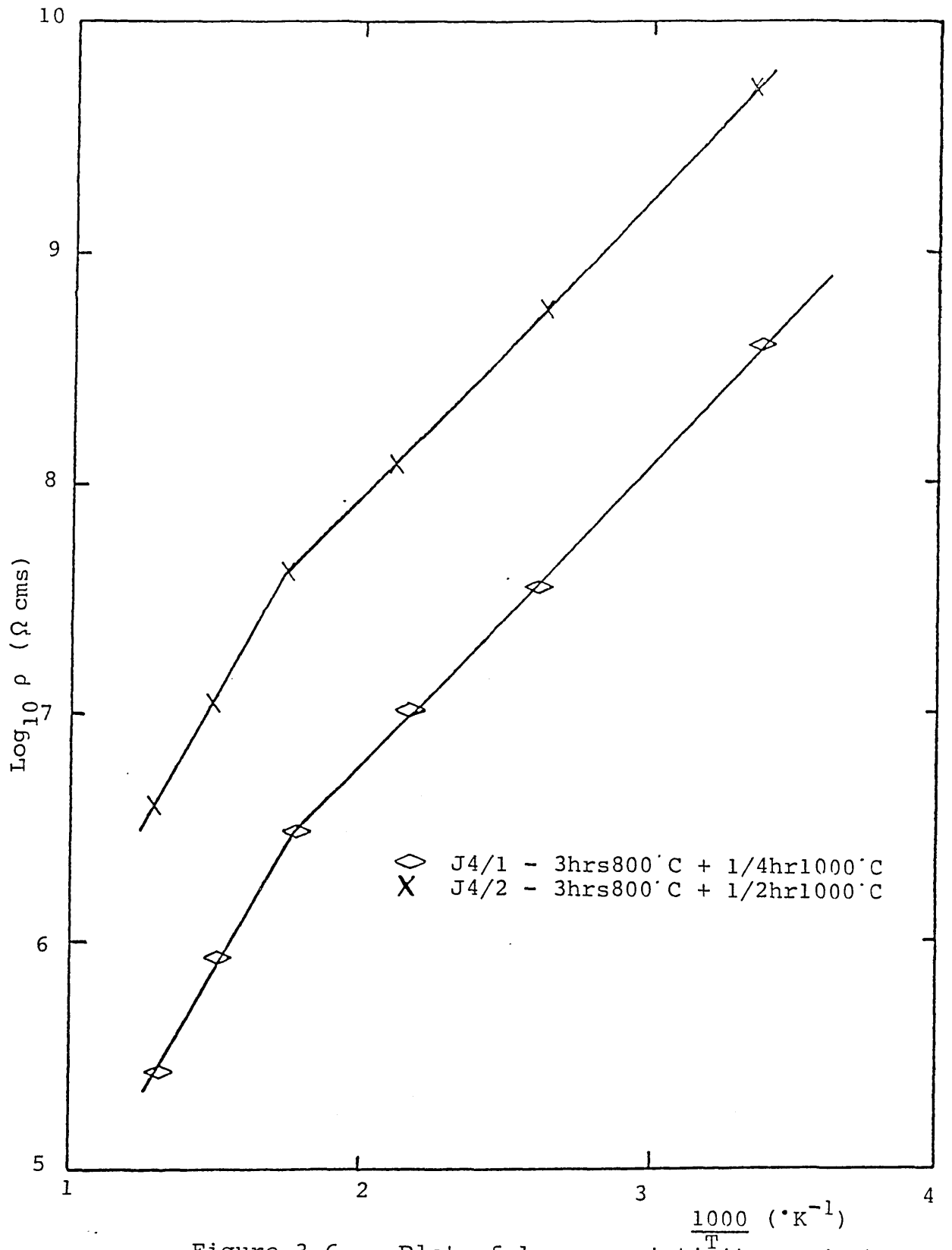


Figure 3.6 Plot of  $\log_{10}$  resistivity against  $1000/\text{temp}$  for partially crystalline samples of J4 glass.

Table 3.14

Heat treatment of J5 glass

Sample	Heat treatment		Optical observation	Crystalline phase
	Time (hrs) at 800°C	+ Time (hrs) at 1000°C		
J5/1	3	0.25	Finely crystalline. Needles in glassy matrix	Rutile
J5/2	3	0.5	↓	Rutile
J5/3	3	1		Rutile
J5/4	3	2		Rutile + trace An
J5/5	3	3		Rutile + An

Table 3.15

Heat treatment of J6 glass

Sample	Heat treatment		Optical observation	Crystalline phases
	Time (hrs) at 800°C	+ Time (hrs) at 1000°C		
J6/1	3	0.25	Fine, stubby needles	Rutile
J6/2	3	0.5	Fine, stubby needles	Rutile
J6/3	3	0.75	Fine, stubby needles	Rutile
J6/4	3	1	Many stubby needles	Rutile
J6/5	3	2	Many stubby needles	Rutile + An
J6/6	3	3	Many stubby needles	Rutile + An

Table 3.16

Heat treatment of J7 glass

Sample	Heat treatment		Optical observation	Crystalline phases
	Time (hrs) at 800°C	+ Time (hrs) at 1000°C		
J7/1	3	0.25	Fine, stubby needles	Rutile
J7/2	3	0.5	Many stubby needles	Rutile
J7/3	3	1	Many stubby needles	Rutile
J7/4	3	2	Many stubby needles	Rutile + trace An
J7/5	3	3	Many stubby needles	Rutile + An

Table 3.17

Heat treatment of J8 glass


Sample	Heat treatment		Optical observation	Crystalline phases
	Time (hrs) at 800°C	+ Time (hrs) at 1000°C		
J8/1	3	0.25	Finely crystalline	Rutile
J8/2	3	0.5		Rutile
J8/3	3	1		Rutile + trace An
J8/4	3	2		Rutile + An
J8/5	3	3		Rutile + An

Table 3.18

Electrical properties of partially crystalline samples of J8  
glass

Sample	Room temperature/ 25°C Log <sub>10</sub> ρ	Activation energy for conduction KJ/mole	eV
J8/1	8.18	21.25	0.22
J8/2	7.77	22.59	0.23
J8/3	7.39	20.20	0.21
J8/4	7.92	24.32	0.25
J8/5	9.68	Low temp 52.08 High temp 18.00	0.54 0.19

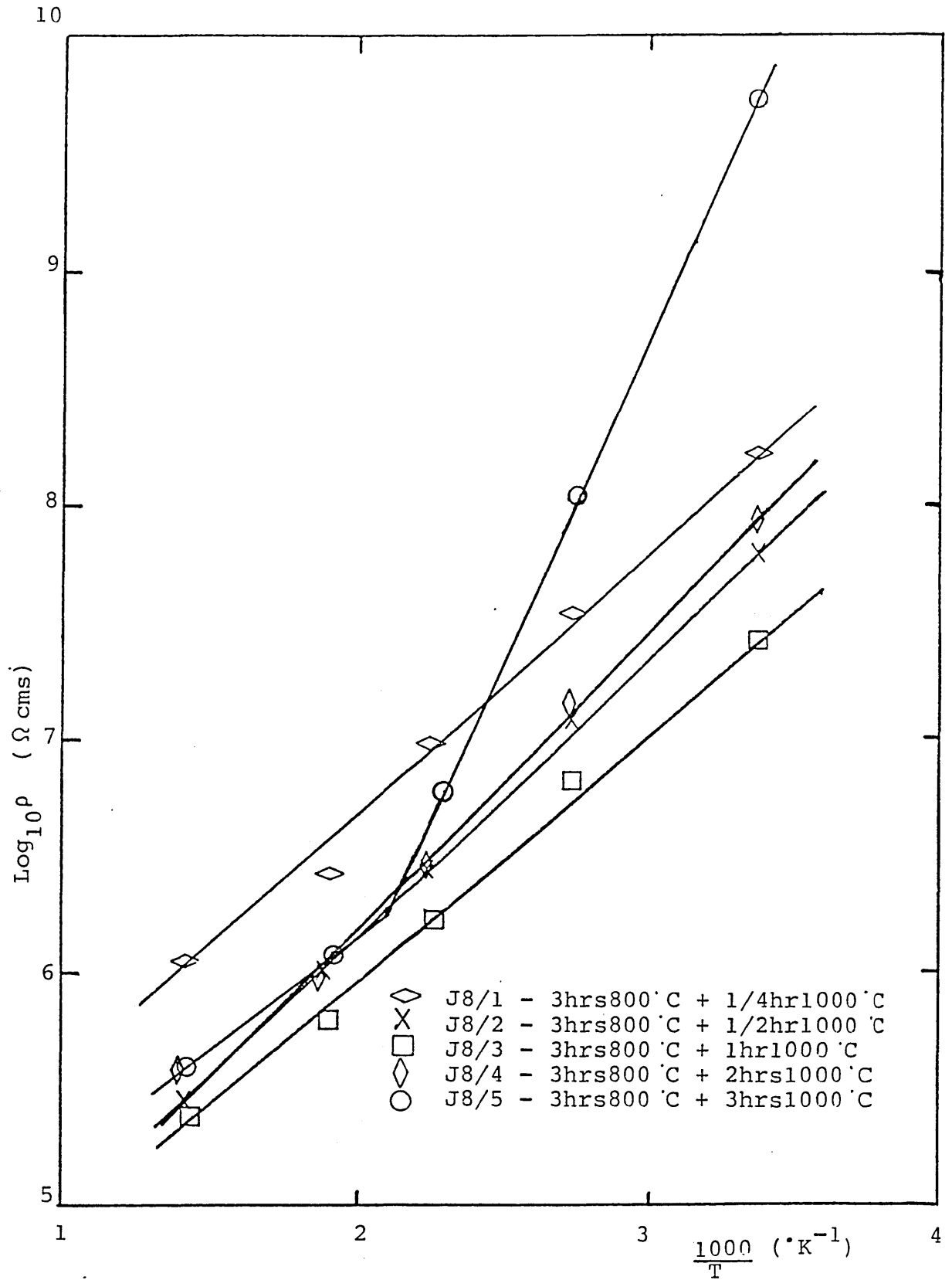


Figure 3.7 Plot of  $\log_{10}$  resistivity against  $1000/\text{temp}$  for partially crystalline samples of J8 glass.

Table 3.19

Heat treatment of J9 glass

Sample	Heat treatment		Optical observation	Crystalline phases
	Time (hrs) at 800°C	+ Time (hrs) at 1000°C		
J9/1	3	0.25	Finely crystalline	Rutile
J9/2	3	0.5	Finely crystalline	Rutile
J9/3	3	1	Finely crystalline	Rutile
J9/4	3	2	Finely crystalline	Rutile + trace An
J9/5	3	3	Finely crystalline	Rutile + An



Table 3.20

Electrical properties of partially crystalline samples of J9  
glass

Sample	Room temperature/ 25°C Log <sub>10</sub> ρ	Activation energy for conduction KJ/mole	eV
J9/1	6.90	19.34	0.20
J9/2	6.72	17.81	0.18
J9/3	6.76	18.29	0.19
J9/4	6.38	17.14	0.18
J9/5	8.24	27.19	0.28

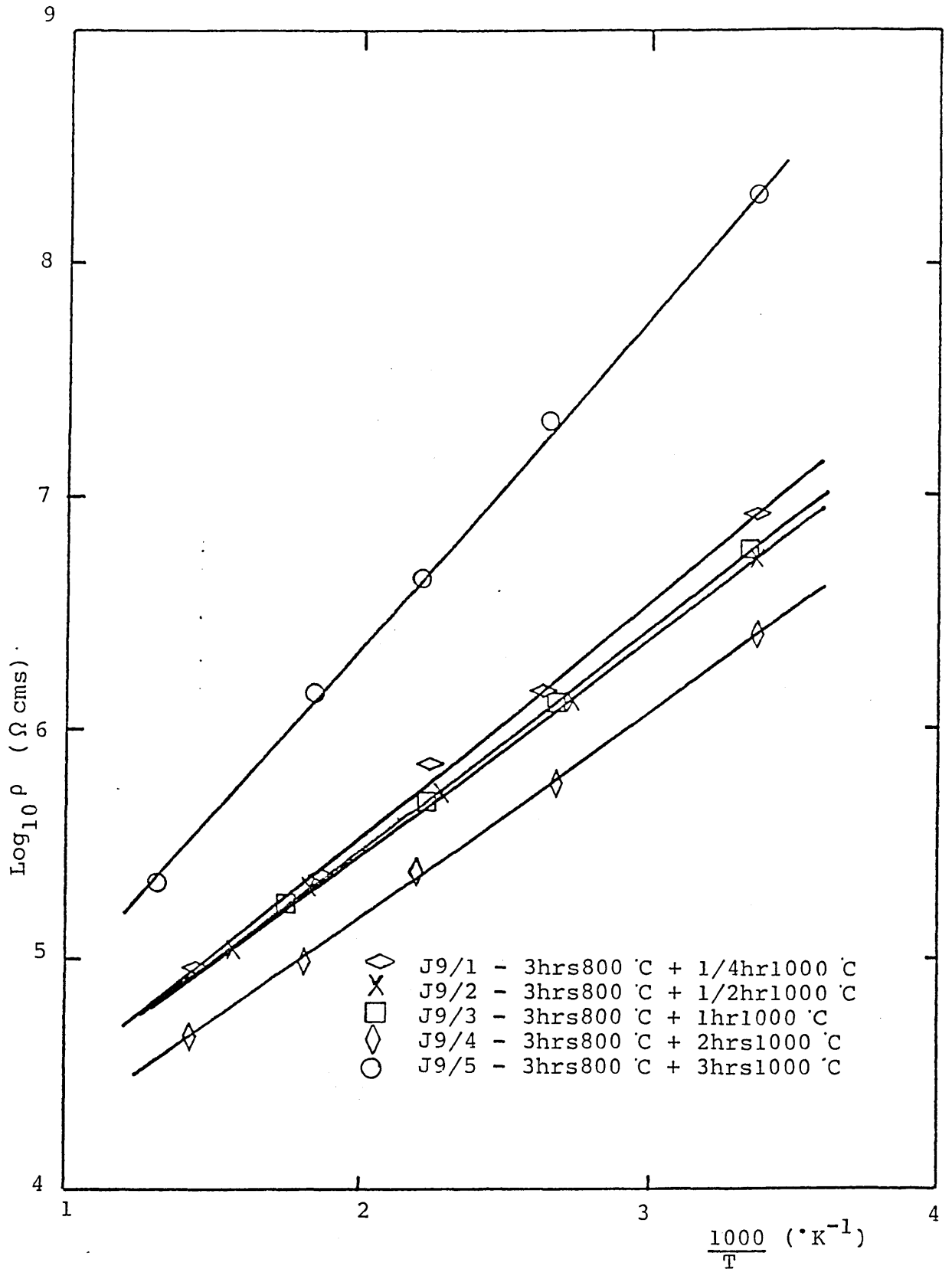


Figure 3.8 Plot of  $\log_{10}$  resistivity against  $1000/\text{temp}$  for partially crystalline samples of J9 glass.

Table 3.21

Heat treatment of J10 glass

Sample	Heat treatment		Optical observation	Crystalline phase
	Time (hrs) at 800°C	+ Time (hrs) at 1000°C		
J10/1	3	0.25	Highly crystalline	Rutile
J10/2	3	0.5	Highly crystalline	Rutile
J10/3	3	1	Highly crystalline	Rutile
J10/4	3	3	Highly crystalline	Rutile + trace An

Table 3.22

Electrical properties of partially crystalline samples of  
J10 glass

Sample	Room temperature/ 25°C Log <sub>10</sub> ρ	Activation energy for conduction KJ/mole	eV
J10/1	7.10	20.30	0.21
J10/2	7.03	21.06	0.22
J10/3	6.62	20.49	0.21
J10/4	6.86	21.25	0.22

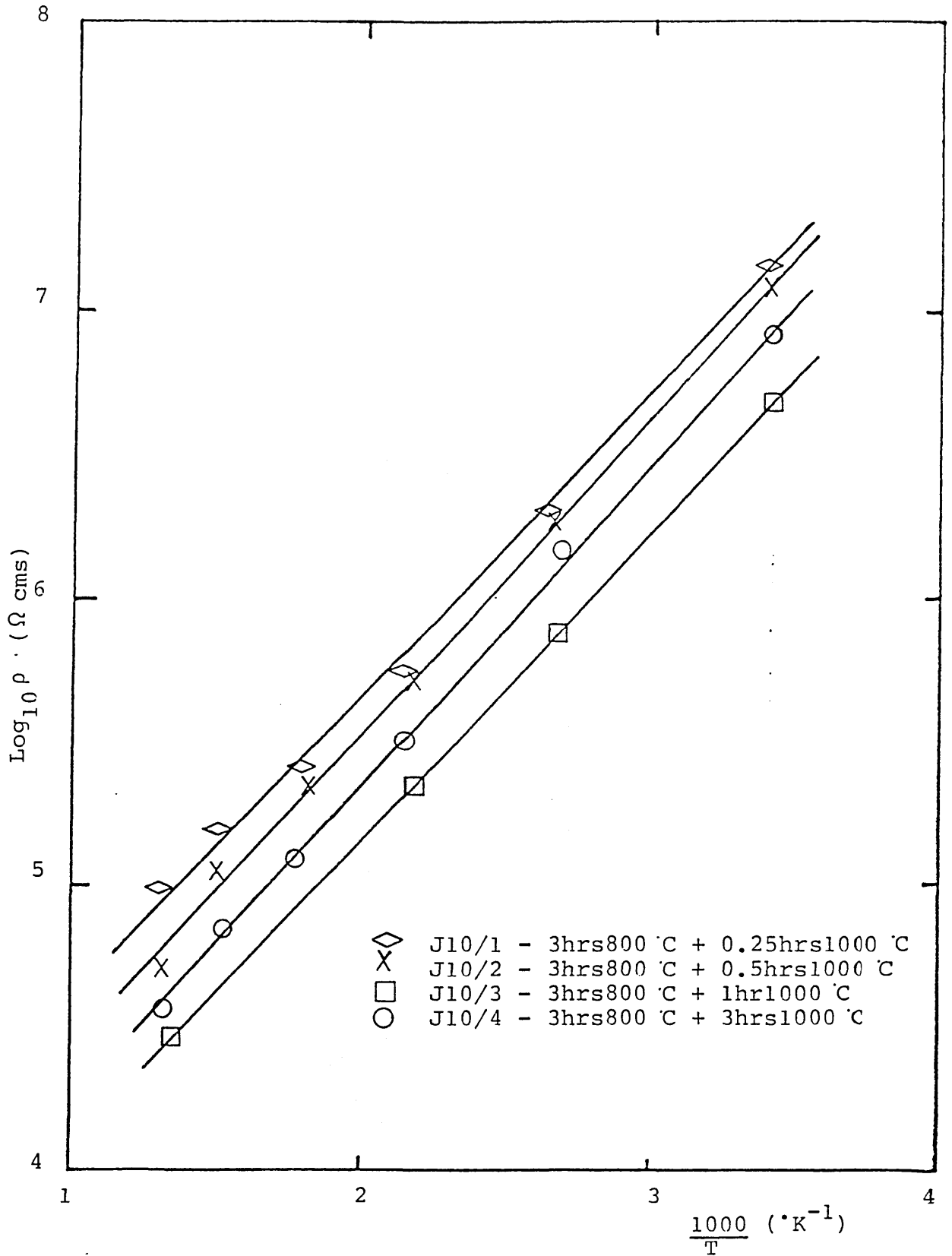


Figure 3.9 Plot of  $\log_{10}$  resistivity against  $1000/\text{temp}$  for partially crystalline samples of J10 glass.

Table 3.23

Heat treatment of J11 glass

Sample	Heat treatment		Optical observation	Crystalline phases
	Time (hrs) at 800°C	+ Time (hrs) at 1000°C		
J11/1	3	0.25	Finely crystalline, many needles	Rutile
J11/2	18	0.25	Finely crystalline	Rutile
J11/3	18	0.5	Finely crystalline	Rutile
J11/4	18	3	Highly crystalline	Rutile + trace An
J11/5	0	3	Highly crystalline	Rutile + An

Table 3.24

Electrical properties of partially crystalline samples of  
J11 glass

Sample	Room temperature/ 25°C Log <sub>10</sub> ρ	Activation energy for conduction	
		Low temp slope (eV)	High temp slope (eV)
J11/1	8.72	0.24	0.35
J11/2	8.57	0.27	0.40
J11/3	8.23	0.26	0.39
J11/4	9.02	0.28	0.37
J11/5	9.47	0.35	0.35

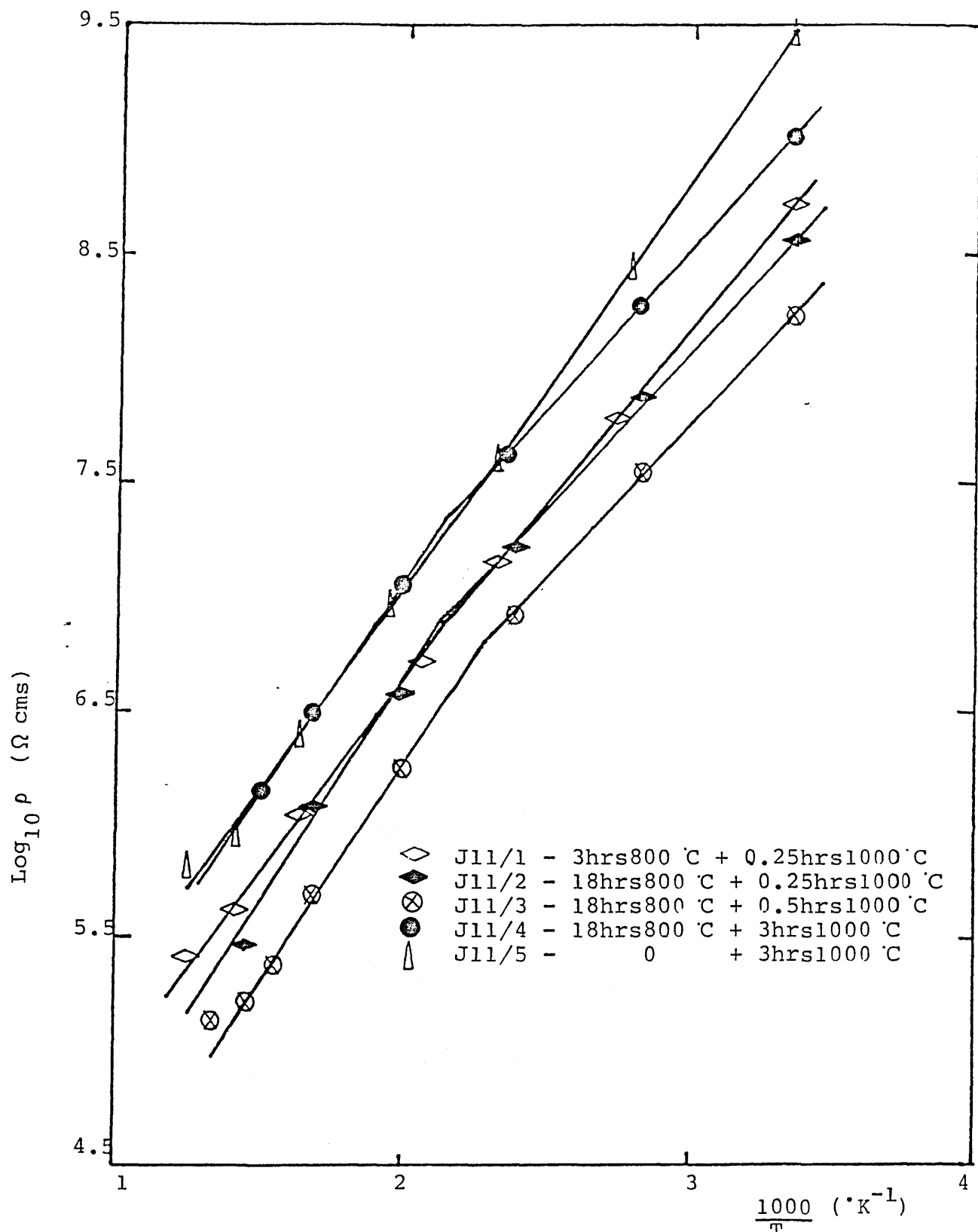


Figure 3.10 Plot of  $\log_{10}$  resistivity against  $1000/T$  for partially crystalline samples of J11 glass.



Table 3.25

Heat treatment of J12 glass

Sample	Heat treatment		Optical observation	Crystalline phases
	Time (hrs) at 800°C	+ Time (hrs) at 1000°C		
J12/1	3	0.25	Finely crystalline, Needles in glassy matrix	Rutile
J12/2	3	0.5	↓	Rutile
J12/3	3	1		Rutile
J12/4	3	2		Rutile
J12/5	3	3		Rutile + trace An

Table 3.26

Electrical properties of partially crystalline samples of  
J12 glass

Sample	Room temperature/ 25°C Log <sub>10</sub> ρ	Activation energy for conduction	
		Low temp slope (eV)	High temp slope (eV)
J12/3	9.12	0.24	0.24
J12/4	9.36	0.26	0.26
J12/5	9.43	0.26	0.41

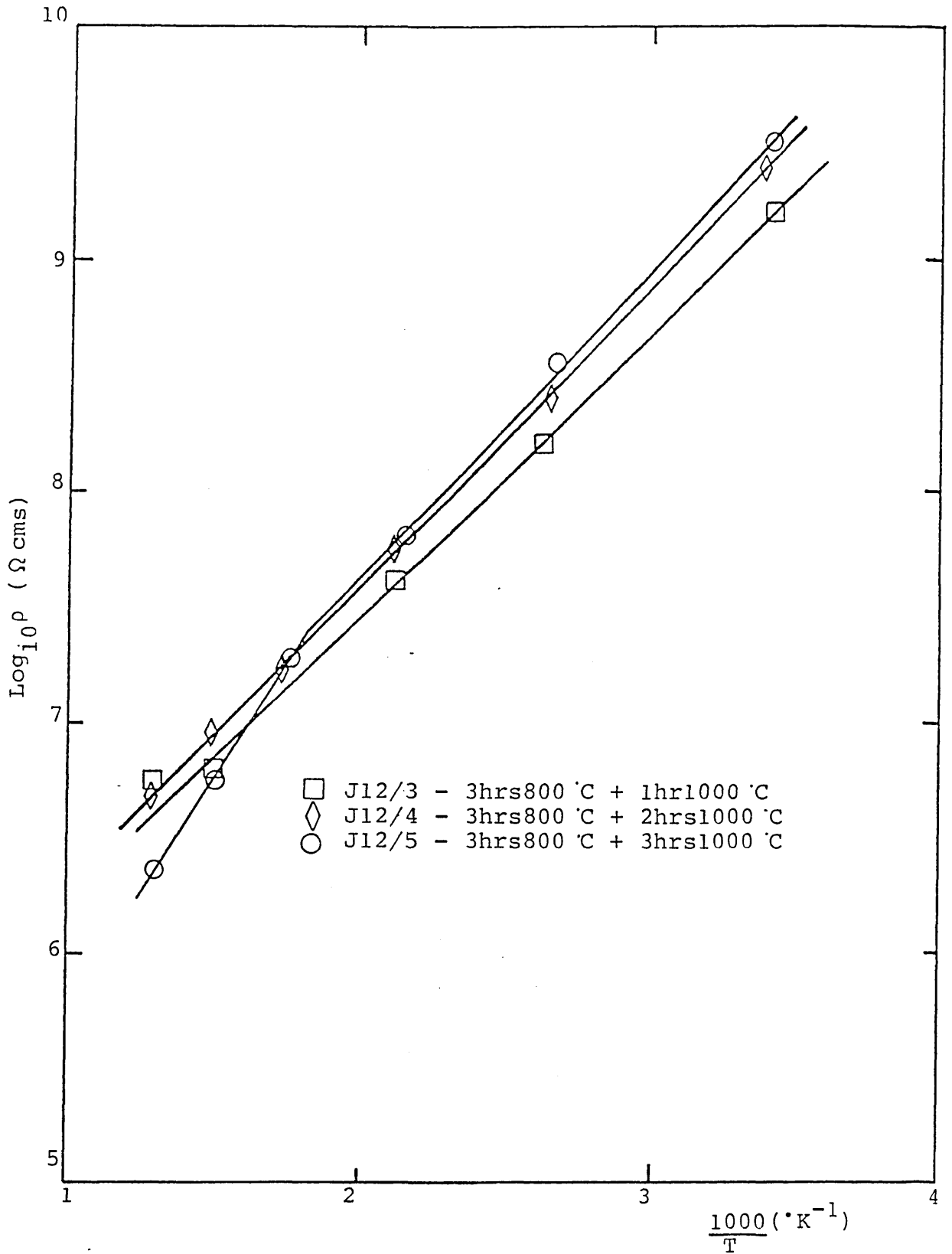


Figure 3.11 Plot of  $\log_{10}$  resistivity against  $1000/\text{temp}$  for partially crystalline samples of J12 glass.

Table 3.27

Heat treatment of J13 glass

Sample	Heat treatment		Optical observation	Crystalline phases
	Time (hrs) at 800°C	+ Time (hrs) at 1000°C		
J13/1	3	0.25	Many stubby needles	Rutile
J13/2	3	0.5	Many stubby needles	Rutile
J13/3	3	1	Many stubby needles	Rutile + trace An
J13/4	3	3	Many stubby needles	Rutile + An

Table 3.28

Electrical properties of partially crystalline samples of  
J13 glass

Sample	Room temperature/ 25°C Log <sub>10</sub> ρ	Activation energy for conduction KJ/mole	(eV)
J13/1	6.72	16.08	0.17
J13/2	6.49	20.68	0.21
J13/3	7.24	27.00	0.28
J13/4	11.58	58.78	0.61

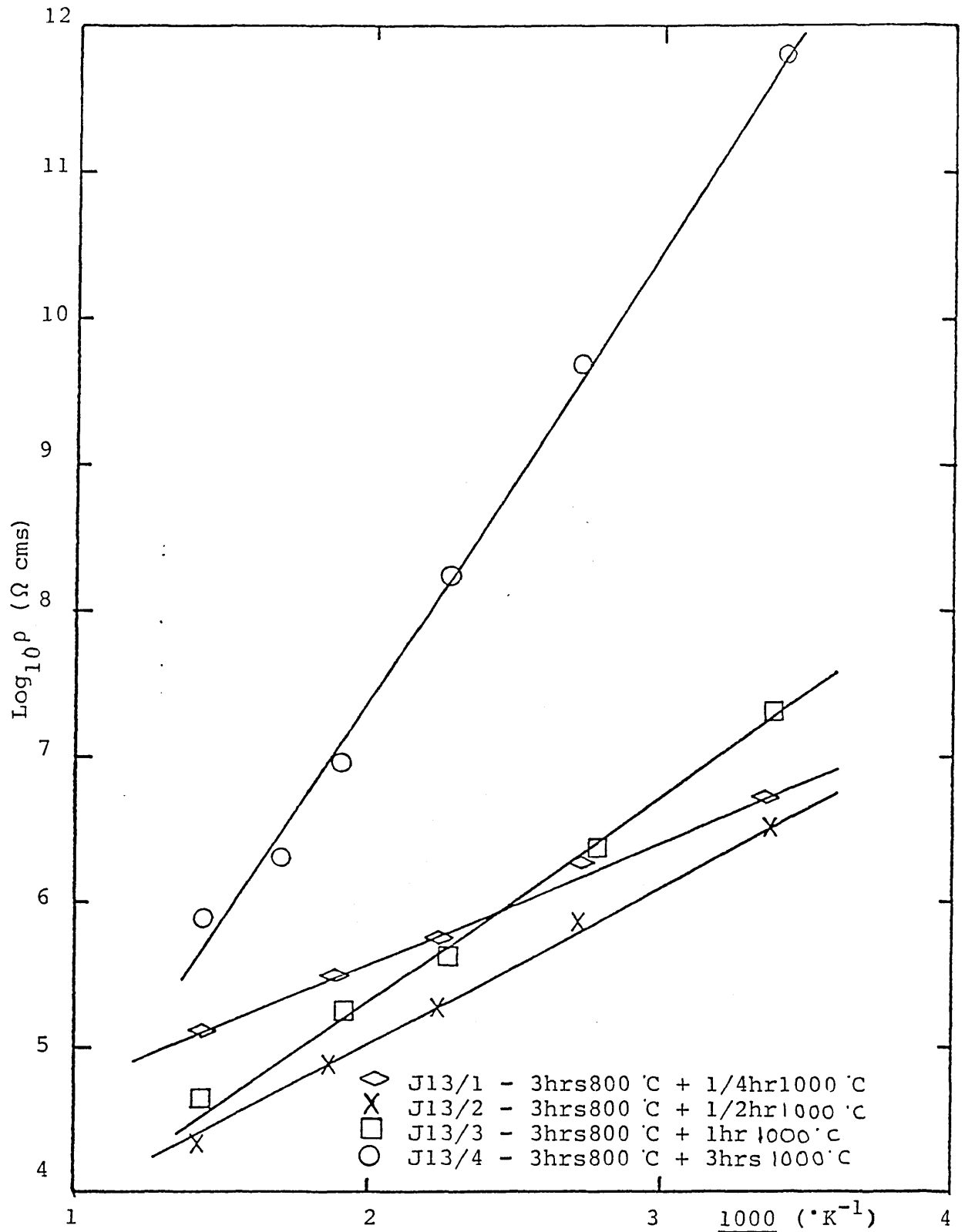


Figure 3.12 Plot of  $\log_{10}$  resistivity against  $1000/\text{temp}$  for partially crystalline samples of J13 glass.

Table 3.29

Heat treatment of JS11 glass

Sample	Heat treatment		Optical observation	Crystalline phase
	Time (hrs) at 800°C	+ Time (hrs) at 1000°C		
JS11/1	3	0.25	Highly crystalline, many needles in a glassy matrix	Rutile
JS11/2	3	0.5	↓	Rutile
JS11/3	3	1		Rutile
JS11/4	3	3		Rutile + trace An

Table 3.30

Electrical properties of partially crystalline samples of  
JS11 glass

Sample	Room temperature/ 25°C Log <sub>10</sub> ρ	Activation energy for conduction	
		Low temp slope (eV)	High temp slope (eV)
JS11/1	8.00	0.23	0.44
JS11/2	8.10	0.24	0.40
JS11/3	7.89	0.29	0.42
JS11/4	9.63	0.42	0.42



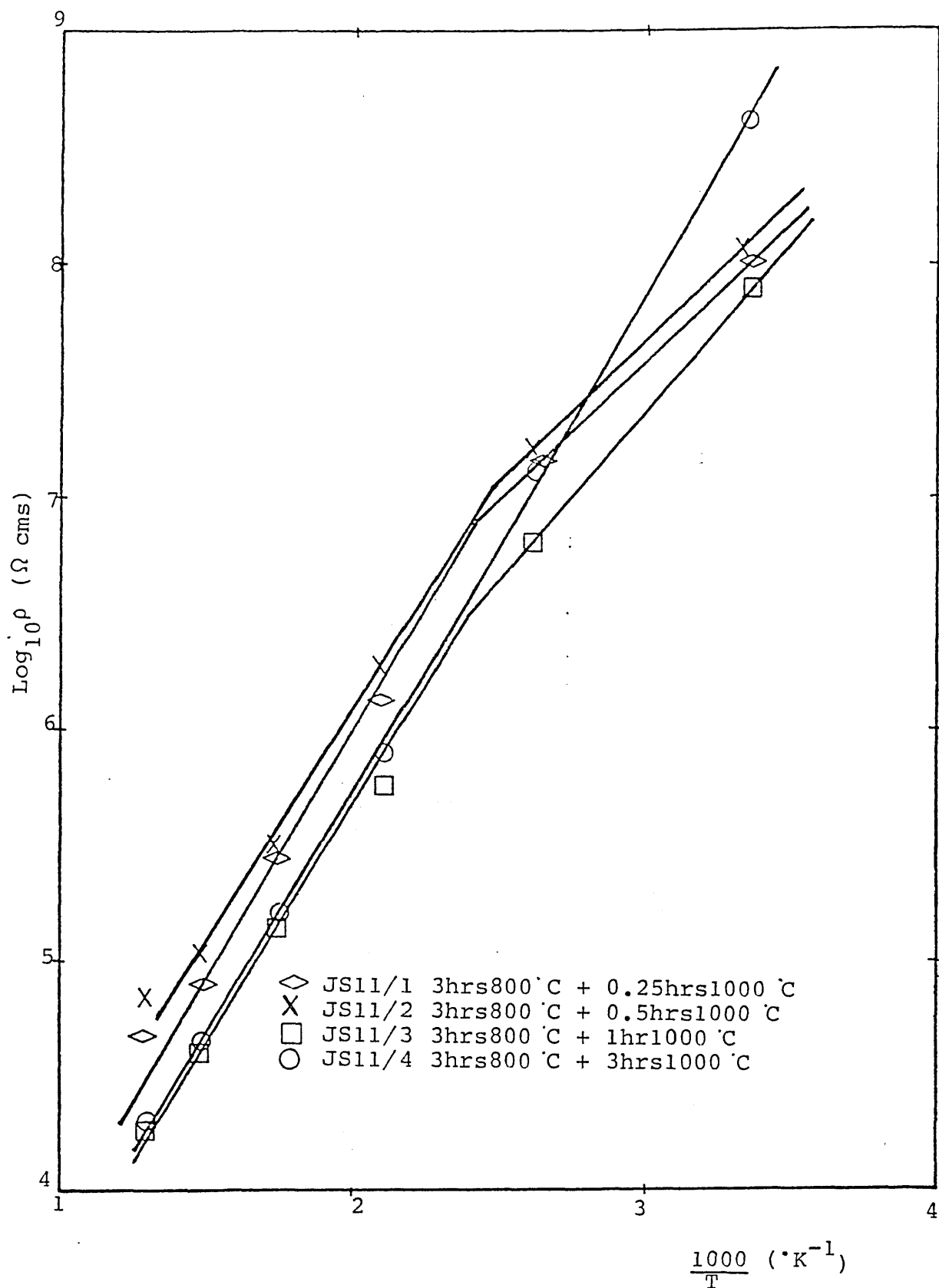


Figure 3.13 Plot of  $\log_{10}$  resistivity against  $1000/\text{temp}$  for partially crystalline samples of JS11 glass.

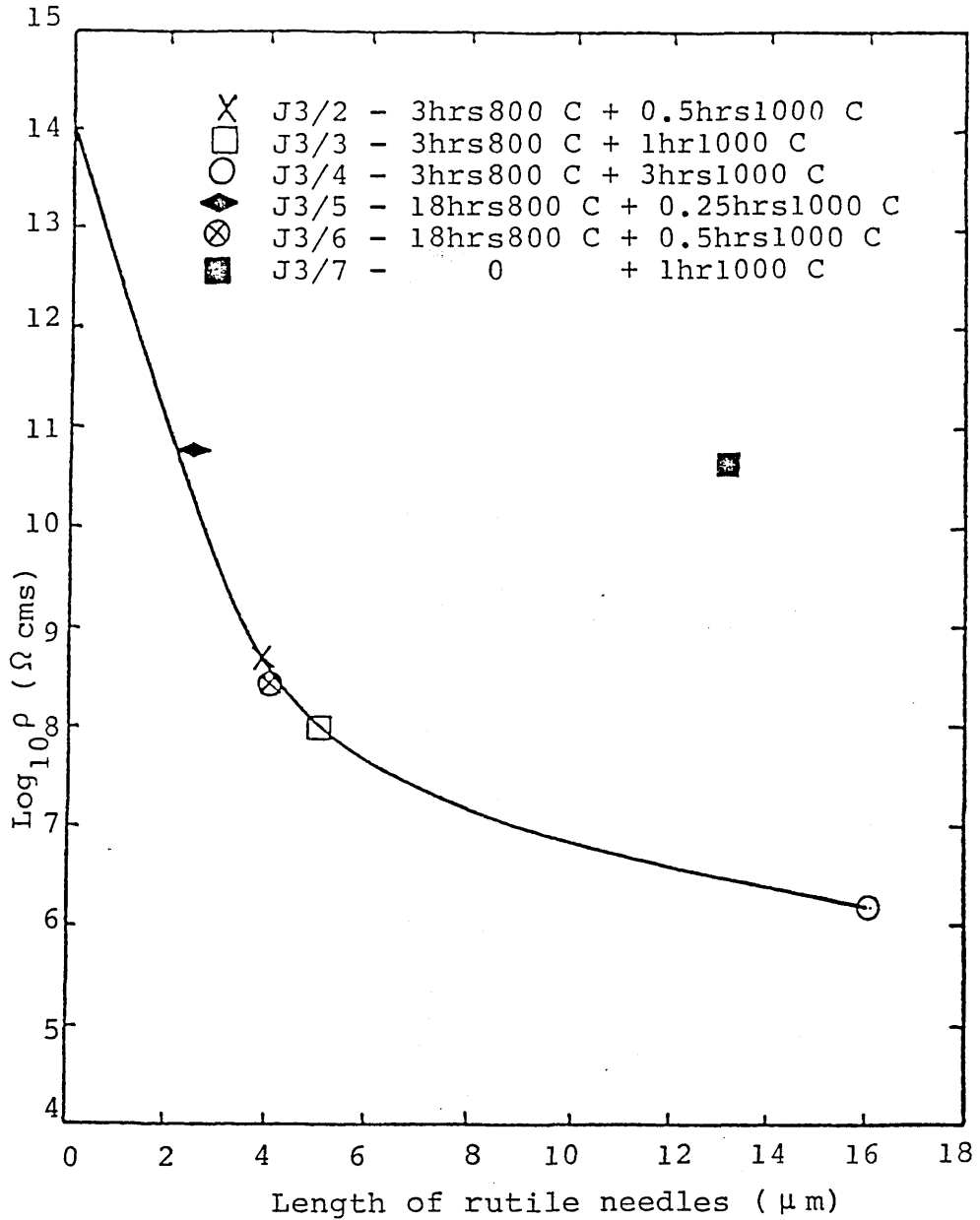


Figure 3.14 Room temperature resistivity of crystallised J3 glass as a function of length of rutile needles. All samples, except J3/7, phase separated prior to crystallisation.

### 3.5 TiO<sub>2</sub>/Nb<sub>2</sub>O<sub>5</sub> Solid Solution Results

The composition of the solid solution samples prepared is shown in table 3.31. A Philips diffractometer was used to detect the small changes in the lattice parameters of the solid solutions. Specific values of  $2\theta^\circ$ , corresponding to lines on the diffraction pattern, were chosen and the lattice spacing,  $d$ , determined using the Bragg Equation:

$$d = \frac{n \lambda}{2 \sin \theta} \quad (3.1)$$

where  $\lambda$  is the wavelength of radiation used (Cu K  $\alpha_1$  = 1.54051 Å and Cu K  $\alpha_2$  , = 1.54434 Å). Values of "d" were obtained from both the  $\alpha_1$  and  $\alpha_2$  diffraction lines and subsequently substituted into the following equation for a crystal with a tetragonal unit cell (eg rutile):

$$\frac{1}{d^2} = \frac{h^2 + k^2}{a^2} + \frac{l^2}{c^2} \quad (3.2)$$

where "a" and "c" are the lattice parameters and h, k and l are the Miller Indices of the plane.

To evaluate the lattice parameter, " $a_0$ ", the requirement was that the particular value of "d" chosen was such that it corresponded to the situation were:

$$hkl = hk0 \quad (3.3)$$

ie lines where "l" was zero. For this purpose the (330), (420), (510) and (440) reflections were chosen. Hence a series of " $a_0$ " values were obtained which were then plotted against  $f(\theta)$ , as shown in figure 3.15(a) and figure

3.16(a), where:

$$f(\theta) = \frac{\cos^2 \theta}{\sin \theta} + \frac{\cos^2 \theta}{\theta} \quad (3.4)$$

The straight line plots were extrapolated back to  $f(\theta) = 0$  to obtain absolute values of " $a_0$ ".

For determination of absolute values of " $c_0$ ", the corresponding absolute value " $a_0$ " was substituted into equation 3.2 for given values of " $d$ " such that " $l$ " was not zero. Then as for the determination of " $a_0$ ", graphs of " $c_0$ " against  $f(\theta)$  (where  $f(\theta)$  is the same as before) were plotted and extrapolated back to  $f(\theta) = 0$ .

Determination of the absolute lattice parameters " $a_0$ " and " $c_0$ " for pure rutile were performed and results are shown in Table 3.32 and 3.33, respectively, whilst plots of " $a_0$ " and " $c_0$ " against  $f(\theta)$  are presented in figure 3.15. The extrapolated plot, in figure 3.15(a), gives an absolute value of " $a_0$ " of 4.59325 Å which compares favourably with the standard value of 4.5933 Å as quoted in the literature<sup>70</sup>.

Similarly, the absolute value of " $c_0$ " is 2.9600 Å, compared with the value of 2.9592 Å quoted in literature<sup>70</sup>.

Diffraction data for sample 2, which represents 1.9 mole% Nb<sub>2</sub>O<sub>5</sub>, are shown in Tables 3.34 and 3.35, with the corresponding plots of " $a_0$ " and " $c_0$ " against  $f(\theta)$  shown in figure 3.16. The absolute values, obtained by extrapolation, for both " $a_0$ " and " $c_0$ " are 4.6042 Å and 2.9627 Å, respectively.

In a similar way, results of the variation of the

lattice parameters of rutile with the addition of  $\text{Nb}_2\text{O}_5$  dopant, for samples 1-7, are shown in Table 3.36. The variation of lattice parameters " $a_0$ " and " $c_0$ " with mole%  $\text{Nb}_2\text{O}_5$  added is shown in figures 3.17 and 3.18. The lattice parameter " $a_0$ " increased with increasing amounts of  $\text{Nb}_2\text{O}_5$  until substitutional saturation became evident at about 8-10 mole%  $\text{Nb}_2\text{O}_5$ . At this point, barely detectable quantities ( $\leq 1\%$ ) of an additional unknown phase were found, but identification was not possible.

Table 3.31      Composition of the solid solution samples

Sample No	Wt% TiO <sub>2</sub>	Wt% Nb <sub>2</sub> O <sub>5</sub>	Mole % TiO <sub>2</sub>	Mole % Nb <sub>2</sub> O <sub>5</sub>
1	100.0	0.0	100.0	0.0
2	94.0	6.0	98.1	1.9
3	90.8	9.2	97.0	3.0
4	83.2	16.8	94.3	5.7
5	76.8	23.2	91.7	8.3
6	71.6	28.4	89.3	10.7

Relative Molecular Mass of TiO<sub>2</sub> = 79.9

Relative Molecular Mass of Nb<sub>2</sub>O<sub>5</sub> = 265.8

Table 3.32

X-ray diffractometer data for determination of absolute lattice parameter "a<sub>0</sub>" for pure rutile, TiO<sub>2</sub>

hkl	Signal	( $\theta$ )	d(Å)	a(Å)	f( $\theta$ )
330	$\alpha_1$	45.450	1.08084	4.5856	0.701
	$\alpha_2$	45.575	1.08122	4.5872	0.697
420	$\alpha_1$	48.675	1.02567	4.58691	0.590
	$\alpha_2$	48.820	1.02594	4.58815	0.585
510	$\alpha_1$	58.825	0.90034	4.59044	0.318
	$\alpha_2$	59.050	0.9004	4.59087	0.313
440	$\alpha_1$	71.6075	0.81171	4.5917	0.106
	$\alpha_2$	72.075	0.81156	4.5909	0.101

$$f(\theta) = \frac{\cos^2 \theta}{\sin \theta} + \frac{\cos^2 \theta}{\theta}$$

Table 3.33

X-ray diffractometer data for determination of absolute  
lattice parameter "c<sub>0</sub>" for pure rutile, TiO<sub>2</sub>

hkl	Signal	c(Å)	f(θ)
402	α <sub>1</sub>	2.95589	0.333
	α <sub>2</sub>	2.95762	0.328
332	α <sub>1</sub>	2.95449	0.255
	α <sub>2</sub>	2.95330	0.250
442	α <sub>1</sub>	2.95644	0.184
	α <sub>2</sub>	2.95795	0.180
303	α <sub>1</sub>	2.95883	0.149
	α <sub>2</sub>	2.95881	0.144

$$f(\theta) = \frac{\cos^2\theta}{\sin\theta} + \frac{\cos^2\theta}{\theta}$$



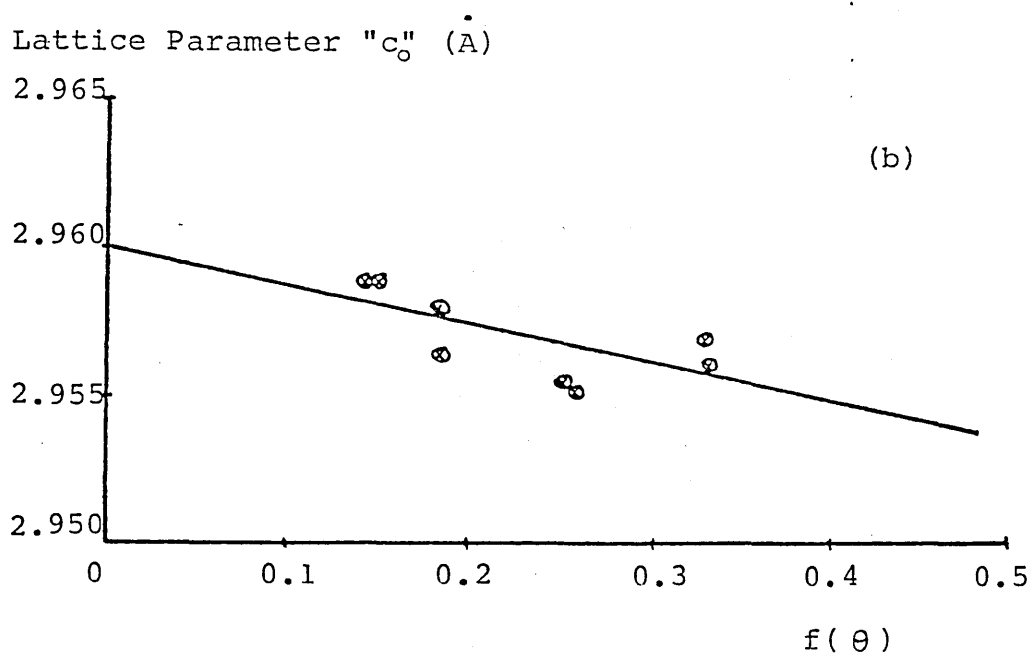
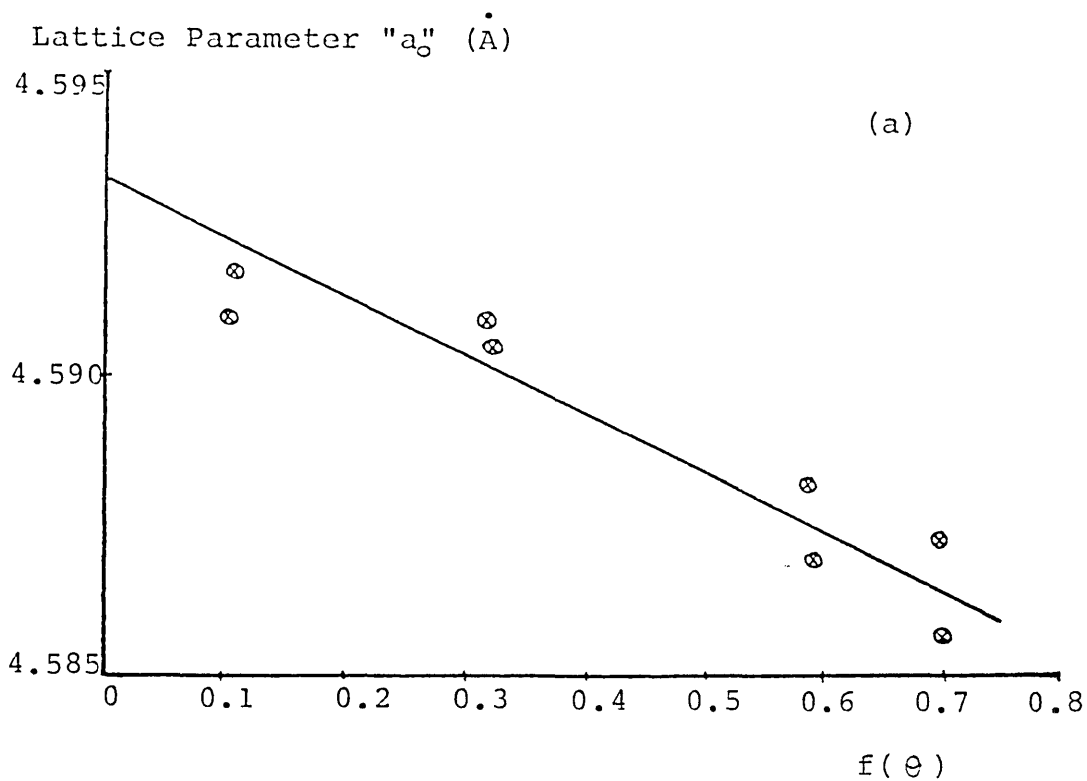


Figure 3.15 (a) Plot of lattice parameter " $a_0$ " against  $f(\theta)$  for pure rutile,  $\text{TiO}_2$ .  
(b) Plot of lattice parameter " $c_0$ " against  $f(\theta)$  for pure rutile,  $\text{TiO}_2$ .

Table 3.34

X-ray diffractometer data for determination of absolute lattice parameter "a<sub>0</sub>" for rutile doped with 1.9 mole% Nb<sub>2</sub>O<sub>5</sub>

hkl	Signal	( $\theta$ )	d(Å)	a(Å)	f( $\theta$ )
330	$\alpha_1$	45.275	1.08411	4.59948	0.708
	$\alpha_2$	45.400	1.08447	4.60101	0.703
420	$\alpha_1$	48.475	1.02883	4.60106	0.596
	$\alpha_2$	48.600	1.02941	4.60365	0.592
510	$\alpha_1$	58.575	0.90265	4.60262	0.323
	$\alpha_2$	58.800	0.90274	4.60308	0.318

Table 3.35

X-ray diffraction data for determination of absolute lattice parameter "c<sub>0</sub>" for rutile doped with 1.9 mole%Nb<sub>2</sub>O<sub>5</sub>

hkl	Signal	c(Å)	f(θ)
402	α <sub>1</sub>	2.96135	0.337
	α <sub>2</sub>	2.96061	0.332
332	α <sub>1</sub>	2.96060	0.260
	α <sub>2</sub>	2.96185	0.255
422	α <sub>1</sub>	2.96146	0.189
	α <sub>2</sub>	2.96272	0.184
303	α <sub>1</sub>	2.96252	0.153
	α <sub>2</sub>	2.96164	0.147

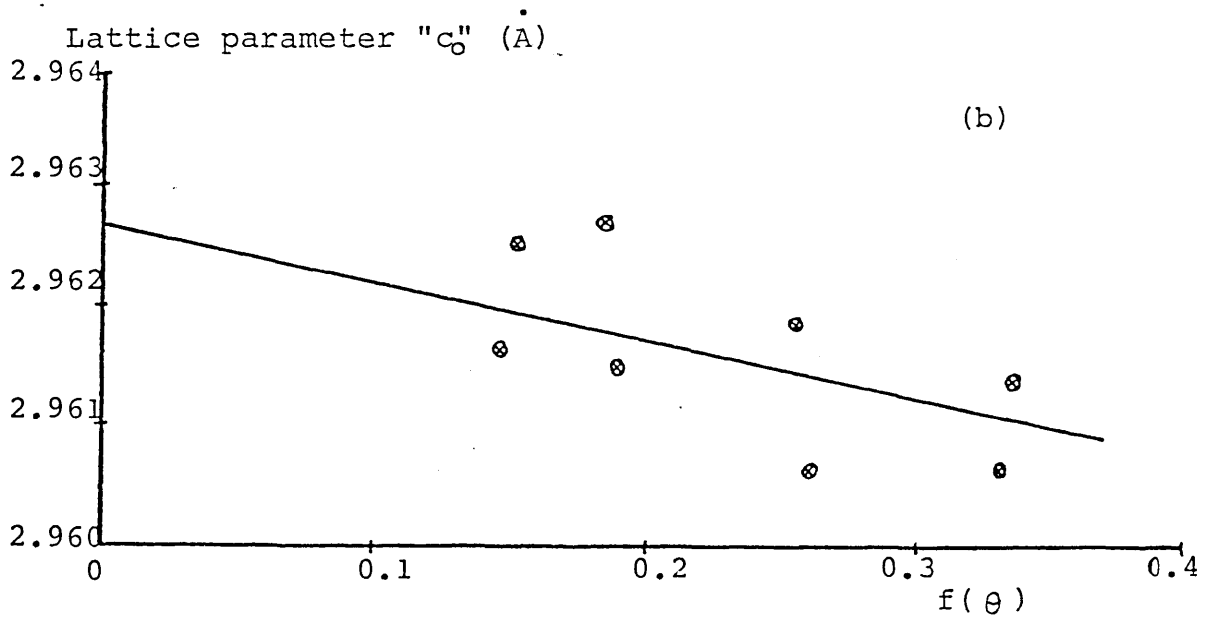
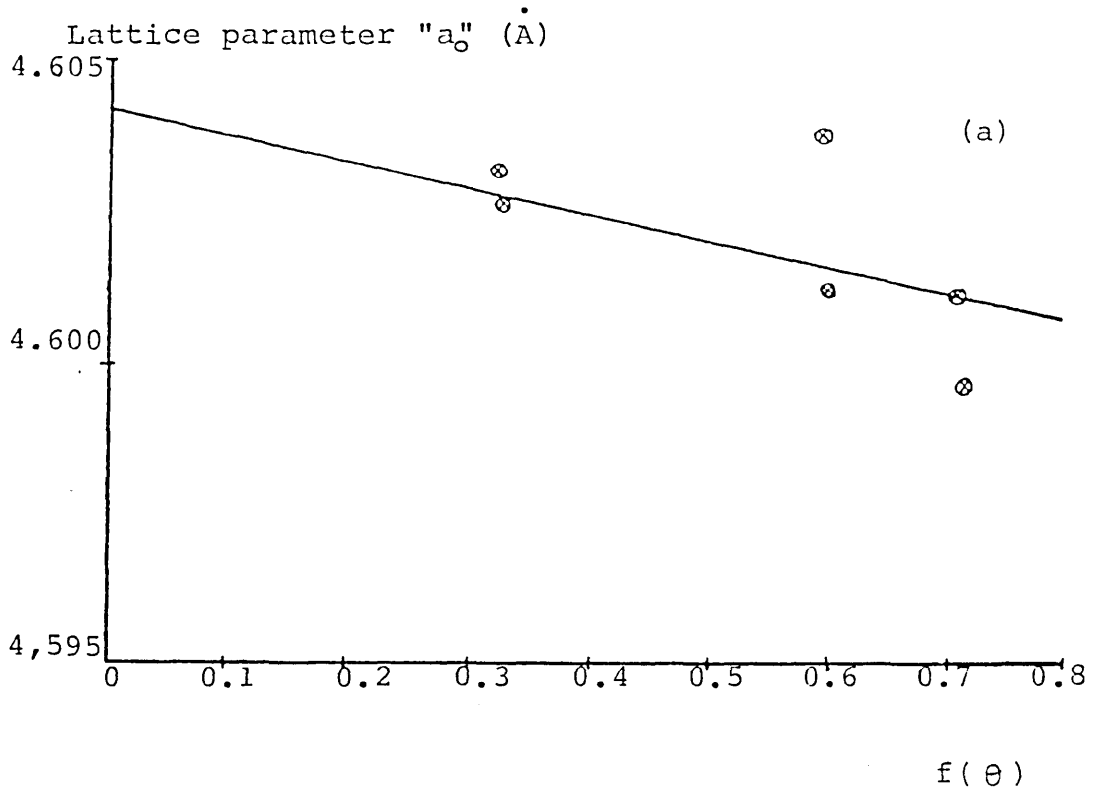


Figure 3.16 (a) Plot of lattice parameter " $a_0$ " against  $f(\theta)$  for rutile doped with 1.9 mole%  $\text{Nb}_2\text{O}_5$ .

(b) Plot of lattice parameter " $c_0$ " against  $f(\theta)$  for rutile doped with 1.9 mole%  $\text{Nb}_2\text{O}_5$ .

Table 3.36

Variation of the lattice parameters of rutile with the  
addition of Nb<sub>2</sub>O<sub>5</sub> dopant

Sample	Mole % Nb <sub>2</sub> O <sub>5</sub>	Lattice Parameters (Å)		Crystalline phases
		a <sub>0</sub>	c <sub>0</sub>	
1	0.0	4.59325	2.9600	Rutile
2	1.9	4.6042	2.9627	Rutile
3	3.0	4.6082	2.9646	Rutile
4	5.7	4.6130	2.9641	Rutile
5	8.3	4.6193	2.9675	Rutile
6	10.7	4.6176	2.9659	Rutile + minute trace of unidentif- ied phase

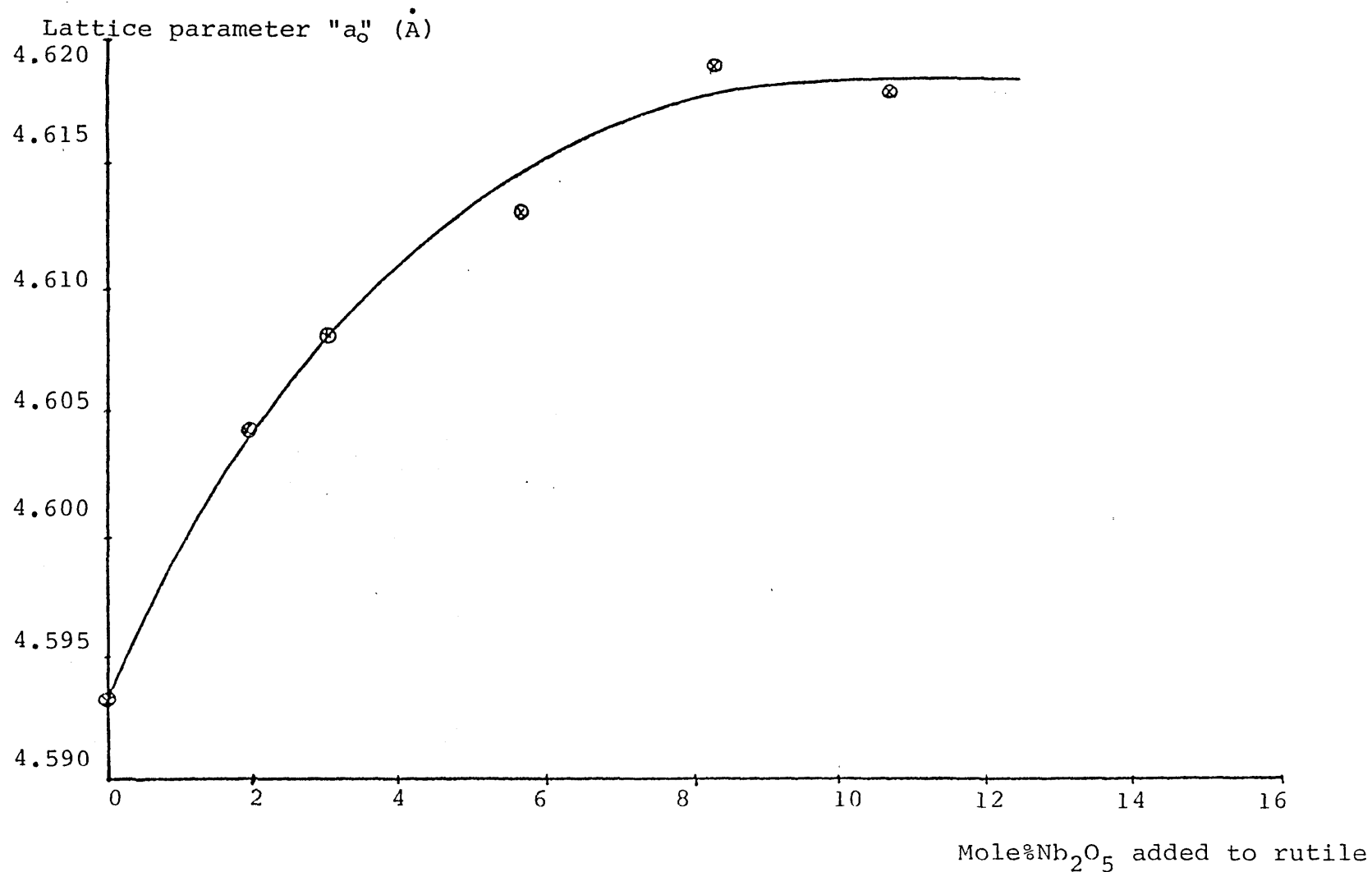


Figure 3.17 Variation in the lattice parameter " $a_0$ " of rutile with mole% addition of  $\text{Nb}_2\text{O}_5$ .

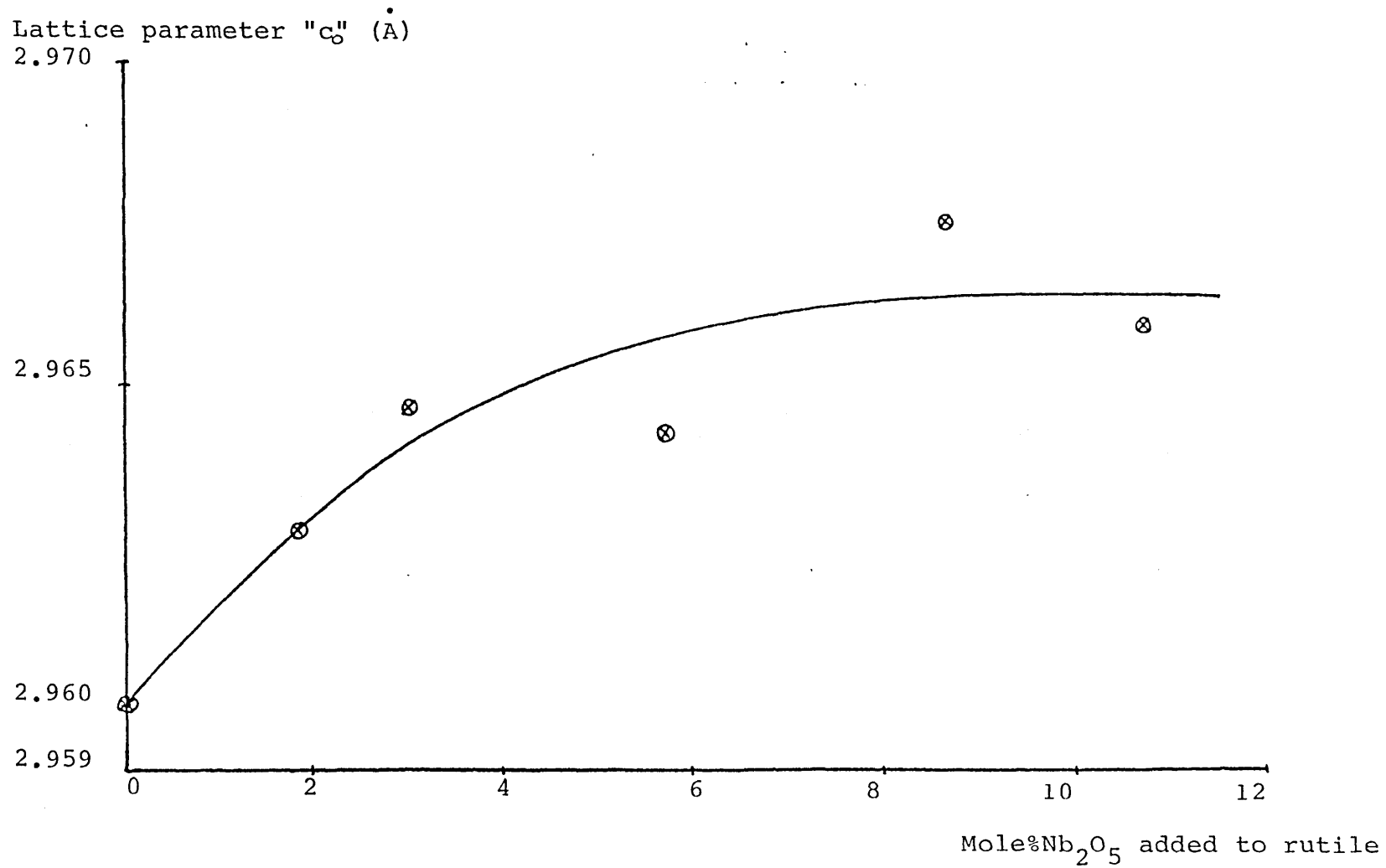


Figure 3.18 Variation in the lattice parameter " $c_0$ " of rutile with mole% addition of  $Nb_2O_5$ .

### 3.6 Determination Of The Wt% Crystalline TiO<sub>2</sub>

Mixtures containing known quantities of TiO<sub>2</sub>, glass and 10wt% NaCl as an internal standard were prepared by thorough mixing in a vibration ball mill for about 2-3 hours. The relationship between the TiO<sub>2</sub>/NaCl peak height ratio, as obtained from XRD analysis, and the wt% TiO<sub>2</sub> in the glass is shown in figure 3.19.

The pairs of points at 2.24, 4.37 and 5.54 wt% TiO<sub>2</sub> in conjunction with the three points at 11.10 wt% TiO<sub>2</sub> represent the number of portions obtained, and subsequently analysed by XRD, from each wt% mixture. Unfortunately, there was only enough of the sample containing 5.7 wt% TiO<sub>2</sub> for one XRD run. For a given wt% TiO<sub>2</sub>, the largest spread in the TiO<sub>2</sub>/NaCl peak height ratio determined was 0.05 on that axis.

Initially, the mixtures were prepared by hand in an agate mortar with pestle, but the results were not reproducible and so have not been reported here since a large scatter in TiO<sub>2</sub>/NaCl peak height ratios was obtained for a given wt% TiO<sub>2</sub>.

Similarly, various crystallised glasses were mixed with 10wt% NaCl and the TiO<sub>2</sub>/NaCl peak height ratio evaluated from XRD analysis. Using the calibration graph (figure 3.19) it was possible to determine the wt% TiO<sub>2</sub> in the various partially crystalline samples - Table 3.37.



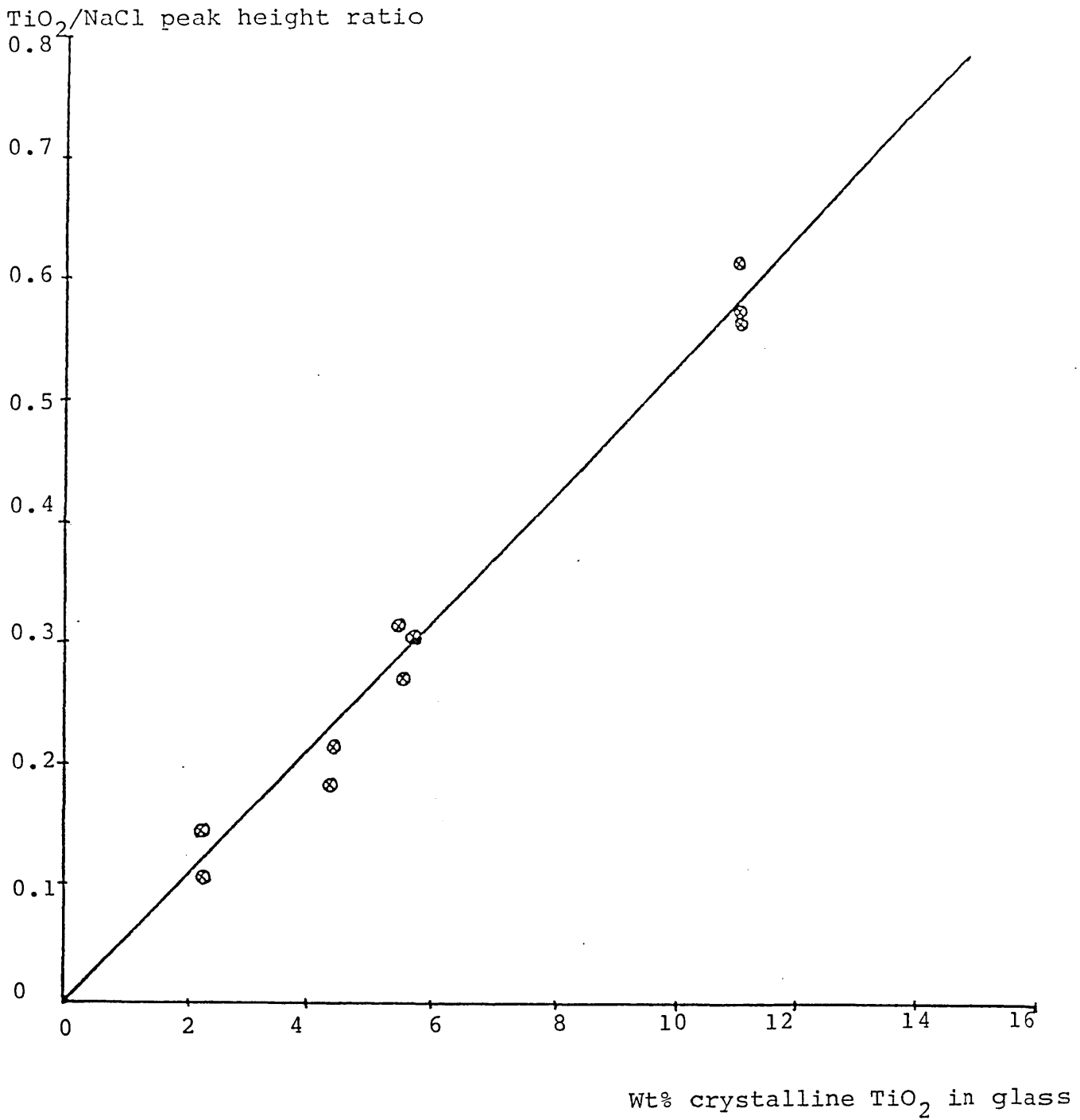


Figure 3.19 Relationship between the TiO<sub>2</sub>/NaCl peak height ratio and the wt% crystalline TiO<sub>2</sub> in a glass/TiO<sub>2</sub> mixture.

Table 3.37

Determination of the wt% of crystalline TiO<sub>2</sub> in partially  
crystalline samples

Sample	wt% crystalline TiO <sub>2</sub>
J1/1	9.3
J1/2	9.5
J1/3	9.3
J1/4	9.9
J1/5	9.8
J3/2	9.5
J3/3	9.1
J3/4	9.5
J3/5	9.0
J3/6	9.4
J3/7	9.6
J9/1	12.5
J9/2	12.5
J9/3	11.8
J9/4	13.0
J9/5	14.9
J10/1	12.7
J10/2	11.6
J10/3	13.3
J10/4	13.5
J13/1	14.6
J13/2	13.9
J13/3	14.7
J13/4	14.8

3.7 Results for the Coefficient of Linear Expansion,  $\alpha$

Results of the dilatometric softening point ( $M_g$ ) and the coefficient of linear expansion ( $\alpha$ ) are reported in Table 3.38. However, not all specimens exhibited a glass transition temperature ( $T_g$ ), but the values for those that did are reported in Table 3.38. The reasons for the absence of  $T_g$  and also the suitability of the glazes for semiconducting material for coating insulators will be discussed in Chapter 4.

Table 3.38

The coefficient of linear expansion,  $\alpha$ , of various samples

Sample	Glass transition temp, $T_g$ , ( $^{\circ}\text{C}$ )	Dilatometric softening point, $M_g$ , ( $^{\circ}\text{C}$ )	$\alpha \times 10^{-6}$ ( $^{\circ}\text{C}^{-1}$ )
J1/1	-	793	5.18
J1/2	-	795	6.26
J1/3	-	797	5.20
J1/4	-	795	6.92
J1/5	-	810	7.29
J/3 glass	710	760	Below $T_g$ , 5.38 Above $T_g$ , 13.98
J3/2	-	780	6.38
J3/3	-	785	6.27
J3/3 annealed	720	790	Below $T_g$ , 7.17 Above $T_g$ , 11.62
J10 phase separated	770	805	Below $T_g$ , 5.72 Above $T_g$ , 12.93
J10/1	730	790	Below $T_g$ , 6.23 Above $T_g$ , 14.26
J10/2	-	790	6.61
J10/3	-	806	6.36
J10/4	753	792	Below $T_g$ , 5.20 Above $T_g$ , 14.06

## CHAPTER 4

### DISCUSSION

#### 4.1 Crystallisation Behaviour of the Glasses

##### 4.1.1 Glass preparation

The choice of glass composition will invariably depend upon the eventual properties required by the glass. As the primary interest was in producing a semiconducting glaze, then appropriately, the base glass composition chosen was that of a calcium aluminosilicate glass. It has long been known that aluminosilicate glasses exhibit good chemical durability and mechanical properties and at the same time the above glass melts would readily dissolve transition metal oxides at glass forming temperatures.

As glazes containing transition metal oxides such as iron oxide, reduced titania and antimony doped tin oxide, which have been used to impart semiconducting properties, have failed in service, then it is quite obvious that any further improvements require a change in the conducting phase of the glaze.

Hobbs and Tantram<sup>71</sup> suggested using valency controlled  $\text{TiO}_2$ , as such a glaze would be more resistant to oxidation and electrolytic attack. However, they proposed that one disadvantage was that since the solubility of  $\text{TiO}_2$  in the glazes was quite high (using high temperature techniques, silica glass containing just under 20wt%  $\text{TiO}_2$  can be prepared<sup>72</sup>) then it would have a tendency to crystallise out as long needles, which would not give the uniformly

dispersed, evenly sized particles that are desired. However, this disadvantage can be easily overcome and will be discussed in the proceeding sections.

The choice of dopant was  $\text{Nb}_2\text{O}_5$  as previously suggested by Binns<sup>10</sup>; the requirement being that the impurity cation ie  $\text{Nb}^{5+}$ , be pentavalent (for n-type semiconduction) and of similar size to the host cation ie  $\text{Ti}^{4+}$ , so as to allow solid solution formation without excessive lattice distortion.

Zinc oxide was added to the glass to act as a network modifier to lower the melting temperature of the glass and at the same time produce a more fluid melt. The exclusion of alkali ions such as  $\text{Na}^+$  was necessary to eliminate any ionic contribution to the overall electronic conduction process by movement of mobile alkali ions through the glaze body under an applied potential.

Glasses containing up to 15wt%  $\text{TiO}_2$  with a pale straw colour have been successfully prepared by the traditional technique of melting and quenching. However, the solubility limit of  $\text{TiO}_2$  in the glass at  $1500^\circ\text{C}$  is exceeded at 20wt%  $\text{TiO}_2$  as borne out by J13 glass which contained a non-uniform layer of undissolved rutile in the bottom of the crucible. By grinding away the undissolved layer it was possible to carry out electrical measurements on the remaining saturated glass.

#### 4.1.2 Phase separation

Many commercial glass systems are seen to undergo

spinodal decomposition, a glass-in-glass phase separation, at subsolidus temperatures, in particular those compositions containing  $\text{TiO}_2$  as the nucleating agent for crystal growth.

Glass in glass phase separation, which was observed by direct transmission electron microscopy to be present (Plates 3.3 and 3.4), effectively separated a homogeneous glass into two glassy phases, one rich in  $\text{TiO}_2$  and the other rich in  $\text{SiO}_2$ . Separation is expected to start on an atomic scale and grow with extended length of heat treatment, leading to a continuous variation of both extremes in composition with time. As the size of the separated regions grew they eventually reached proportions, representative of an equilibrium composition, with the same dimensions as the wavelength of visible light ( $\approx 0.5 \mu\text{m}$  diameter) and a subsequent light scattering phenomenon was observed.

The temperature and time chosen for the nucleation treatment (3 hours at  $800^\circ\text{C}$ ) was one that was effective in providing the desired microstructure of a fine dispersion of  $\text{TiO}_2$  rich droplets in a silica rich matrix. It should be pointed out that although phase separation was observed for glasses heat treated for 18 hours at  $750^\circ\text{C}$ ,  $780^\circ\text{C}$  and  $800^\circ\text{C}$  the only reason for choosing the 3 hours at  $800^\circ\text{C}$  treatment as a nucleation process prior to crystallisation was on the grounds of cost effectiveness, in that the time taken at  $800^\circ\text{C}$  was much less than at other temperatures.

The importance of this glass-in-glass phase separation

is in providing a uniform dispersion of small particles of a second phase. Although spinodal decomposition has always had a tendency to be associated with a high degree of inter-connectivity of second phase non-spherical particles, it must be pointed out that a lowering of the free energy of the system can result by a coarsening process leading to dispersed spheroids. In this respect, the system can be wrongly interpreted to have undergone a nucleation and growth mechanism but quite obviously the nuclei for such a mechanism would show random distributions of particle sizes and positions in the matrix. There was no evidence to suggest that this mechanism had operated for this glass system.

#### 4.1.3 Crystal growth

At sub-solidus temperatures the  $\text{TiO}_2$  was much less soluble and the glass became supersaturated with respect to  $\text{TiO}_2$ . A single stage crystallisation treatment produced a glass which contained a non-uniform distribution of sizes and uneven dispersion of rutile needles. Obviously, this bulk effect was due to internal nucleation and crystal growth occurring randomly within the glass. After a time the crystal growth became diffusion dependent, inevitably due to the six component nature of the glass, as the diffusion distance for  $\text{Ti}^{4+}$  ions to the advancing crystal growth interface increased.

Prolonged heat treatment of the glass produced a second crystalline phase,  $\text{CaO} \cdot \text{Al}_2\text{O}_3 \cdot 2\text{SiO}_2$ , namely anorthite. Since



the composition of the base glasses lies within the primary field of anorthite in the  $\text{CaO} - \text{Al}_2\text{O}_3 - \text{SiO}_2$  system<sup>73</sup> it is not surprising that this phase also crystallised from the glass, needles or dendrites being a common form for this phase. Also trace amounts of a titanite,  $\text{CaO} \cdot \text{TiO}_2 \cdot \text{SiO}_2$ , were found by x-ray diffraction analysis for samples heat treated at higher temperatures and for extended times.

By comparison, a two stage heat treatment at  $800^\circ\text{C}$  and  $1000^\circ\text{C}$  produced a much finer and more uniform distribution of  $\text{TiO}_2$  needles. The difference in microstructure was entirely due to the heat treatment at  $800^\circ\text{C}$  which allowed glassy sub-micron  $\text{TiO}_2$ -rich droplets to separate from a silica rich matrix. This enabled a very fine dispersion of  $\text{TiO}_2$  needles to grow when the temperature was raised to  $1000^\circ\text{C}$ .

During the crystallisation step, the rutile needles are expected to grow rapidly at first due to the high local concentration of  $\text{TiO}_2$ , eventually the rate decreasing as the diffusion dependency for  $\text{Ti}^{4+}$  becomes important.

Although the maximum growth rate obtained ( $1.5 \mu\text{m}/\text{min}$ ) occurred at  $1100^\circ\text{C}$ , this was not chosen as the experimental crystallisation temperature since the relative quantity of anorthite at this temperature was high. As anorthite was a non-conducting crystalline phase, its presence was considered as a possible source for impairing the electrical properties. Therefore it was felt necessary to keep the concentration of anorthite down to a minimum. This was

achieved by crystallising at a lower temperature of 1000°C, where the growth rate of rutile was still reasonable but the anorthite content was low. Though it must be pointed out, that even at this temperature, appreciable amounts of anorthite crystallised out with prolonged treatment.

EPMA analysis performed on selected partially crystalline samples did not shown conclusively that niobium was associated with the rutile needles. Clearly, with needles less than 1 µm across, analysis would be representative of needles and the surrounding glassy matrix since the resolution of the electron beam is 4-5 µm. Specimens were initially coated with sputtered gold to prevent charging under the electron beam but it became evident that the AuK<sub>α</sub> line was superimposed on the NbK<sub>α</sub> line and so evaporated carbon was used instead.

#### 4.2 Solid Solution Formation in the TiO<sub>2</sub>/Nb<sub>2</sub>O<sub>5</sub> System

Various authors have reported the existence of solid solution formation between TiO<sub>2</sub> and Nb<sub>2</sub>O<sub>5</sub> at various temperatures (as mentioned in section 1.9) but none have presented any values for the shift in the lattice parameters of rutile.

By heating the powdered oxides at a relatively high temperature of 1450°C, but still below the melting point of Nb<sub>2</sub>O<sub>5</sub> (≈ 1500°C), it was felt that solid solution formation would be greatly encouraged; and a period of one week at 1450°C was considered appropriate for equilibrium conditions to be attained.

The Végard plot (figure 3.17) shows quite clearly the increase in lattice parameter " $a_0$ " of rutile with small additions of  $\text{Nb}_2\text{O}_5$  in solid solution. The limit of  $\text{Nb}_2\text{O}_5$  solubility at  $1450^\circ\text{C}$  lay between 8-10 mole%  $\text{Nb}_2\text{O}_5$  after which substitutional saturation was observed. This latter observation was confirmed by the appearance of a minute trace of an unidentified crystalline phase as well as the presence of rutile solid solution in the sample containing 10.7 mole%  $\text{Nb}_2\text{O}_5$ , whereas the only crystalline phase detected below this dopant level was rutile. Roth and Coughanour (Ref 63, figure 1.15) report a value of approximately 11 mole%  $\text{Nb}_2\text{O}_5$  in solid solution at  $1450^\circ\text{C}$ , which compares favourably with the results obtained in this study.

However, it should be pointed out that the values of " $a_0$ " obtained for pure rutile and that of 1.9 mole%  $\text{Nb}_2\text{O}_5$  in solid solution, were absolute values, as they were obtained by the extrapolations shown in figures 3.15 and 3.16, respectively. In effect, they are values with the least errors incurred as they represent high  $2\theta$  angles [approximating to  $180^\circ(2\theta)$ ]. The value of " $a_0$ " obtained for pure rutile ( $4.59325 \text{ \AA}$ ) compared favourably with the value quoted in literature,  $4.5933 \text{ \AA}^{70}$ . A value of  $4.6042 \text{ \AA}$  was obtained for the 1.9 mole%  $\text{Nb}_2\text{O}_5$  sample showing the expected increase in " $a_0$ " with mole% addition of  $\text{Nb}_2\text{O}_5$  on forming a solid solution; this being confirmed by x-ray diffraction analysis indicating the presence of rutile only.

The values of " $a_0$ " for the remaining samples were also obtained through samples sent to the CEGB but did not represent absolute values. They were obtained from diffraction lines in the region  $115-123^\circ(2\theta)$  and no such extrapolation was possible. It was considered that as the difference between the value for " $a_0$ " obtained by the extrapolation method and that obtained at the highest measurable  $2\theta$  angle was only approximately  $0.0015\text{\AA}$ , then only the third decimal place was affected by at most two units. Hence, the actual trend in " $a_0$ " values would remain pretty much the same by just using the higher values of measured  $2\theta$ .

The absolute value of the lattice parameter " $c_0$ " obtained for pure rutile was  $2.9600\text{\AA}$  which again compared favourably with the value of  $2.9592\text{\AA}$  quoted in literature<sup>70</sup>. Similarly, an absolute value for " $c_0$ " was obtained for  $\text{TiO}_2$  containing 1.9 mole%  $\text{Nb}_2\text{O}_5$  using the extrapolation method. Again, a margin of error of  $0.0015\text{\AA}$  was possible for the difference between the highest measured  $2\theta$  angle and that obtained on extrapolating. The values obtained for the remaining samples (which were not absolute) appeared to show an increase in the lattice parameter " $c_0$ " with increasing addition of  $\text{Nb}_2\text{O}_5$  (figure 3.18).

As the Pauling radii for the ions  $\text{Ti}^{4+}$  and  $\text{Nb}^{5+}$  are  $0.68$  and  $0.70 \text{\AA}$ , respectively, then one would expect there to be an increase in the " $a_0$ " and " $c_0$ " lattice parameters of rutile for the substitutional replacement of  $\text{Ti}^{4+}$  ions by

the larger  $\text{Nb}^{5+}$  ions. Owing to the similarity in the size of the two ions one would expect the increase to be very small. However, the expansion parallel to the "c" axis was not as large as that parallel to the "a" axis and it is therefore necessary to discuss the structural implications.

The structure of rutile is not close-packed and from figure 4.1 it can be seen that in the unit cell, titanium is octahedrally coordinated (with slight distortion) to six oxygens and that each oxygen is in planar three coordination with titanium ions at the corners of a nearly equilateral triangle<sup>74</sup>. The structure of the oxide can be described as chains of edge sharing octahedra of composition  $(\text{TiO}_4)^{4-}$  condensed by sharing the remaining vertices (figure 4.2). It would therefore appear that the asymmetric expansion in the lattice parameters of rutile must be due to the non-close packed structure of rutile.

#### 4.3 Wt% Crystalline $\text{TiO}_2$ in Partially Crystalline Samples

As predicted by equation (2.12) the curve (figure 3.19) for  $\text{TiO}_2/\text{NaCl}$  peak height ratio against weight fraction of crystalline  $\text{TiO}_2$  is linear and passes through the origin.

Strictly speaking equation (2.12) is only valid for integrated intensities but as the diffraction lines were sharp and did not vary in shape from sample to sample then measurements of the maximum intensities does not give rise to large inaccuracies, so long as all the patterns were obtained under the same experimental conditions.

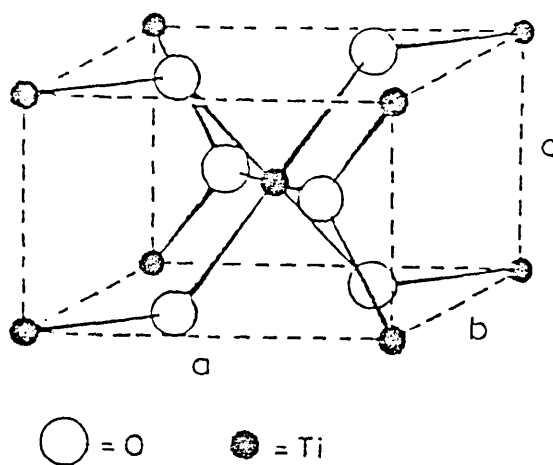


Figure 4.1 The structure of rutile,  $\text{TiO}_2$

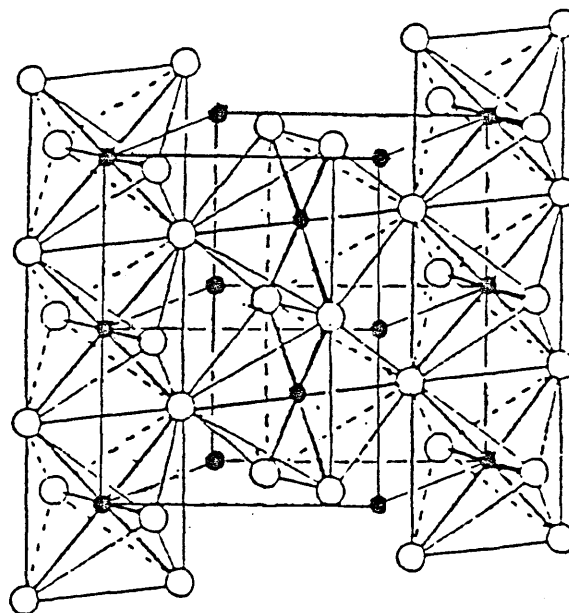


Figure 4.2 An overall view of rutile emphasizing the arrangement of the octahedral chains, and showing the relation to Figure 4.1

Certain drawbacks with this technique are those associated with preferred orientation, microabsorption and extinction, but these can all be greatly reduced by finely grinding the samples before analysis. The effects of microabsorption and extinction do not invalidate this technique because the effects are essentially constant from sample to sample and minimal. The determination of the wt% crystalline  $\text{TiO}_2$  in partially crystalline samples is accurate to within  $\pm 0.5$  wt%  $\text{TiO}_2$  (Table 3.37) as obtained from the calibration graph (figure 3.19).

Assuming the glasses to be homogeneous and containing a uniform distribution of titanium, one would expect an increase in the wt% crystalline  $\text{TiO}_2$  with extended crystallisation heat treatment. From Table 3.37 for partially crystalline samples of J1 glass, with 10 wt%  $\text{TiO}_2$  added, it is quite apparent that the data suggest a high initial growth rate which decreases rapidly with extended treatment; as borne out by the relatively high wt% crystalline  $\text{TiO}_2$  in J1/1 (9.30%) followed by the progressively small increase thereafter. The value for J1/3 appears rather lower than expected, possibly due to non-homogeneity. Similarly, a high initial growth rate is suggested for J3 glasses.

For J9 and J10 glasses, which both contained 15 wt%  $\text{TiO}_2$ , a large initial growth rate was suggested by the results, and the wt%  $\text{TiO}_2$  generally increased with extended heat treatment, though any discrepancies such as J9/3 and

J10/2 must invariably be due to non-homogeneity.

A much clearer picture emerges on evaluating the volume % crystalline TiO<sub>2</sub> contained in the samples.

By using the wt% of crystalline TiO<sub>2</sub> determined from experiment (Table 3.37) and taking the density of rutile <sup>75</sup> as 4.26 g/cm<sup>3</sup> it was possible to evaluate the volume occupied by crystalline TiO<sub>2</sub> in 100 g of partially crystalline sample. Simple density measurements, using the displacement of water, were used to determine the volume occupied by 100 g of the partially crystalline samples. Using the simple ratio:

$$\frac{\text{Vol of TiO}_2 \text{ in 100 g sample}}{\text{Vol of 100 g of sample}} \times 100\% \quad (4.1)$$

it was possible to calculate the vol% of crystalline TiO<sub>2</sub> (Table 4.1). It is evident that the 10 wt% TiO<sub>2</sub> glasses contained 6.1-6.5 vol% crystalline TiO<sub>2</sub> whilst the 15 wt% TiO<sub>2</sub> glasses contained 8.0-10.1 vol% crystalline TiO<sub>2</sub>. The glass J13, which would represent the solubility limit of TiO<sub>2</sub> in the glass at 1500°C, contained 10.1-10.8 vol% crystalline TiO<sub>2</sub>; higher than the other two as might be expected. These results will be discussed in more detail in conjunction with the conductivity results which follow.



TABLE 4.1

Volume% of crystalline TiO<sub>2</sub> in partially crystalline samples

<u>Sample</u>	<u>Vol% crystalline TiO<sub>2</sub></u>
J1/1	6.1
J1/2	6.2
J1/3	6.1
J1/4	6.5
J1/5	6.4
J3/2	6.5
J3/3	6.2
J3/4	6.5
J3/5	6.1
J3/6	6.4
J3/7	6.5
J9/1	8.5
J9/2	8.5
J9/3	8.0
J9/4	8.9
J9/5	10.1
J10/1	9.2
J10/2	8.4
J10/3	9.7
J10/4	9.8
J13/1	10.6
J13/2	10.1
J13/3	10.7
J13/4	10.8

#### 4.4 DC Resistivity Measurements of the Glasses

Essentially, all the parent glasses and subsequently phase separated samples were non-conducting, in the sense that measurements of sample resistance greater than  $10^{13}$  ohms were not possible. However, the "anomalous current" effect was observed, in which an initial surge in current was recorded which decreased exponentially with time and was no longer detected after a minute or so. This can invariably be assigned to a slow dielectric relaxation within the glass. All the conducting samples were ohmic between 5-40 V dc applied.

##### 4.4.1 Glasses containing 10wt% TiO<sub>2</sub>

J0 glass containing 10wt% TiO<sub>2</sub> but excluding Nb<sub>2</sub>O<sub>5</sub> showed no signs of electronic conductivity, as did the partially crystalline samples where the only detected crystalline phase was rutile; although anorthite crystallised out with prolonged treatment. However, partially crystalline glasses containing both TiO<sub>2</sub> and Nb<sub>2</sub>O<sub>5</sub> have been shown to be electronically conducting. Hence, the obvious conclusion drawn from this experimental observation is that Nb<sub>2</sub>O<sub>5</sub> and crystalline TiO<sub>2</sub> must both be present to impart electronic conductivity.

J1 glass which contained 0.5 wt% Nb<sub>2</sub>O<sub>5</sub> exhibited activation energies of 0.16-0.19 eV which lie in the region indicative of semiconductive properties. The room temperature resistivities and activation energies for conduction are seen to rise with extended heat treatment.

As it has already been shown that the 10 wt% TiO<sub>2</sub> glasses contain between 6.1 to 6.5 volume% crystalline TiO<sub>2</sub>, it is envisaged that it may be possible for the Nb doped rutile needles, possessing high aspect ratio, to form a continuous connected network through the glass, giving rise to the observed conductivity. However, the crystallisation of anorthite, a non-conducting phase, might be expected to lower the conductivity of the system as it grows from the rutile needles, potentially lowering the number of rutile-rutile needle contacts.

Sample J11/1 appeared to have the lowest resistivity ( $5.25 \times 10^5$  ohm.cm) measured of all the samples studied in the present work; no other sample had a room temperature resistivity value less than  $10^6$  ohm.cm. Since microscopically, its structure was typically of a fine distribution of rutile needles, then it was considered that this anomaly must be some function of the rutile defect structure, possible exsolution of Nb from the rutile needles with extended heat treatment after 1/4 hr at 1000°C. Hence J1 glass was phase separated and then crystallised from a lower temperature of 975°C. At this temperature, the 1/4 hr treated sample did not conduct, presumably due to the lower crystal growth rate compared with 1000°C. This would reduce the size of rutile needles and hence the probability of needle-needle contact giving rise to a continuous crystalline network. The resistivity decreased with extended heat treatment time up to 1 hr and then increased

again after 3 hrs at 975°C. This phenomenon can be explained by assuming that after 1/2 hr at 975°C a continuous network of doped rutile needles is achieved, where the number of contacts increases with heat treatment time. Eventually somewhere between 1-3 hrs, sufficient anorthite had crystallised to reduce the conductivity by over an order of magnitude.

The two slope behaviour encountered here cannot be readily explained. In transition metal oxide glasses this phenomenon is observed quite often and various explanations have been offered, such as electron hopping between transition metal ions of different coordination sites<sup>76</sup>. This has the effect of introducing a  $\Delta U$  term<sup>(57)</sup> to the polaron hopping activation energy term to account for the site differences. However, in the crystalline needles of  $TiO_2$ , such structural differences would not be expected although the contacts between needles may play a role, but it is not known what. Johnson<sup>61</sup> showed that crystalline  $TiO_2$  containing 0.5 mole%  $Nb_2O_5$  solid solution exhibited a change in slope in the conductivity versus temperature plot at around 300°C; and suggested oxidation of  $Ti^{3+}$  or exsolution of  $Nb_2O_5$  as playing important roles. His samples also showed voltage dependent conductivity, though this was not observed in the present system on applying up to about 120 V/cm.

Similar results were obtained for J2 glass samples, where the 1/4 hr at 1000°C treatment was non-conducting but

a treatment of 1/2 hr at 1000°C produced a continuous network of doped rutile needles which exhibited semiconducting properties. Extended treatment resulted in more needle-to-needle contacts which increased the conductivity but eventually as more and more anorthite crystallised out, a reduction in conductivity was observed. Again, two slope behaviour was noted.

For J3 glass samples, the general trend was an increase in conductivity with heat treatment, even for a sample crystallised for 3 hours at 1000°C (J3/4). It would appear that this latter observation is quite different from that observed for J1 and J2 glasses where the conductivity for the 3 hr treated samples tended to decrease, associated with the increased anorthite content. However, the microstructure of J3/4 revealed the presence of larger needles and a smaller density of nuclei than was apparent for all the other partially crystalline samples. Presumably, J3/4 had not been phase separated extensively prior to crystallisation. However, it was difficult to say whether or not the needles were homogeneously dispersed, but it was quite apparent that a continuous network of doped rutile needles was present.

From figure 3.5, samples J3/3 and J3/7 were both heat treated at 1000°C for 1 hr but J3/3 had undergone a prior phase separation treatment of 3 hrs at 800°C. As can be seen from the figure the conductivity of J3/3 was almost 3 orders of magnitude higher than that for J3/7. This must be

due to the difference in microstructure. J3/3 had a fine distribution of evenly sized  $\text{TiO}_2$  needles whereas the non-phase separated sample merely had irregular sized needles randomly dispersed. As the activation energies for conduction for J3/3 and J3/7 are 0.19 and 0.22 eV, respectively, ie very similar, then it is expected that a similar conduction mechanism operates.

J3/2 and J3/6 which were phase separated for 3 hrs and 18 hrs at  $800^\circ\text{C}$ , respectively, and then both crystallised for 1/2 hr at  $1000^\circ\text{C}$ , exhibited similar room temperature resistivities, as might be expected since their microstructures were similar. All the samples exhibited two slope behaviour except for J3/6.

For J4 glass, only two partially crystalline samples were conducting, namely J4/1 and J4/2, even when a repeat batch was made up and crystallised. The conductivity for J4/1 was an order of magnitude greater than J4/2 whilst the remaining samples which had undergone extended heat treatments did not conduct. Previously, this had been accounted for by the increased anorthite content, but in this situation, J4/3 did not conduct, nor did it contain detectable amounts ( $\geq 1\%$ ) anorthite. Hence, the possibility arises that the  $\text{Nb}_2\text{O}_5$  may not be going into solid solution in  $\text{TiO}_2$ , with prolonged heat treatment for a  $\text{TiO}_2/\text{Nb}_2\text{O}_5$  ratio of 10/3. As no other crystalline phase apart from anorthite was detected, it appears that  $\text{Nb}_2\text{O}_5$  may remain in the glass with prolonged treatment, though the reason for

this is unknown.

Alternatively, it could be that such large quantities of  $\text{Nb}^{5+}$  in  $\text{TiO}_2$  form couples with  $\text{Al}^{3+}$  for example, thus rendering the  $\text{TiO}_2$  non-conducting<sup>61</sup>, though there is no evidence for this.

Partially crystalline samples of J5, J6 and J7 glasses which contained 3.5, 4 and 6 wt%  $\text{Nb}_2\text{O}_5$  showed no signs of conduction. Again, the only crystalline phase present was rutile, although with extended heat treatment increasing quantities of anorthite crystallised out.

At this stage it was questioned whether there was a critical  $\text{TiO}_2/\text{Nb}_2\text{O}_5$  ratio or if instead it was the total  $\text{Nb}_2\text{O}_5$  content which was important with respect to the cut off in observed electrical conductivity. To test this hypothesis J12 glass was prepared which contained 13.3 wt%  $\text{TiO}_2$  and 4wt%  $\text{Nb}_2\text{O}_5$ . As partially crystalline samples of this glass exhibited semiconducting properties it was deduced that it was in fact the  $\text{TiO}_2/\text{Nb}_2\text{O}_5$  ratio which was an important quantity and that it was possible to obtain semiconducting glasses containing up to 4 wt%  $\text{Nb}_2\text{O}_5$ . It should be pointed out that although the samples J12/2 which had been crystallised for 1/2 hr at  $1000^\circ\text{C}$  appeared to display a fine microstructure in which the crystalline network appeared continuous, it did not show signs of electrical conduction. Again, with such a relatively high wt%  $\text{Nb}_2\text{O}_5$  content, the conductivity-microstructure relationship still appears to be rather complicated.

#### 4.4.2 Glasses containing 15 wt% TiO<sub>2</sub>

The determination of the volume% of crystalline TiO<sub>2</sub> in the glasses has shown (section 4.3) the presence of between 8.0-10% crystalline TiO<sub>2</sub>. Such values are in good agreement with those reported by Binns<sup>5</sup> (9-11%) for the formation of a continuous network of conducting crystals within the glassy matrix.

For partially crystalline samples of J8 glass, the room temperature resistivities decreased with heat treatment for up to 1 hr at 1000°C. This would be in line with a picture representing an increase in the number of needle-needle contacts. However, after 1 hr, increasing amounts of anorthite are present and a corresponding increase in resistivity is observed. All the samples except J8/5 exhibited similar activation energies (0.21-0.25 eV) which suggested that conduction mechanisms were similar. Single slope behaviour was observed except for J8/5, which had a much higher (0.54 eV) low temperature activation energy and which decreased above 230°C (0.19 eV). The high temperature activation energy is expected to possibly represent a conduction mechanism similar to the other samples but it is difficult to speculate on the rather higher low temperature activation energy. Any ionic contribution to the conductivity can be discarded as polarisation effects were not observed at these temperatures.

Partially crystalline samples of J9 glass exhibited the lowest resistivities of all the glasses studied. Single



slope behaviour was observed and activation energies between 0.18-0.2 eV were encountered, which were marginally smaller than, but similar to those obtained for J8 samples; although J9/5, at 0.28 eV, was slightly higher.

The room temperature resistivities decreased from  $7.9 \times 10^6$  to  $2.4 \times 10^6$  ohm.cms with extended heat treatment for up to 2 hrs at 1000°C. However, as before, increasing amounts of anorthite crystallised out with prolonged heat treatment, thus reducing the conductivity for the sample heat treated for 3 hours at 1000°C.

Partially crystalline samples of J10 glass exhibited properties very similar to J9 glass. Both single slope behaviour and similar activation energies (0.21.-0.22 eV) were observed. The resistivity was at a minimum after 1 hr at 1000°C and then started to rise again for the 3 hrs at 1000°C treatment, which was shown to contain small amounts of anorthite. It would have been interesting to see whether a 2 hour heat treated sample exhibited a lower resistivity than the 1 hr treated sample; though it is envisaged that the resistivity will be similar to that of the 1 hr heat treated sample, but less than the 3 hr sample.

Two slope behaviour was apparent for samples of J11 glass which contained 3 wt% Nb<sub>2</sub>O<sub>5</sub>. The conductivity increased with increasing heat treatment up to 1/2 hr at 1000°C after which anorthite was detected and subsequently the conductivity decreased. The low temperature activation energies were all in the range 0.24-0.28 eV,

although J11/5 which had not had prior phase separation exhibited single slope behaviour with an activation energy of 0.35 eV. The microstructure typically showed irregular sized needles randomly dispersed; anorthite also being present. As the high temperature activation energies for the other samples lay in the region 0.35-0.40 eV, possibilities existed for their high temperature conduction mechanisms to be similar to that for J11/5.

Phase separation of this glass for 3 hrs and 18 hrs at 800°C, prior to crystallisation (J11/1 and J11/2), did not appear to make a substantial difference in resistivity, as might have been expected since both treatments produced a similar microstructure. It would have been useful to prepare a sample that had been crystallised for 1 hr at 1000°C to note whether a decrease in resistivity occurred before the 3 hour treatment resulted in a subsequent increase.

Glass JS11 was analogous to J11 except that a  $\text{TiO}_2/\text{Nb}_2\text{O}_5$  solid solution was prepared prior to glass formation. The microstructure of both glasses appeared similar as did the two slope behaviour of their log resistivity against  $1000/\text{Temp}$  plots. Low temperature activation energies for conduction in JS11 samples (0.23-0.29 eV) were also in a similar range to J11 samples suggesting the mechanism for conduction was similar; although the actual resistivity values for JS11 were slightly lower.

The high temperature activation energies were in the

range 0.40-0.44 eV, slightly higher than the J11 counterparts but still in a similar region.

From the analysis it followed that the optimum  $\text{TiO}_2/\text{Nb}_2\text{O}_5$  ratio had been established, as being represented by J9 glass (15 : 0.5 respectively). It was decided to try this ratio out in a glass containing 20 wt%  $\text{TiO}_2$  (J13) to observe whether or not it had improved electrical properties. Hence, J13 glass was prepared, but apparently the solubility limit of  $\text{TiO}_2$  in the base glass at 1500°C had been exceeded. Nevertheless, by grinding away the deposit of undissolved  $\text{TiO}_2$  at the bottom of the crucible, it was possible to carry out the electrical measurements on the remaining glass. Partially crystalline samples exhibited semiconducting properties with activation energies in the range 0.17-0.28 eV although, the 3 hr heat treated sample (J13/4) gave a much higher value of 0.61 eV.

From the volume%  $\text{TiO}_2$  determinations, between 10.1-10.8 vol% crystalline  $\text{TiO}_2$  was present, allowing the formation of a continuous network of touching rutile needles. The activation energies were comparable with J9 samples (except for J13/4) as also were the room temperature resistivities.

The microstructure of J13/4 was typical of a fine dispersion of rutile needles, with the presence of anorthite expected to lower the conductivity. However, the size of the activation energy leads one to believe that the mechanism for conduction is rather more complicated.

On plotting the minimum value in  $\log \rho$  at 25°C for each

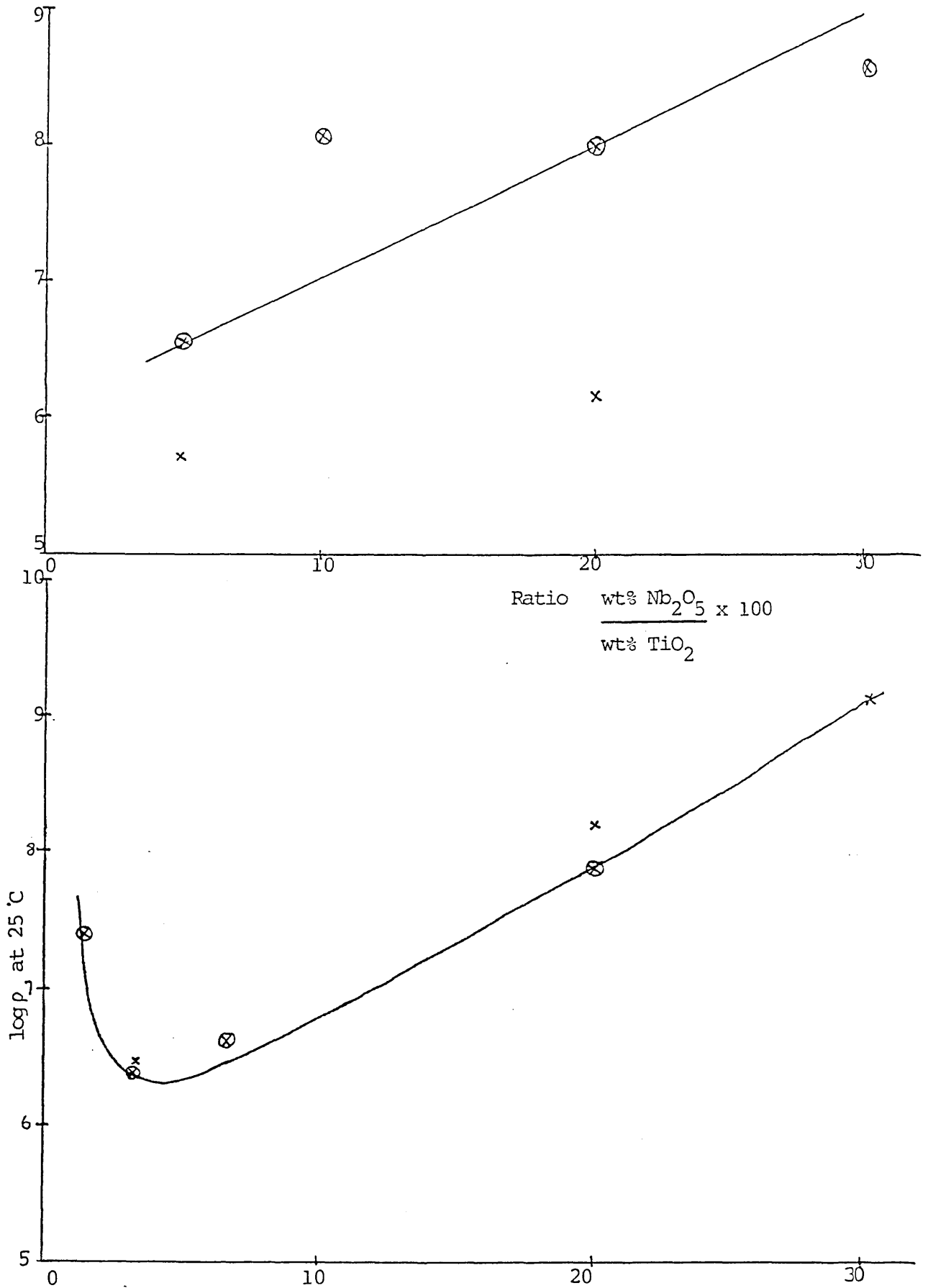


Figure 4.3 Variation between the minimum value in  $\log \rho$  at 25 °C and the ratio of wt% Nb<sub>2</sub>O<sub>5</sub> to wt% TiO<sub>2</sub> for

- a) 10 wt% TiO<sub>2</sub> glasses
- b) 15 wt% TiO<sub>2</sub> glasses

series of glasses against the ratio of wt% Nb<sub>2</sub>O<sub>5</sub> to wt% TiO<sub>2</sub> expressed as a percentage, the curves shown in figure 4.3 were obtained. From figure 4.3(a) there appeared to be a general increase in log ρ with an increase in the ratio Nb<sub>2</sub>O<sub>5</sub> : TiO<sub>2</sub>. However, at the ratios 5 and 20% Nb<sub>2</sub>O<sub>5</sub> : TiO<sub>2</sub> there are two sets of log ρ values. The points in "⊗" notation were more typical of the trend within that glass system, whilst the points in "X" notation were somewhat anomalous in their conductivity versus heat treatment results.

However, when one looks at figure 4.3(b) one notices a minimum in the plot, corresponding to a ratio of 4-5%. This in turn gives a value of 1.3 - 1.5 when the Nb<sub>2</sub>O<sub>5</sub> : TiO<sub>2</sub> ratio is expressed in mole% which is of the same order of magnitude as the amount of Sb<sub>2</sub>O<sub>5</sub> used in doped tin oxide glazes<sup>50</sup>. Similar plots for doped tin oxide glazes show a minimum in resistivity corresponding to about 2.5 mole% Sb<sub>2</sub>O<sub>5</sub>.

The points in "⊗" notation represent the highest conductivity samples for each glass system, whilst the "X" point at the Nb<sub>2</sub>O<sub>5</sub> : TiO<sub>2</sub> ratio of 20% represented a sample that had been phase separated for 18 hrs at 800°C instead of 3 hrs. The "X" points at the ratios of 3.4 and 30.1 % represent J13 and J12 glasses, which originally contained 20 and 13.3 wt% TiO<sub>2</sub>, respectively. With the higher wt% TiO<sub>2</sub> glasses, there appears to be less scatter in the points.

In summary, a fine dispersion of TiO<sub>2</sub> rich droplets in

a silicate matrix enables a very fine dispersion of rutile needles to form when the temperature is raised to allow crystal growth. Both the initial glasses and subsequently phase separated glasses have been shown to be non conducting. However, once the rutile needles start to grow, the conductivity increases rapidly. It has been shown that a glass prepared without  $\text{Nb}_2\text{O}_5$  and crystallised in a similar manner remained non-conducting after heat treatment.

Niobium is therefore responsible for producing a semiconducting material. It has been shown that solid solutions of  $\text{TiO}_2$  containing up to 9 mole%  $\text{Nb}_2\text{O}_5$  may be prepared, however, the change in lattice parameters with solid solution is extremely small and attempts to confirm that the precipitated rutile needles are in fact solid solutions were unsuccessful. However, it is not unreasonable to assume that even trace amounts of  $\text{Nb}_2\text{O}_5$  in solution in  $\text{TiO}_2$  would produce a defect lattice structure. A semiconducting material can be produced when a mass of interlocking and touching doped  $\text{TiO}_2$  needles precipitate from the glass. However, the point is reached when a second non-conducting crystalline phase, anorthite, eventually starts to grow and reduces the needle-needle contacts and so leads to an increase in the resistivity.

The 15 wt%  $\text{TiO}_2$  glazes (8.0-10 vol% crystalline  $\text{TiO}_2$ ) had much improved electrical properties when compared to the 10 wt%  $\text{TiO}_2$  glazes. Two slope behaviour was more commonly observed for the 10 wt%  $\text{TiO}_2$  glazes and is most probably

associated with the relatively high Nb content or the low vol% TiO<sub>2</sub> or possibly both, but the mechanism is uncertain, though it could also be a function of the needle-needle contacts. 10 wt% TiO<sub>2</sub> glazes containing greater than 3 wt% Nb<sub>2</sub>O<sub>5</sub> were non-conducting suggesting a lower limit of Nb<sub>2</sub>O<sub>5</sub> for the production of a defect lattice structure in TiO<sub>2</sub>.

#### 4.5 Suitability of TiO<sub>2</sub> Aluminosilicates as Insulator Glaze Material

Before assessing the suitability of the TiO<sub>2</sub> glazes as insulator glaze material, it would be useful to briefly mention the shortcomings of the previously used commercial glazes.

The iron oxide based glazes had much better performance under polluted conditions than insulators coated with a standard glaze. Unfortunately, under polluted conditions the glazes deteriorated in a relatively short period of time and the semiconducting properties were lost. The main cause for loss in conductivity was considered to be electrolytic corrosion arising from currents passing between the pollution layer and the glaze while spark discharging was considered to be a secondary cause. The wet pollution layer was considered to have a much smaller resistance than the semiconducting glaze, and when a dry band formed, electrolysis occurred where the current passed from pollution deposit to glaze and vice versa. Hence the magnitude of the electrolytic current was greatest at the edges of dry bands and corrosion was thought to occur here.

However, the transfer of current from pollution to glaze was necessary to prevent flashover of the dry band. Smith<sup>4</sup> showed that the corrosion rate was higher, the more complex the spinel. It was considered that the corrosion rate was increased by having oxides of different electrode potentials within the glaze. If the conducting phase was made up of one phase uniformly dispersed, then the corrosion would be uniform and large defects in the glaze surface would take longer to form. Uneven size distribution was considered as a possible source for the deterioration of iron oxide glazes. These glazes were also unsuitable because of their high temperature coefficients of resistance, so while keeping the surface of the insulator dry, this could lead to failure of the glaze due to overheating. Another contributing factor was the rather high coefficient of thermal expansion of the spinels which led to the glaze surface being in tension rather than compression.

The reduced titania glazes had very good corrosion resistant properties while their expansion coefficients were low in accordance with the requirements of glazes for electrical porcelains. Their temperature coefficient of resistance was about half that for the spinel based glazes and so the likelihood of thermal damage was much reduced. However, their mechanism for failure seemed to be attributed to local spark discharges oxidising the non-stoichiometric oxide, again associated with the non-uniform distribution of conducting phase.



Sb<sub>2</sub>O<sub>5</sub> doped tin oxide glazes had temperature coefficients of resistivity, expansion coefficients and corrosion resistance which were all comparable with reduced titania based glazes. However, they too failed due to electrolytic corrosion with a secondary cause of deterioration being spark erosion leading to electrical puncturing; again associated with the uneven distribution of crystallites.

Bearing these points in mind, it is evident that the doped TiO<sub>2</sub> glazes with their finer and more uniform microstructure would be strong contenders for HV insulators. By careful control of heat treatment a range of resistivities can be imparted to the glazes; and they will not re-oxidise with time to be rendered non-conducting (unlike the reduced TiO<sub>2</sub> glazes).

The corrosion resistance of the glazes as shown by Smith<sup>4</sup> is high, in accordance with the requirements for such a glaze. T<sub>½</sub> values are about 45°C which compare favourably with the value of 50°C quoted by Powell<sup>8</sup>.

With regards to the practical aspects of glazing, one must consider the expansion coefficient of the glaze. In this respect, samples were chosen and their relative glass transition temperatures, dilatometric softening points and linear expansion coefficients measured and are reported in table 3.38.

#### 4.5.1 Coefficients of linear expansion, $\alpha$

Between ambient and the glass transition temperature

( $T_g$ ) the coefficient of linear expansion of a glass is approximately linear; expansion and contraction curves of a well annealed glass are identical and reversible.

The diagram below shows a typical plot of increase in length,  $\Delta L$ , against temperature,  $T$ .

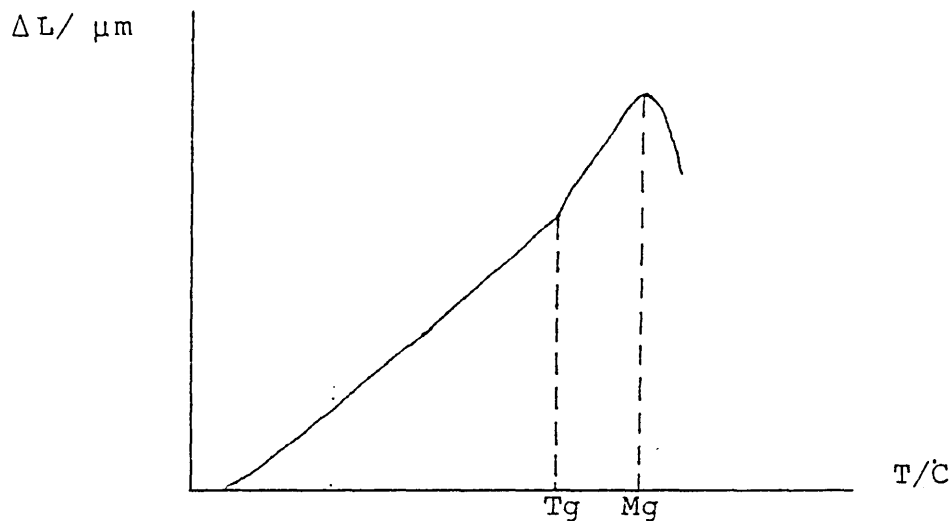


Figure 4.4

$T_g$  represents the "glass transition temperature" and corresponds to the temperature at which the coefficient of expansion of the sample shows a marked increase. It is defined as the temperature at which the viscosity is equal to  $10^{12.4}$  Pa.s ( $10^{13.4}$  Poise).

$M_g$  represents the "glass softening point" and corresponds to the temperature and viscosity at which the specimen starts to deform or decrease in length. The contraction after  $M_g$  is a direct consequence of the method of measurement. Use of a dilatometer will invariably put the glass sample under axial compression whilst the

measurements are made. As the viscosity of the glass samples will decrease with increasing temperature, there is a temperature at which the glass flows under the applied compressive stress. This corresponds to a viscosity of  $10^{6.6}$  Pa.s ( $10^{7.6}$  Poise).

The rapidly quenched partially crystalline glasses showed an apparent contraction as  $T_g$  was approached. This contraction can be explained by introducing the term "Fictive Temperature"<sup>77</sup>. When a glass is cooled quickly from  $1000^\circ$ , say, the room temperature configuration of the glass will be best represented by a rather more open structure corresponding to a high temperature configuration. The glass is then said to have a high fictive temperature. This would be the case for samples heat treated at  $1000^\circ\text{C}$ . The contraction is due to structural changes towards a more dense form corresponding to the equilibrium configuration. The densification may be so marked as to outweigh the thermal expansion due to increased amplitude of atomic vibration with increasing temperature. Having attained the equilibrium configuration, the glass then expands as normal. A possible way to overcome this contraction is to anneal slowly from above the transformation temperature, but this would tend to affect the microstructure and hence alter the resistivity of the samples. Generally, the samples exhibit low temperature expansion coefficients of between  $5.2 - 7.3 \times 10^{-6} \cdot\text{C}^{-1}$ , which compare favourably with the values quoted by Bloor<sup>78</sup> for electrical porcelains,  $4 - 6.8 \times 10^{-6} \cdot\text{C}^{-1}$ .

Bloor suggests that the expansion coefficient of the porcelains can be altered by changing the  $(\text{Na}_2\text{O} + \text{K}_2\text{O}) : (\text{Al}_2\text{O}_3 + \text{SiO}_2)$  ratio; an increase in the ratio giving an increase in the coefficient of expansion. Changes in the coefficient of expansion of the experimental glazes could be made by changing the ratio of modifying to network forming oxides in the glass. A decrease in the  $\text{CaO} : \text{SiO}_2$  ratio would lower the coefficient of expansion, thus enabling a glaze to be produced which would be in compression when applied to the surface of high tension insulators.

## CHAPTER 5

### CONCLUSIONS AND SUGGESTIONS FOR FUTURE WORK

#### 5.1 Conclusions

1. Calcium aluminosilicate glasses containing from 10 to 15 wt%  $\text{TiO}_2$  have been prepared by fusion of the oxides at  $1500^\circ\text{C}$ .
2. At subsolidus temperatures, the glass becomes supersaturated with respect to  $\text{TiO}_2$  and crystalline needles of rutile ( $\text{TiO}_2$ ) may be nucleated and grown.
3. Heat treatment of the glass at  $850^\circ\text{C}$  or below induces the glass to separate into two immiscible glassy phases by a process of spinodal decomposition. This produces a dispersion of sub-micron regions rich in  $\text{TiO}_2$  dispersed in a silica rich matrix. With prolonged heat treatment the  $\text{TiO}_2$  regions grow in size.
4. At temperatures of  $900^\circ\text{C}$ , or above, crystal growth of rutile takes place. A glass which has been given a prior glass in glass phase separation treatment produces a much finer and more uniform dispersion of rutile needles than one which has been given a single crystallisation treatment.
5. The volume per cent of  $\text{TiO}_2$  which crystallises from glasses containing 10 and 15 wt%  $\text{TiO}_2$  has been determined by x-ray diffraction techniques to range from 6 to 10 vol%.
6. Examination of crystallised glasses has shown that even at 6 vol% of crystalline  $\text{TiO}_2$ , a continuous network of

interlocking and touching needles is achieved. This is due to the high aspect ratio of the rutile needles crystallising from this system.

7. The glasses and crystallised glasses, themselves, were electrically non-conducting. However, the addition of a few weight per cent  $\text{Nb}_2\text{O}_5$  to the glass gave crystallised glasses which exhibited semiconducting properties.
8. Electron microprobe analysis was unable to confirm that the  $\text{Nb}_2\text{O}_5$  containing glasses gave needles containing  $\text{Nb}^{5+}$  ions. This was due to the extremely small ( $<1\mu\text{m}$ ) width of the needles being less than the resolution of the electron beam.
9. A separate study on the formation of solid solutions in the system  $\text{TiO}_2 - \text{Nb}_2\text{O}_5$  has shown that approximately 9 mole%  $\text{Nb}_2\text{O}_5$  may be taken into solid solution at  $1450^\circ\text{C}$ . The change in the lattice parameters of  $\text{TiO}_2$  with increasing amounts of  $\text{Nb}_2\text{O}_5$  is extremely small due to the similar size of the  $\text{Ti}^{4+}$  and  $\text{Nb}^{5+}$  ions.
10. The electrical conductivity of the crystallised glasses has been shown to be strongly related to the length of the rutile needles. The needles grow rapidly at first giving many point to point contacts, with the resistivity dropping rapidly. As the rate of needle growth decreases and the number of additional contacts falls, a plateau in the conductivity is reached.

11. With extended heat treatment, a second crystalline phase, anorthite ( $\text{CaO} \cdot \text{Al}_2\text{O}_3 \cdot 2\text{SiO}_2$ ), grows and the resistivity of the samples rises.
12. When the log resistivity as a function of reciprocal temperature was investigated, two slope behaviour was observed. Activation energies for electronic conduction from 0.13 to 0.61 eV were observed with most values in the range 0.18 - 0.25 eV.
13. Crystallised glasses containing 10 wt%  $\text{TiO}_2$  and greater than 3 wt%  $\text{Nb}_2\text{O}_5$  were non-conducting, suggesting that this represents an upper limit of  $\text{Nb}_2\text{O}_5$  to produce a defect lattice structure in  $\text{TiO}_2$ .
14. Glasses containing 15 wt%  $\text{TiO}_2$  generally exhibited single slope behaviour and gave optimum electrical conductance for a  $\text{Nb}_2\text{O}_5$  :  $\text{TiO}_2$  ratio of 1 : 30 [J9 glass].
15. The change in resistivity with temperature of the semiconducting partially crystalline glasses gave temperature coefficients which would make the materials highly suitable for semiconducting glazes on H V insulators.
16. The coefficient of thermal expansion of the glass and crystallised products is close to that of electrical porcelains. It would therefore be possible to apply these materials to the surface of high tension insulators.

## 5.2 Suggestions For Further Studies

This investigation has shown that it is possible to produce semiconducting materials by a novel process of glass in glass phase separation and crystallisation, which should be highly suitable for semiconducting coatings for high tension insulators.

While the electrical properties of the potential glaze materials have been investigated in some detail, a lack of time has prevented a study of the problems which may be encountered when the glaze is applied to an insulating ceramic substrate. Previous investigations have shown that interactions between the applied glaze and the electrical porcelain may occur during the coating process. A study of the inter diffusion of ions between the glass and the porcelain should be undertaken. Long term conductivity tests and possible corrosion phenomena would form an essential step in the evaluation of the glazes. Changes in the composition of the base glass to assist in the glazing operation, ie achieving flow properties at the application temperature, would require some further study. Similarly the effect of base glass composition on the coefficient of thermal expansion requires a more detailed study to ensure that the glaze surface is in compression and thus free from cracks or microflaws.

The effects of dopants other than  $\text{Nb}_2\text{O}_5$ , for example  $\text{Ta}_2\text{O}_5$  and  $\text{Sb}_2\text{O}_5$  could well provide an enhanced range of semiconducting materials for glaze and resistor



applications.

Finally new methods of glass preparation and of producing glassy coatings via the sol-gel method have recently been developed. This technique based on the precipitation of hydroxides from alcoholic solutions of metal alkoxides produces extremely homogeneous glass at much lower temperatures than conventional fusing of metal oxides/carbonates. The technique would seem highly appropriate for the application of strongly bonded and thin semiconducting layers of glaze materials to the surface of high tension insulators.

ACKNOWLEDGEMENTS

The author would like to express his thanks to all the members of the academic and technical staff of the department of Metallurgy and Materials Science at Imperial College who have assisted in various ways with this project. In particular the author wishes to thank his supervisor, Dr J Williamson, for his patience, guidance and continual help throughout the period of this work.

Thanks must also go to Dr J Robertson and Dr B Meadowcroft of the CEGB for stimulating and rewarding discussions.

The author is extremely grateful of Ms M Heydon for carefully typing this thesis; and S Groves and M Campbell for commenting on the text. Finally, the provision of a research studentship by the Science and Engineering Research Council and financial assistance from the CEGB is gratefully acknowledged.

REFERENCES

- 1 J S Forrest; J Inst Electr Eng, 89 (2), (1942), 60-80
- 2 T E Bradburn, G R Rigby; Trans Brit Ceram Soc, 52, (1953), 417-435
- 3 D H Lucas; Brit J Appl Phys, 3, (1952), 293-296
- 4 E J D Smith; Trans Brit Ceram Soc, 58, (1959), 277-300
- 5 D B Binns; Trans Brit Ceram Soc, 70, (1971), 253
- 6 C H W Clark, R B Turner, D G Powell; Trans Brit Ceram Soc, 60, (1961), 330
- 7 C H W Clark; Electrical Review, 15, (1964), 740-744
- 8 D G Powell; Bull Am Ceram Soc, 52, (1973), 600-603
- 9 E J Verwey, P W Haayman, F C Romeijn, G W Van Oosterhout; Phillips Res Rep 5 (1950), 173-187
- 10 D B Binns; Trans Brit Ceram Soc, 73, (1974), 7-17
- 11 O Nigol, J Reichman, G Rosenblatt, IEEE conference, Vancouver 1973.
- 12 V Bourgsdorf; CEGB report T4548, (1976), 44
- 13 R H Taylor; J Mat Sci, 12, (1977), 873-883
- 14 R H Taylor, D L Allinson, T I Barry; J Mat Sci, 13, (1978), 876-884
- 15 P M Morgan, J Robertson, R H Taylor; J Non Cryst Solids, 31, (1979), 367-375
- 16 J Robertson; CEGB report, VC 443, April 1980
- 17 A A Lebedoff; Trans Optical Inst Petrograd, 2, No 10 (1921); J Soc Glass Technol, Abs, 6, (1922) 110
- 18 W H Zachariasen; J Am Chem Soc, 54, (1932), 3841-3851
- 19 V M Goldschmidt; Skrifter Norske Videnskaps Akad (Oslo) I Math-naturwiss Kl No 8, (1926), 7-156
- 20 G W Morey; J Am Ceram Soc, 17, (1934), 315-328

- 21 B E Warren, H Krutter, D Morningstar; J Am Ceram Soc, 19, (1936), 202-206
- 22 A Smekal; J Soc Glass Technol; 35, 411-420, (1951)
- 23 J E Stanworth; J Soc Glass Technol; 30, 54-64 T, (1946) and 32, 154-172T and 32, 366-372T and 36, 217-241T and Nature, 169, 581
- 24 A Winter; Verres Réfract, 9, 147-156, (1955)
- 25 K H Sun; J Am Ceram Soc, 30 277-281, (1947)
- 26 H Rawson; "Proc 4th Int Cong on Glass, Paris", 62-69, Imprimerie Choix, Paris
- 27 Gibbs - see D R Uhlmann; J Non Cryst solids, 25, Nos 1-3, (1977)
- 28 A Dietzel, M Wickert; Glastechn Ber, 29, 1-4, (1956)
- 29 A C J Havermans, J M Stevels, H N Stein; J Non Cryst Solids, 5, 66, (1970)
- 30 D Turnbull; Contemp Phys, 10, 473, (1969)
- 31 P T Sarjeant, R Roy; Matls Res Bull, 3, 265 (1968)
- 32 D R Uhlmann; J Non Cryst Solids, 25, Nos 1.3, (1977)
- 33 A Hruby; Czech J Phys, B22, 1187 (1972)
- 34 D D Thornburg; Matls Res Bull, 9, 1481 (1974)
- 35 H A Davies, B G Lewis; Scripta Met, 9, 1107 (1975)
- 36 W Vogel; "Structure and crystallisation of glasses", Pergamon Press (1971)
- 37 D Turnbull, W B Hillig; J Phys Chem, 24, 914, (1956)
- 38 F E Wagstaff; J Am Ceram Soc, 52, 650, (1969)
- 39 R J Kirkpatrick; Am Miner, 40, 798 (1975)
- 40 J Williamson, P S Rogers; UK Patent 1462035
- 41 P W McMillan, "Glass-Ceramics", Academic Press, (1979), 2nd Edition
- 42 S M Ohlberg et al; "Symposium on nucleation and crystallisation in glasses and melts", Ed by Am Ceram Soc, Columbus, Ohio (1962) 55-62

- 43 W Vogel, K Gerth; as above pp 11-22
- 44 R D Maurer; as above pp 5-9
- 45 S Ya Bobovich; The Structure of Glass, vol 3, Consultants Bureau, New York, (1963) pp 93-95
- 46 G T Petrovski et al; as above, Vol 7 (1966)
- 47 E V Pudushko, A B Kozlova; as above, Vol 3, (1963)
- 48 T I Barry; J Mat Sci, 4, (1969) 596 and 5 (1970) 117
- 49 W B Hillig; as reference 42 but pp 77-89 (1962)
- 50 R W Gress, J A Murphy, A T Talkwalker; Ber Dtsch, Keram Ges, Vol 47, (10), 643-7
- 51 N F Mott, E A Davies, "Electronic Processes in Non-Crystalline Materials", (1978) Oxford Press
- 52 P W Anderson; Phys Rev, 109, 1492 (1958)
- 53 M H Cohen, H Fritzsche, S R Ovshinsky; Phys Revs Letts, 22, 1065 (1969)
- 54 M H Cohen; J Non Cryst Solids, 4, 391 (1970)
- 55 N F Mott; J Non Cryst Solids, 8-10, (1972)
- 56 D Emin; "Electronic and Structural Properties of Amorphous Semiconductors", Ed LeComber, PG and Mort, J, (Academic Press, London and NY), 261, (1973)
- 57 I G Austin; J Non Cryst Solids, 2, (1970), 474
- 58 G N Greaves; J Non Cryst Solids, 11, (1973), 427-446
- 59 V N Bogmolov et al; Soviet Phys Solid State, 9, (1968), 2502
- 60 A Miller, E Abrahams, Phys Rev, 120, (1969), 745
- 61 G H Johnson; J Am Ceram Soc, 36, No 3, March 1953
- 62 N P Bogoroditskii, V Kristya, Ya I Panova; Soviet Phys Solid State, 9, No 1 (1967)
- 63 R S Roth, L W Coughanour; J Res Nat Bur Standards, 55, No 4, October 1955
- 64 N G Error, D M Smyth; The Chemistry of Extended Defects in Non Metallic Solids", Ed by L Eyring and M O'Keefe (North Holland, Amsterdam, 1970) p 62

- 65 J F Baumard, E Tani; J Chem Phys, Vol 67, No 3, Aug 1977
- 66 F A Kroger; "The Chemistry of Imperfect Crystals", North Holland, Amsterdam, 1964
- 67 G J May; J Mat Sci, 14, (1979), 633-639
- 68 B D Cullity; "Elements of x-ray diffraction"; Addison Wesley, 396-400 (1967)
- 69 "Inorganic X-ray Powder Diffraction File", published by Joint Committee on Powder Diffraction Standards, Pennsylvania, USA
- 70 X-ray Powder Diffraction Files, 1979
- 71 B S Hobbs, A D S Tantram; "Degradation of H V "Insulators", Electrical Research Association project No 41/01/5039, Report No 72-112 pp 58 (1972)
- 72 P C Shultz; J Am Ceram Soc, 59, (1976), 214
- 73 Phase Diagrams for Ceramists, Fig.630, pp 219, publ. by Am. Ceram. Soc. (1964)
- 74 D M Adams; "Inorganic Solids", ed by John Wiley and Sons, (1978), pp 74
- 75 "Handbook of Chemistry and Physics", published by CRS Press, Inc, Boca Raton, Florida 33431, B-138 (1981)
- 76 D Warner; "Electrical Properties of Oxide Glasses Containing Iron and Manganese", thesis submitted Nov 1981. London University PhD
- 77 H Rawson; "Properties and Applications of Glass", published by Elsevier, 1980, (Glass Science and Technology 3) pp 69
- 78 E C Bloor; pp 227-279 in "Ceramics, a Symposium", by A T Green (1953), publ. by British Ceramic Soc.